A STUDY OF MODEL MATCHING TECHNIQUES FOR THE DETERMINATION OF PARAMETERS IN HUMAN PILOT MODELS

By G. A. Bekey, H. F. Meissinger and R. E. Rose

2 MAY 1964

Contract NAS 1-2582

Prepared for
LANGLEY RESEARCH CENTER
NATIONAL AERONAUTICS AND SPACE ADMINISTRATION
Langley Field, Virginia

TRW SPACE TECHNOLOGY LABORATORIES
THOMPSON RAMO WOOLDRIDGE INC.

A STUDY OF MODEL MATCHING TECHNIQUES FOR THE DETERMINATION OF PARAMETERS IN HUMAN PILOT MODELS

By G. A. Bekey, H. F. Meissinger and R. E. Rose

8 MAY 1964

Contract NAS 1-2582

Prepared for
LANGLEY RESEARCH CENTER
NATIONAL AERONAUTICS AND SPACE ADMINISTRATION
Langley Field, Virginia

TRW SPACE TECHNOLOGY LABORATORIES
THOMPSON RAMO WOOLDRIDGE INC.

STUDY OF MODEL MATCHING TECHNIQUES FOR THE DETERMINATION OF PARAMETERS IN HUMAN PILOT MODELS (FINAL REPORT)

8426-6006-RU-000

2 May 1964

Prepared by: G. A. Bekey

G. A. Bekey

H. F. Meissinger

H. F. Meissinger

R. E. Rose

R. E. Rose

Approved by: R. K. Whitford

R. K. Whitford, Director
Inertial Guidance and Control
Laboratory

TRW SPACE TECHNOLOGY LABORATORIES
One Space Park - Redondo Beach, Calif.

ACKNOWLEDGMENT

The authors wish to acknowledge the participation by Mr. R. E. Humphrey, formerly a member of the Technical Staff of STL, in the early portion of the study and his contribution to the formulation of the computer approach presented here. The authors are also indebted to Mr. J. J. Adams and Dr. R. Saucer of the Guidance and Control Branch, Space Mechanics Division, of NASA/Langley Research Center for valuable comments made in the course of this study and for their review of progress reports.

Mr. R. W. Taylor of the Office of Advanced Research and Technology, NASA Headquarters, has given this research effort continuous support and encouragement, and his helpful comments are gratefully acknowledged.

ABSTRACT

24040

This report presents the results of a study of techniques for the determination of parameters in mathematical models of the human pilot. The study was conducted by Space Technology Laboratories under NASA Contract NAS 1-2582. Earlier company-sponsored research, initiated in 1961, on the dynamics of the human operator in manual control tasks provided valuable background which is also reflected in this report.

The study departs from conventional approaches where the pilot is characterized by transfer functions or quasi-linear describing functions, progressing into the domain of time-variant and nonlinear operations and representative models of this type. The final portion of the study is concerned with manual tracking in two axes where the operator is modeled as a multiple input-multiple output system.

The emphasis has been placed primarily on development of computational methods and, hence, model matching experiments on synthetic pilots with known parameters were required. The resulting methodology was successfully applied to actual pilot tracking data and provided new insight into the pilot's dynamic response. The experimental results are presented in the report. A part of the study was devoted to the comparison of continuous and iterative parameter adjustment methods. In addition, significant analytical results were derived pertaining to the nature of parameter optimization by the gradient method. The report concludes with a recommendation of areas for further study of mathematical pilot models.

author

TABLE OF CONTENTS

LIST OF FIGURES

LIST OF FIGURES

1. INTRODUCTION

An important problem in the design of aircraft and manned space vehicles is that of describing the dynamic response of the human pilot mathematically. Numerous previous studies have had the objectives of expressing the pilot's input-output characteristics in quantitative terms. The techniques employed in these studies limit the tasks that can be considered to a class of manual operations where the pilot response can be approximated by a linear time-invariant system having a single input and a single output. However, in many situations of practical interest the pilot acts as a multiple input, multiple output system, and his response is essentially time-varying or nonlinear.

The purpose of this study is to examine new techniques for obtaining mathematical models of the human pilot that permit a departure into the regime of time-varying and nonlinear operations and into multi-axis control situations. Ideally, the methods to be investigated should allow incorporation of known mechanisms of human performance into the mathematical model so as to make maximum use of existing knowledge. The methods should also provide a means for continuously monitoring pilot performance in the process of determining optimum model parameter values.

The basic strategy used in the model matching procedure is optimization of parameters by a steepest descent method or by related methods of finding the minimum of a suitably chosen criterion function. This optimization may be performed by a continuous or by a step by step procedure. Both techniques have been the subject of investigation in this study.

To develop these techniques and to explore their applicability to model matching of human pilots in the larger class of operating conditions described above, the research study was subdivided into four parts. The first part was primarily concerned with developing the model matching approach and suitable computational strategies which were applied to the case of single axis manual tracking. The tracking task performed by the operator was chosen so as to emphasize linear and time-invariant performance. After test and validation of the model matching technique in this relatively simple first task, the study progressed to

the more complex tasks of time-varying, nonlinear, and two-axis tracking.

In each of these investigations the computer approach of model matching was tested on systems with known sets of parameters to ascertain accuracy of results. Each phase of the study concluded with matching of human operator's tracking data. The experimental results are presented in Section 6 and Appendix A of this report.

A review of the experimental procedures employed and the various computer programs implemented during Part 1, 2, 3 and 4 of the study is presented in Sections 3 and 4. Significant analytical results regarding the nature of the model matching process were obtained and are presented in Section 5. The analytical results include: a derivation of properties of the criterion function used in model matching and of the gradient of this function; an explanation of the dynamics of parameter adjustment in terms of stability, convergence, and parameter interaction; and an analysis of the relative precision of parameter determination.

Section 7 presents conclusions derived from the results of Parts 1 through 4 and recommendations for future study of mathematical pilot's models. Appendix B presents a detailed comparison of the continuous parameter adjustment techniques used in this study with the techniques, based on transfer function notation, which have been used by Whitaker (1), Adams (2), and others.

The use of analog rather than digital computation was motivated by economy of operation, flexibility of experimentation, ease of processing of pilot output data in analog form, and the convenience offered by the analog computer in operating on a real-time basis. The relatively simple analog computer implementation of the techniques investigated offers advantages for use in the laboratory or in field applications.

2. MODEL MATCHING TECHNIQUES OF PARAMETER IDENTIFICATION

2.1 Historical Background

Previous investigations of the dynamic response of human operators have been based on one of three general techniques, Fourier analysis, spectral analysis or model matching techniques. The methods based on spectral analysis and Fourier analysis have been well documented in the literature (3) and will not be reviewed.

Early model matching studies have been based on visual matching of the time response of an assumed model and that of a pilot in a specific control task. This operation requires manual parameter adjustment on a trial-and-error basis. Such a study was performed at Goodyear Aircraft Corporation (4). Two studies in the literature on human operator models have used automatic techniques for the adjustment of the parameters of an assumed model. Ornstein (5) applied an automatic technique for determination of parameters in an assumed linear model of the human operator. The method used has been described by Graupe (6) and consists of adjusting parameters in such a way as to minimize a particular error called the "equation error." Wertz (7) has applied the "learning model" or "output error" technique described by Margolis (8) to adjust automatically the parameters according to a specified criterion. Humphrey and Bekey (9,10) extended these methods to the determination of parameters in nonlinear models. Studies by Elkind and Green (11) have represented the human operator by means of a linear model composed of a set of filters whose impulse responses are orthonormal. The filter outputs are weighted and summed to yield the output. The weights are chosen to minimize the mean squared matching error over a particular time interval.

The objective of this study has been to extend these earlier concepts and to define and solve some of the problems inherent in the model matching approach. The scope of this study only permitted the investigation of the output error method and was limited to operations involving compensatory tracking tasks. A further broadening of the program in future model matching studies to include pursuit tracking tasks as well would be most desirable.

2.2 Statement of the Problem

The methods of parameter optimization considered in this research are based on the comparison of performance of an assumed mathematical model with that of the human pilot, as indicated in Figure 2-1. An automatic parameter adjusting strategy must be selected which determines the optimum values of the model parameters, in the sense that the model performance approximates as closely as possible the human pilot performance. It can be seen that the mechanization of techniques of this type involves three primary considerations:

(a) A mathematical model must be selected and the adjustable parameters fully identified. The evidence available in the literature on human dynamic response provides justification for the selection of a second order differential equation as a model for the operator's performance.

(b) A criterion function must be selected which can serve as an index of the validity of the mathematical model. Minimization of this criterion or performance function by adjustment of model parameters results in the closest possible agreement between pilot output and model output.

(c) An automatic technique for performing the required parameter adjustments must be selected.

This section presents a brief discussion of the rationale which underlies the selection of the type of criterion function used in the experiments and to present three different adjustment strategies which were employed. The results obtained with these strategies are given in Sections 5, 6, and Appendix A.

2.3 Choice of Performance Criterion

The criterion which compares the performance of system and model must be selected with care. Consider first the mathematical description of the model and pilot behavior. Dynamic systems are described by means of differential equations. A system of order n is described by a single nth order differential equation or by n first order equations. Thus a model of order n and having m parameters α_i can be described by

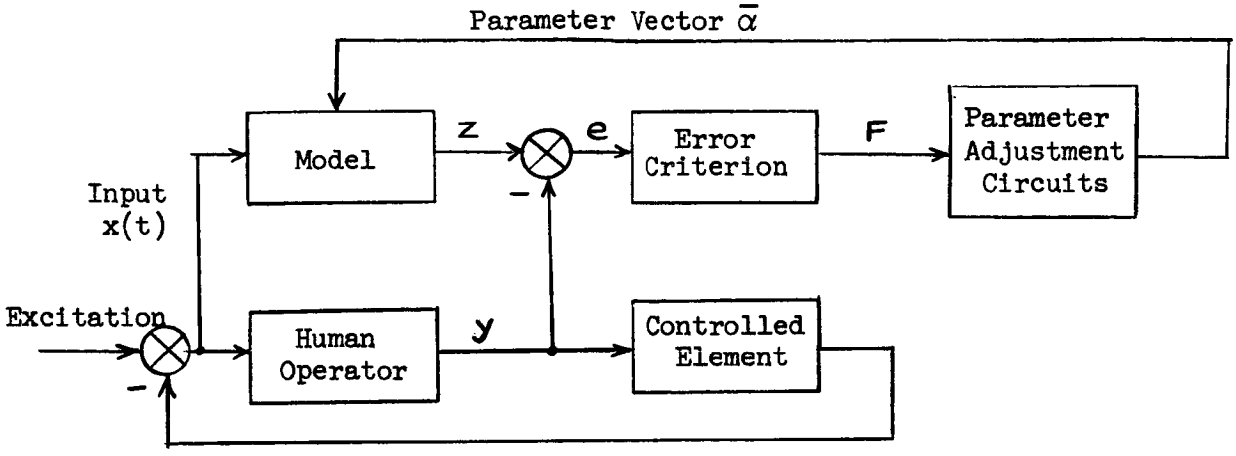

Figure 2-1. Model Matching Block Diagram

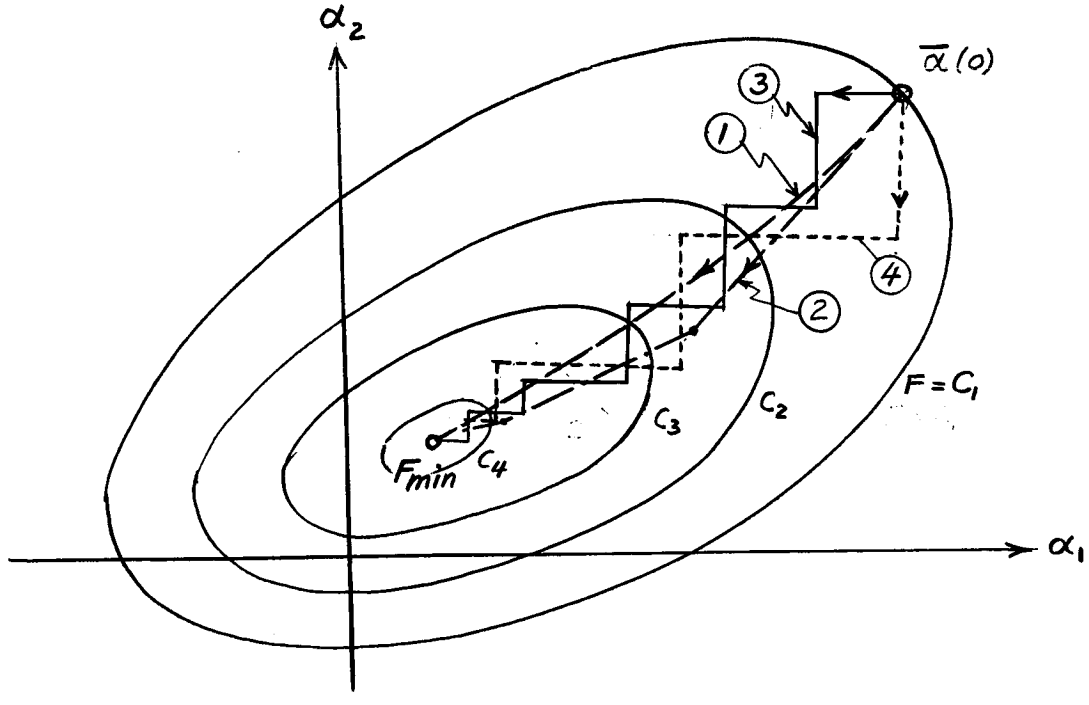

Figure 2-2. Adjustment Paths in Parameter Space

the set of equations*

$$\dot{z}_i = f_i\,(z_1, z_2 \ldots z_n;\ t;\ \alpha_1, \alpha_2, \ldots \alpha_m) \qquad (2.1)$$

$$i = 1, 2, \ldots n$$

The z_i can be considered to be the corresponding time derivatives of the model output, viz.,

$$z_i = \frac{d^i z}{dt^i} \qquad (2.2)$$

Time t appears explicitly in Equations (2.1) since the model output also depends on the time dependent input x. To completely characterize any dynamic system a set of initial conditions is required in addition to the system equations and these are given by

$$z_i(0) = c_i \qquad i = 1, 2, \ldots n \qquad (2.3)$$

where c_i represents the value of the ith derivative at the initial time. Since the set of variables z_i provide a complete description of model behavior at any particular time, they are commonly referred to as state variables. The variables z_i may also be considered as components of a state vector $\bar{z}$. Similarly the m adjustable parameters $\alpha_1, \alpha_2, \ldots \alpha_m$ can be considered the components of a parameter vector $\bar{\alpha}$. The set of first-order differential equations described by Equation (2.1) can then be stated as a single vector differential equation

$$\dot{\bar{z}} = \bar{f}\,(\bar{z},\ t,\ \bar{\alpha});\quad \bar{z}(0) = \bar{c}$$

where $\bar{c}$ represents the initial state of the system. The model matching problem consists in selecting a particular parameter vector $\bar{\alpha}$ such that the model response approximates as closely as possible the response of the human pilot.

The state of the system to be identified, in this case the human pilot, can be denoted by means of the vector $\bar{y}$. However, whereas the order of the model represented by $\bar{z}$ is assumed (in Equation 2.1 the order is n) the system to be modeled, represented by the vector $\bar{y}$,

*For explanation of symbols see the Glossary on page 162.

is of unknown order and may in fact be only partly deterministic.

The problem of formulating a performance function is one of determining a distance between the vectors $\bar{z}$ and $\bar{y}$. In order to qualify as a distance function or metric in a function space, the criterion function must satisfy certain properties. A typical criterion function may be formulated as

$$F = \int_0^T \left[y_1(t) - z\ (\bar{\alpha},\ t) \right]^2 \ dt \qquad (2.5)$$

where z_1 and y_1 represent the output positions of the model and pilot respectively. It is important to note that the criterion function F is an ordinary function of the parameter vector $\bar{\alpha}$. That is, a selection of particular values for the parameters will result in a given number for the criterion function upon evaluation of the definite integral in Equation (2.5). Using this criterion function the parameter optimization problem can proceed on the basis of ordinary calculus by determining the maxima or minima of functions. On the other hand the instantaneous criterion function defined by

$$f = \frac{1}{2}\left[y_1(t) - z\ (\bar{\alpha},\ t) \right]^2 \qquad (2.6)$$

depends not only on the parameter values but on the entire time history of the model output and consequently represents a functional whose maximization or minimization is the concern of the calculus of variations.

2.4 Possible Adjustment Strategies

The three parameter adjustment strategies employed during this study plus an additional strategy developed but not proven experimentally, can be visualized conveniently with reference to Figure (2-2) which illustrates contours of constant criterion function F in a parameter plane determined by the two adjustable parameters α_1 and α_2. Parameter optimization begins with an arbitrary initial set of values denoted by $\bar{\alpha}\ (0)$, as indicated in the figure, and proceeds automatically to the

particular value of the parameter vector which minimizes the criterion function. Four possible paths are illustrated in Figure (2-2):

(a) Path 1 proceeds from the initial position along the gradient vector, i.e., in a direction always normal to the contour lines, and terminates at the minimum value. This is the path known as "path of steepest descent." (See Ref.12).

The adjustment strategy is based on choosing a rate of adjustment of the parameters which is proportional to the negative of the gradient vector;

$$\dot{\bar{\alpha}} = -K \ \overline{\nabla F} \tag{2.7}$$

where K is a positive constant.

This equation corresponds to the two scalar equations

$$\begin{aligned} \dot{\alpha}_1 &= -K \ \frac{\partial F}{\partial \alpha_1} \\ \dot{\alpha}_2 &= -K \ \frac{\partial F}{\partial \alpha_2} \end{aligned} \tag{2.8}$$

At the minimum of F the gradient as well as the rate of change of the parameters approach zero and the solution becomes stationary.

(b) The steepest descent path can be approximated by straight line segments by means of an iterative procedure which adjusts the parameter vector in a series of discrete steps. (See Ref.13). Thus beginning at the initial value $\bar{\alpha}^{(0)}$ the components of the gradient

$$\overline{\nabla F}\ (\bar{\alpha}^{(0)}) = \left[\frac{\partial F(\bar{\alpha}^{(0)})}{\partial \alpha_1}, \quad \frac{\partial F(\bar{\alpha}^{(0)})}{\partial \alpha_2} \right] \tag{2.9}$$

Using the gradient at $\bar{\alpha}^{(0)}$ a discrete parameter change vector can now be computed by means of the relationship

$$\bar{\triangle} \alpha^{(0)} = -K \ \overline{\nabla F}\ (\bar{\alpha}^{(0)}) \tag{2.10}$$

and the process is repeated. If the steps are sufficiently small path 2 can be a good approximation to path 1 in Figure (2-2).

(c) Path 3: The major disadvantage of the computational strategy involved in path 1 is the need to compute the gradient vector at each point. In order to implement Equation (2.10) it is necessary to compute and store all n components of the gradient vector. This procedure requires either n computer circuits operating in parallel in order to obtain all n components of the gradient vector, or n memory cells which can be used to store the components when they are computed one at a time. Methods of computation of the gradient are discussed below.

Path 3 is an iterative technique based on cyclical parameter adjustment. Assume that the initial value of the parameters is again given by $\bar{\alpha}^{(0)}$. Now compute one component of the gradient, say

$$\frac{\partial F(\bar{\alpha}^{(0)})}{\partial \alpha_1} \tag{2.12}$$

then the parameter α_1 only is adjusted to yield

$$\alpha_1^{(1)} = \alpha_1^{(0)} - K \left.\frac{\partial F(\bar{\alpha}^{(0)})}{\partial \alpha_1}\right|_{\bar{\alpha}^{(1)}} \tag{2.13}$$

and the new parameter vector $\bar{\alpha}^{(1)}$ is defined as

$$\begin{aligned} \bar{\alpha}^{(1)} &= \left[\alpha_1^{(1)}, \alpha_2^{(0)}, \alpha_3^{(0)}, \ldots . \alpha_n^{(0)}\right] \\ &= \left[\alpha_1^{(1)}, \alpha_2^{(1)}, \alpha_3^{(1)}, \ldots . \alpha_n^{(1)}\right] \end{aligned} \tag{2.14}$$

Parameter α_2 is now adjusted to yield the next point in the parameter space, etc. The process is continued until the nth parameter has been adjusted and then the cycle is repeated.

(d) Path 4 is obtained by a so-called relaxation procedure which consists of adjusting each parameter in turn until the performance function is minimized with respect to that parameter. With reference to Figure (2-2), if the relaxation process is begun by adjustment of parameter α_1 this parameter is adjusted until the path reaches a relative minimum. At this point α_1 is held constant and adjustment is switched to α_2 until a new minimum is reached. The process is repeated in this manner.

In the experimental studies of Phase 1 the cyclical or iterative technique of path 3 and the relaxation method of path 4 were instrumented by means of an analog computer using the criterion function of Equation (2.5). Path 1 was approximated by using a continuous parameter adjustment procedure based on a minimization of the time-dependent criterion function given in Equation (2.4). However, the gradient of the latter criterion function is not strictly defined when the parameters are varied and consequently this adjustment strategy may be considered an approximation to a continuous steepest descent path, with the degree of approximation being dependent on the rate of change of the parameters. The nature of the approximation and the resulting path are discussed and illustrated in Section 5. Some of the mathematical considerations involved in the formulation of the adjustment strategies and their effect on the convergence and stability of the process are also discussed in Section 3.

2.5 Computation of the Gradient

Two different methods were used for the computation of gradient components $\partial F/\partial \alpha_i$. The iterative strategy denoted by path 2 in Figure 2-2 was based on computation of components of the gradient from the relation

$$\frac{\partial F(\bar{\alpha}^{(k)})}{\partial \alpha_i} = \frac{F(\alpha_1^{(k)}, \alpha_2^{(k)} \ldots, \alpha_i^{(k)} + \Delta\alpha_i, \ldots \alpha_n^{(k)} - F(\bar{\alpha}^{(k)})}{\Delta\alpha_i} \tag{2.15}$$

where the subscript k represents the computation of the kth iteration. Clearly this computation requires either the use of two parallel mathematical models, or some form of data storage to permit computation of the finite differences $\Delta F(\bar{\alpha}^{(k)})$.

The continuous or approximate steepest descent adjustment strategy was based on the computation of components of the gradient vector by means of the method of influence coefficients (14). This method is discussed briefly in Section 4.

2.6 Formulation of an Assumed Mathematical Model of the Human Pilot in Single Axis Tasks

The parameter optimization techniques described in the preceding paragraphs are based on the formulation of a model equation suitable for representing the unknown system. A finite number of parameters are to be adjusted in the model to minimize a particular criterion function. The rationale used here for postulating a general model structure conforms to the approach commonly used in engineering analysis, namely to formulate the model equation on the basis of past experience and observation of typical input-output characteristics.

The extensive work on human dynamic response reported by McRuer and Krendel (3) suggests that in many single axis tracking tasks, human operators may be characterized by a quasilinear describing function of the form

$$H(j\omega) = \frac{K\,(1 + j\omega T_1)e^{-j\omega\tau}}{(1 + j\omega T_2)(1 + j\omega T_3)} \qquad (2.16)$$

where K, T_1, T_2, T_3 and τ are parameters which depend on the forcing function bandwidth and on the controlled element dynamics. It has been shown that when the forcing function contains negligible energy above -.75 cps, the describing function (2.16) may represent as much as 80 - 90% of the total power in the operator's output. Consequently, the form of (2.16) was suitable for the single axis models used in this research. However, since τ is typically very small in continuous tracking (τ = 0.15 sec) and since a number of experimental difficulties

are encountered when attempting to match a pure time delay, the term τ was set equal to zero, and the following human pilot model was formulated

$$\ddot{z} + \alpha_1 \dot{z} + \alpha_2 z = \alpha_3 \dot{x} + \alpha_4 x \qquad (2.17)$$

where x is the pilot (and model) input and z is the model output. This equation corresponds to (2.16), viz.

$$K = \frac{\alpha_4}{\alpha_2}, \quad T_1 = \frac{\alpha_3}{\alpha_4}, \text{ and } T_2, T_3 \text{ are the roots of}$$

$$\left(\frac{1}{\alpha_2} s^2 + \frac{\alpha_1}{\alpha_2} s + 1\right)$$

The model was formulated as a differential equation (rather than a describing function) in order to make possible a direct extension to the time-varying and nonlinear case. This model is similar to the one employed by Adams (2) with the exception of the denominator term. The STL form allows for two complex roots, whereas Adams' model is restricted to two identical real roots.

2.6.1 Extension to the Time-Varying Case

The model of Equation (2.17) can be used to represent directly linear invariant and linear time-varying cases of human operator response. In the former case the human pilot is assumed to behave in an approximately stationary manner. In the latter case, the controlled element dynamics is time-varying, thus inducing time variation in the pilot's response. The same model form was used in both cases and time variations in the α's were investigated. The results of these studies are reported in Sections 5 and 6 below.

2.6.2 Extension of the Model to the Nonlinear Case

The model structure was modified to include nonlinear terms primarily to test the applicability of the model matching techniques, rather than as a valid hypothesis of human dynamic response in the given tracking situation.

Two representative nonlinearities were selected for the model: namely, a cubic term $f_1(x) = x^3$ and a deadzone term,

$$x_d = f_2(x) = \begin{cases} x - \alpha_6, & x > \alpha_6 \\ 0 \quad , \text{ if} & |x| \leq \alpha_6 \\ x + \alpha_6, & x < -\alpha_6 \end{cases} \tag{2.18}$$

where α_6 is a positive constant. These nonlinearities were selected for two reasons:

(1) They represent two important classes of nonlinear behavior: $f_1(x)$ is an analytic function of x while $f_2(x)$ has slope discontinuities. It was necessary to test the model matching techniques with both types of nonlinearities.

(2) $f_1(x)$ and $f_2(x)$ represent behavior similar to that observed in human tracking records. $f_1(x)$ is an amplitude-dependent gain characteristic which corresponds to a "hardening" or "softening" spring. $f_2(x)$ corresponds to threshold phenomena which are known to occur in tracking. In addition, an amplitude limiter was used in some experiments as a third form of nonlinear response.

The human operator was assumed to behave as a second order nonlinear system governed by the equation

$$\ddot{y} + a_1\dot{y} + a_2 y = a_3\dot{x}_d + a_4 x_d + a_5 x_d^3 \tag{2.19}$$

where x_d is the output of a deadzone of width $2a_6$. Furthermore, the system output y is subject to amplitude limiting at a level a_7. The model was of the same form as (2.19) and had 7 adjustable parameters $\alpha_1, \alpha_2, \ldots \alpha_7$.

2.7 Formulation of a Two-Axis Model of the Human Operator

2.7.1 Extension of Single-Axis Model

As a straightforward approach to formulating a two-axis model of the human operator for the purposes of this study, a direct extension was made of the single-axis model discussed above. A symmetrical two-axis tracking task was selected in which the excursions of the controlled element are assumed independent of each other.

The human operator's response to vertical and horizontal error signals was expressed in terms of two uncoupled, second order linear differential equations.

For the vertical axis:

$$\ddot{y}_v + a_{1v}\,\dot{y}_z + a_{2v}\,y_v = a_{3v}\,x_v + a_{4v}\,\dot{x}_v \qquad (2.20)$$

For the horizontal axis:

$$\ddot{y}_h + a_{1h}\,\dot{y}_h + a_{2h}\,y_h = a_{3h}\,x_v + a_{4h}\,\dot{x}_h \qquad (2.21)$$

where x_v and x_h are the vertical and horizontal deflections of a dot on an oscilloscope display, i.e., the inputs to the human operator. In accordance with earlier notation the model differential equations used to match the human operator output y_v, y_h are written in terms of z_v and z_h with unknown coefficients α_{iv} and α_{ih}, e.g.

$$\ddot{z}_v + \alpha_{1v}\,\dot{z}_v + \alpha_{2v}\,z_v = \alpha_{3v}\,x_v + \alpha_{4v}\,\dot{x}_v \qquad (2.22)$$

(The subscripts v and h will be omitted subsequently where no misunderstandings can arise.)

The controlled element dynamics did not contain cross-coupling between axis, hence the operator's responses in each axis can be assumed as essentially independent. This initial assumption is supported by the results of a symmetrical two-axis tracking experiment conducted by Humphrey (15). However, the possibility of cross-coupling in the operator's responses must also be considered.

2.7.2 Cross-Coupling Effects

The integrated display of two tracking error components on the display screen, and the integration of two-axis control into a single fingertip controller introduces a problem in the interpretation by the operator of visual stimuli and kinesthetic feedback. When observing the displayed tracking error in two dimensions the operator probably does not consciously resolve the error vector into cartesian coordinates, x_v, x_h, when manipulating the control stick. He may actually interpret

the display error and the stick deflection in terms of polar coordinates (see Figure 2-3). The displacement element expressed in polar coordinates r and φ is obtained by a linear transformation of the cartesian elements dx_v, dx_h:

$$dr = dx_h \cos\varphi + dx_v \sin\varphi$$
$$r d\varphi = dx_h \sin\varphi + dx_v \cos\varphi \qquad (2.23)$$

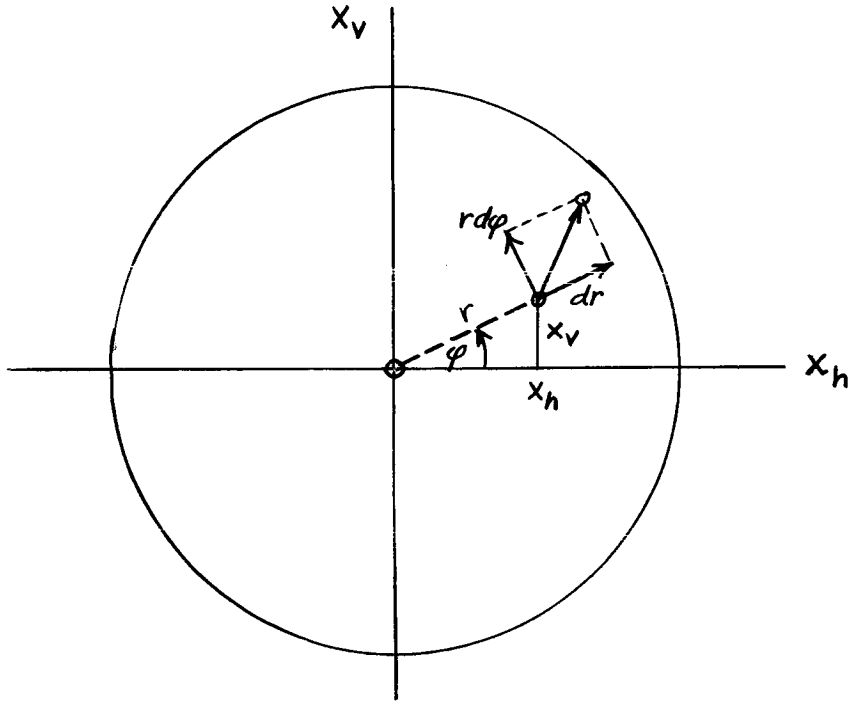

Figure 2-3

Resolution of Coordinate Changes on Display

The operator could not perform this resolution (or its inverse) with precision even if he knew the individual deflection elements. This suggests that there are interactions in his responses to error stimuli regardless of whether they are perceived in terms of cartesian or polar coordinates. A further complication stems from the fact that a finger-tip controller of the type used in this study (see Section 3) does not provide a clear "proprioceptive" feedback of stick deflections in the horizontal or vertical sense. Hence the operator's control deflections in the two axes contain inevitable interactions.

2.7.3 Mathematical Model of Cross-coupling Effects

On the basis of these considerations it is reasonable to expect unintentional cross-coupling of varying degree to exist in the tracking responses of the operator. The model equation (2.22) should therefore be modified as follows for the vertical channel:

$$\ddot{z}_v + \alpha_1 \dot{z}_v + \alpha_2 z_v + \underline{\beta_1 z_h + \beta_2 \dot{z}_h + \gamma_1 z_v z_h} = \alpha_3 x_v + \alpha_4 \dot{x}_v + \underline{\beta_3 x_h + \beta_4 \dot{x}_h + \gamma_2 x_v x_h} \qquad (2.24)$$

and similarly for the horizontal channel. The additional, underlined terms on the left and right hand sides of the equation are the various types of cross-coupling having unknown coefficients β_i and γ_i.

The following distinction is made as to the sources and form of the cross-coupling terms added to the equation: The effects of the excitation signal x_h or its derivative will be termed perceptual or input cross-coupling. The effects of the variable z_h will be termed motor or output coupling. The terms may appear in linear or nonlinear form. The latter case may occur under conditions where a heavy task load occurs simultaneously in both channels and causes a deterioration of manual control action with unintentional response in the wrong channel. The coefficients β_i, γ_i are used to denote these different coupling phenomena as follows:

	Output (Motor)	Input (Perceptual)
Linear	β_1, β_2	β_3, β_4
Nonlinear	γ_1	γ_2

As will be discussed in Section 6 some experimental computer runs were included in this study to detect the presence of cross-coupling in the operators' performance and to observe, if possible, a quantitative improvement in model matching by the introduction of individual cross-coupling terms.

For further study of these phenomena it would be of great interest to introduce display cross-coupling artificially,e.g.

$$x_v' = x_v + m_1 x_h$$
$$x_h' = x_h + m_2 x_v \qquad (2.25)$$

and to retrieve the coefficients m_1, m_2 in the operator's response by model matching techniques. It would also be of considerable practical value to study control tasks which are essentially asymmetrical and exhibit inherent coupling phenomena. Such tasks probably tend to induce reverse cross-coupling in the operator's responses after the operator has learned to cope with this situation.

3. EXPERIMENTAL PROCEDURE

3.1 General Approach

The philosophy of model matching in this study is based on the "output error method" illustrated in Figure 2-1. The same input signal is applied to the human operator and to an adjustable mathematical model. The outputs of model and operator are compared and the output error is used in generating an appropriate performance function. The parameter adjustment program utilizes the performance function and computes the parameter changes required to minimize the performance function. The input and output quantities were obtained by having the human operator perform a simple closed loop control task as depicted in Figure 3-1. This task performed by the operator is commonly referred to as a compensatory tracking task, i.e., a signal proportional to the tracking error is displayed to the operator who in response produces corrective actions by means of a hand controller.

An analog computer was utilized for generating the input signals, simulating the controlled element, and driving the display during the experiment. The analog computer also performed the parameter optimization process. Most of the model matching experiments used the continuous parameter adjustment technique which requires only conventional analog computer programming. The iterative parameter optimization technique was instrumented on an iterative analog computer with provisions for independent control of the operating modes on each integrator, permitting the use of any integrator as a track-and-hold channel. The details of the computer implementation for each technique are given in Section 4.

3.2 Description of the Tracking Task

3.2.1 Experimental Arrangement

The tracking tasks performed during each of the four phases of the study were similar. The pilot was seated in a fixed-base cockpit shielded as much as possible from external disturbances. Figure 3-2 illustrates the cockpit used in the experiments. Changes in the tracking task required for different phases of the study are described in Sections 3.3 - 3.6.

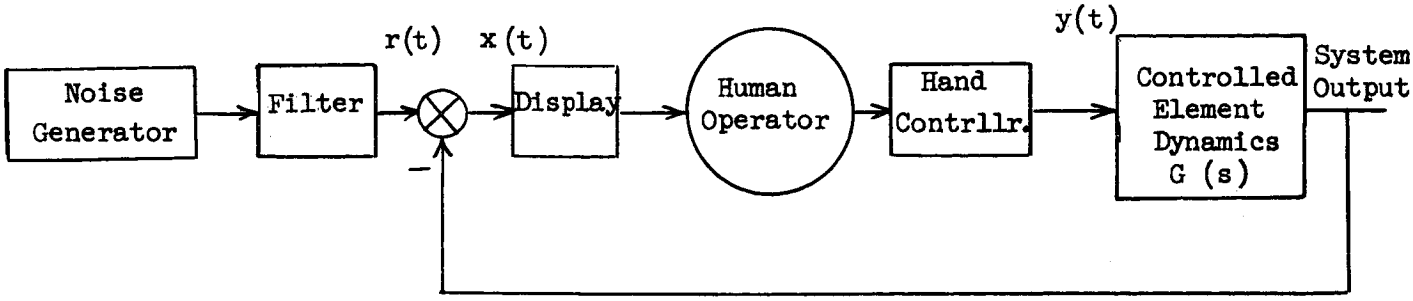

Figure 3-1

Tracking Task of the Human Operator

TABLE 3-1

Human Operator Tracking Tasks

	Phase I (Linear Invariant)	Phase II (Time Varying)	Phase III (Non-linear)	Phase IV (Two-Axis)
Type of Input Disturbance r(t)	Random Noise	Random Noise	Random Noise	Random Noise
Filter G(s)	$\frac{50s}{(10s+1)(s+1)^3}$	$\frac{20}{(2s+1)^2}$	Same as Phase I	$\frac{40}{(4s+1)^2}$ (both axes)
Controlled Element Dymanics				
$G_1(s)$	$\frac{12.5}{s(s+1)}$	Variable (see Section 3.4)	Same as Phase I	$\frac{10}{s(s+1)}$ (both axes)
$G_2(s)$	$\frac{12.5}{s^2}$			
$G_3(s)$	$\frac{12.5}{s+1}$			

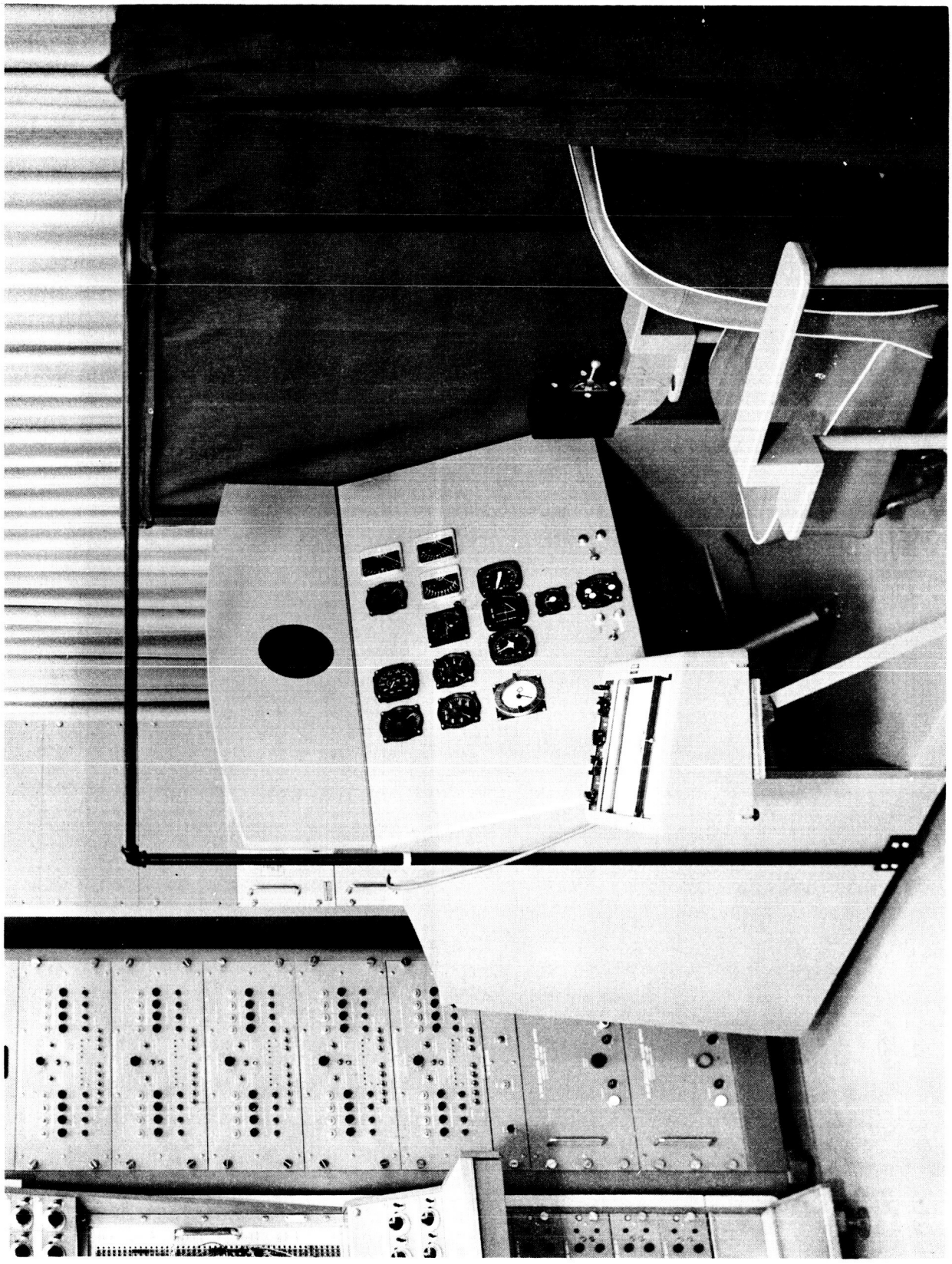

Figure 3-2. Experimental Facility

3.2.2 Display and Control Configuration

A 5" oscilloscope having a reticle calibrated in 1 centimeter units was used as display instrument. The tracking errors were indicated by proportional displacement of a dot from the center of the oscilloscope screen. A three-degree-of-freedom spring centered fingertip controller used had a lever arm of approximately 4-1/2 inches and a maximum angular deflection of $\pm$ 30 degrees in horizontal and vertical direction. Horizontal and vertical stick deflections, y_h and y_v and corresponding oscilloscope displays, x_h, x_v, were activated as required for single or two-axis control tasks. The controller exhibits negligible inertia and damping and was used as a position controller.

3.2.3 Input Disturbance

Low frequency Gaussian noise generators were used as sources of the input disturbance signal, r(t). The output noise had a power spectral density, N_o = 2.41 volts^2/cps at zero frequency, the power spectrum was flat up to approximately 100 rad/sec. This noise was fed through a low-pass filter to obtain desired input signal characteristics. Different filters were employed as required for each task of the study. The characteristics of the filters are given in Table 3-1.

3.2.4 Controlled Element Dynamics

Three simple controlled element configurations were simulated on an analog computer and utilized in the experiments. These configurations are described by

$$G_1(s) = \frac{K_1}{s\,(s+1)} \qquad (3.1)$$

$$G_2(s) = \frac{K_2}{s^2}$$

$$G_3(s) = \frac{K_3}{s\,(s+1)}$$

Values of the gains employed are listed in Table 3-1.

3.2.5 Recording of Data

In order to apply identical experimental data to several model matching strategies for purpose of comparison, it was necessary to record the input signals and the human operator responses in a variety of experimental situations, and to use the recorded information subsequently as input to the computer program. These signals were recorded on a Precision Instrument Company FM magnetic tape recorder, appropriately coded for each experiment. Voltage pulses which served to control the analog computer were recorded simultaneously on an adjacent track.

3.2.6 Operation Instructions and Training

In order to obtain approximately invariant tracking performance, the two subjects were given extensive training sessions for both the single-axis and the two-axis tracking tasks before any data were recorded. After proficiency and consistent performance in one axis tracking had been demonstrated, an additional period of one hour (12 five minute tracking runs) was devoted to training in the two-axis task. The importance of adequate training was pointed out and quantitatively demonstrated in a two-axis tracking study by Humphrey (15). The operators were instructed to achieve and maintain minimum display error, as measured by the distance between the dot and the center of the scope. They were also instructed to avoid excessively large and rapid control stick deflection as much as possible. Data taking was initiated only after the operators had acquired reasonable tracking proficiency.

3.3 Experimental Procedure - Task 1: Linear Invariant Models

The objective of this task of the experimental study was to examine different model matching techniques and select those most promising for subsequent tasks. Four methods were considered, the so-called "continuous," "sequential," "iterative," and "relaxation" processes discussed in Section 2.4. The continuous, iterative, and relaxation techniques showed sufficient promise and ease of implementation and were therefore implemented on analog computers as described in Section 4. The results of these tests are presented in Sections 5 and 6.

Each method was tested for convergence and stability by first matching the parameters of a known system, i. e. a differential equation identical to the model but having known parameters. After passing this test, human tracking data previously recorded was applied to each method. Parameter values were obtained and compared for consistency. During this phase of the study, only the basic stability and convergence of the methods were investigated.

Data characterizing the input disturbance function and controlled element dynamics are given in Table 3-1. Two human operators were used, each performing three runs with each of three different controlled element configurations (a total of 18 runs). While nine runs for each of two trained operators are not sufficient to establish the statistical characteristics of the experiment, they form an adequate sample for evaluating the feasibility of the parameter optimization methods.

Each individual tracking run lasted five minutes. From these runs sample intervals of 30 seconds were selected and re-recorded on tape loops to supply input signals for iterative parameter adjustment as described in Section 4.

The same experimental data were used with each of the different computational strategies in order to avoid ambiguities due to variability of human pilot performance.

3.4 Experimental Procedure - Task 2: Linear Model with Time-Varying Parameters.

The emphasis of Task 2 was directed to the improvement of the parameter tracking ability of the continuous method. Task 2 was divided into three parts: optimization of convergence time to parameters in known time-invariant systems, convergent to time varying parameters in known systems, and application of the technique to human tracking.

Task 2-1

In order to gain a better understanding of the adjustment process as well as to improve the system stability and response time, the effects of parameter adjustment gain K and the rate compensation term, $q\dot{e}$, were given primary consideration. These terms are described in detail in Section 4.

Task 2-2

This task was concerned with the identification of a time-varying parameter in the original system. A sinusoidal or square wave was used to perturb the system parameter in question. The parameter adjustment circuit of the model system tracked the parameter perturbations.

Task 2-3

In this task the model matching technique was applied to identification of human pilot model parameters while the pilot performed a time varying single-axis tracking task. The controlled element, or plant, was made time-variant by the following time sequence: For the first two minutes of a five minute run, the plant was described by the differential equation

$$\ddot{p} + \dot{p} = 20y$$

or by the transfer function

$$\frac{P}{Y} = \frac{20}{s\,(s + 1)}$$

During the third minute of the run the gain was increased at a constant rate for 10 seconds until it reached a value of 45. This value of gain was held for one minute and 50 seconds. During a subsequent 10 second interval, one coefficient in the plant differential equation was changed at uniform rate according to

$$\ddot{p} + (1 - 0.1t)\,\dot{p} = 45y$$

After ten seconds, the plant transfer function was thus given by

$$\frac{P}{Y} = \frac{45}{s^2}$$

and these characteristics were obtained for 50 seconds. After a total elapsed time of four minutes of tracking, the plant was again returned to its initial state and remained in this condition for the final 50 seconds of a five-minute tracking run. The same program was used in four runs by two operators. As in Task 2-2, the data was recorded on magnetic tape and subsequently analyzed by the continuous model matching method.

3.5 Experimental Procedure - Task 3: Non-Linear Models

The first part of the experiments was concerned with verification of the convergence of the nonlinear parameter adjustment technique described in Section 4 of this report. The technique of matching the system to a nonlinear model with known characteristics was employed.

Methods for implementing influence coefficients of analytic nonlinearities had been discussed in the literature previously (14). However, no such background was available for non-analytic nonlinearities and the required computer circuits were developed and tested.

The second part of the study was concerned with the effect of additive noise on the performance of model matching techniques. The same system as in Task 1 was used, but the output of the simulated pilot was defined as

$$y' = y + cn(t)$$

where n(t) is the output of a Gaussian noise generator and c is a constant. This noise simulates random fluctuations of the operator.

The third part of the study was restricted to application of the results of the first phase to human tracking data previously obtained. The general approach, the display and control configuration and the controlled element dynamics are described in Section 3.2 and Table 3-1. Since a unique solution could not be obtained for all seven variable parameters of the nonlinear method, the linear parameters were first adjusted and then held constant while improvement in the error criterion was attempted by varying the parameters associated with the nonlinear terms.

3.6 Experimental Procedure - Task 4: Two Axis Tracking Tasks

A block diagram of the two-axis control system is illustrated in Figure 3-3.

Two uncorrelated random excitation signals r_v and r_h activating the vertical and horizontal channels, respectively, were generated by two separate noise generators, each having a zero frequency spectral density N_o = 2.41 volts^2/cps and a flat power spectrum from zero to approximately 100 rad/sec. The input signals, the controlled system

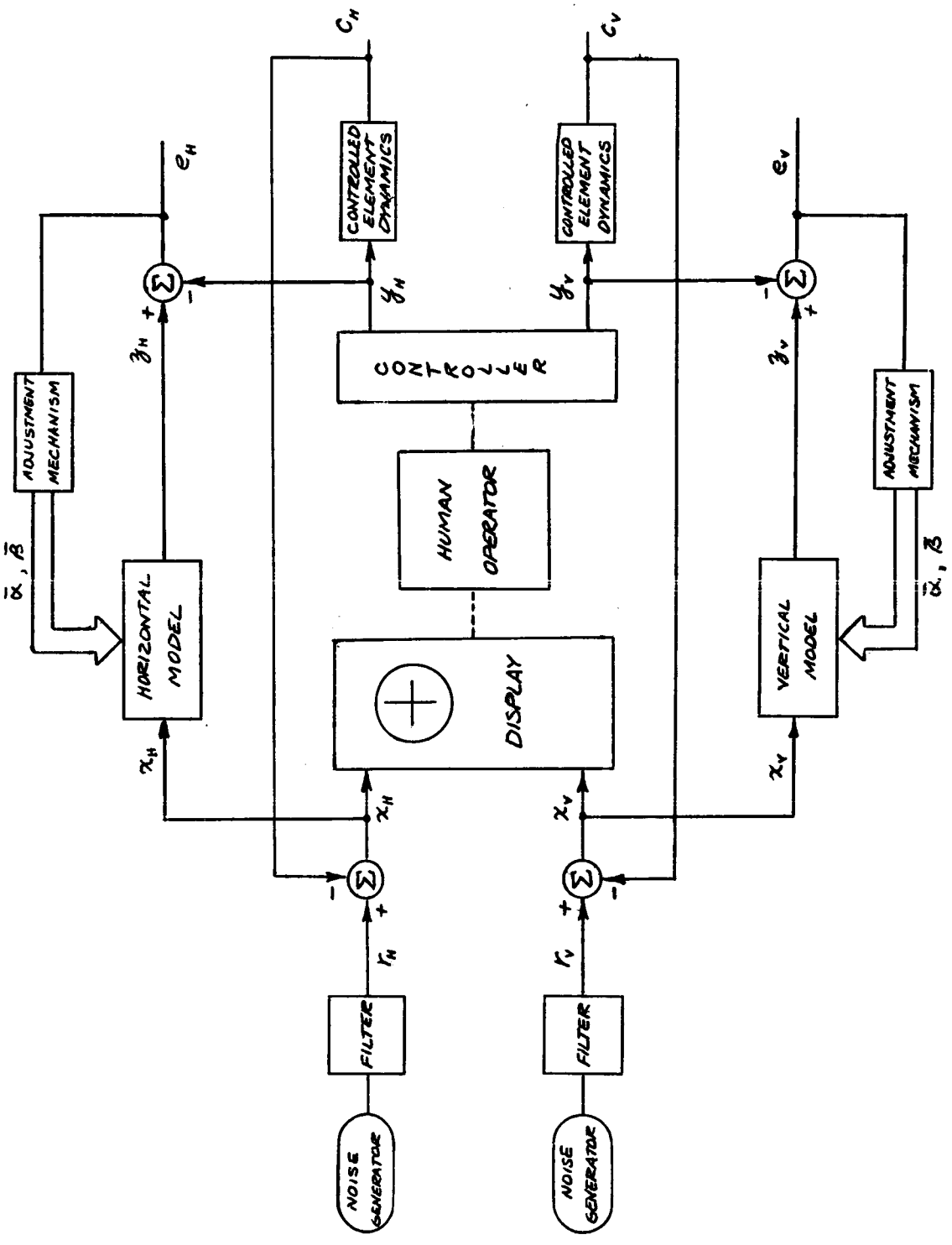

Figure 3-3. Block Diagram of Two-axis Control System

dynamics and filters employed are given in Table 3-1. The two axes of the control task did not include cross coupling. The displayed quantities x_v (vertical deflection on the scope) and x_h (horizontal deflection) as well as the operator's output signals y_v (control stick vertical position, normalized in terms of full stick deflection) and y_h (control stick horizontal position) were recorded on magnetic tape for repeated use. Sufficient tracking runs were performed to study the feasibility of the model matching techniques, but extensive coverage of operator characteristics was not attempted.

Two human operators performed three tracking tasks each with three replications: 1) single axis tracking in horizontal direction, 2) single axis tracking in vertical direction, 3) two-axis tracking. All runs were of 5 minutes duration. The mean squared values of excitation signals, $\overline{r_h^2}$ and $\overline{r_v^2}$, displayed errors $\overline{x_h^2}$ and $\overline{x_v^2}$, and operator output, $\overline{y_h^2}$ amd $\overline{y_v^2}$ were recorded for each run.

A mathematical model was fitted to the human operator data by means of the continuous method described in Section 4. Data obtained from two-axis tracking was analyzed separately and model matching was performed individually for each of the two channels. Repeated model matching runs of the same recorded data were required in some instances to minimize interactions between parameter adjustment which occurred when starting from arbitrarily chosen initial parameter settings. This procedure was found necessary to provide dependable parameter values for subsequent evaluation of the dependence of adjustment gains, damping terms, and cross-coupling terms on the model matching performance.

In order to be able to evaluate the adequacy of the model, the mean square residual matching error,

$$\overline{e^2} = \frac{1}{T}\int_0^T e^2\, dt$$

was used as a "matching accuracy criterion."

During the search for cross coupling β in the model (see Equation 2.24) the coefficients α were held fixed to avoid interaction between the adjustment loops. The model parameters of the uncoupled system were held near their optimum values during attempts of finding a further improvement of the matching criterion by the introduction and adjustment of various cross-coupling terms.

Off-line model matching procedures involving the repeated use of taped operator tracking data were necessary(1) in order to minimize computational complexity and(2) to provide greater assurance of deriving valid results. This point will be further discussed in Section 5 in terms of the model matching results presented there.

4. COMPUTER IMPLEMENTATION

4.1 Computer Programming for Continuous Parameter Adjustment

The continuous method of parameter adjustment described in Section 2.4 is related to similar techniques used by Margolis (8), Whitaker (1), and Adams (2). It uses the parameter influence programming technique developed by Meissinger (14). Figure 2-1 shows the computer implementation of parameter adjustment schematically. Continuous adjustment of the parameter values from arbitrarily chosen initial values is effected by feedback signals generated by the computer on the basis of the measured error criterion.

The criterion function selected here is

$$f = \frac{1}{2} \ (e + q \dot{e})^2 \tag{4.1}$$

where q is a constant and $q \dot{e}$ constitutes a rate compensation term. Steepest descent requires parameter adjustment at a rate proportional to the local slope of the error criterion function.

$$\dot{\alpha} = -K \overline{\nabla f} \quad , \tag{4.2}$$

where K is a positive gain constant. The gradient components $\frac{\partial f}{\partial \alpha_i}$ are expressed in terms of the parameter influence coefficients $\frac{\partial z}{\partial \alpha_i} = u_i$ of the model output variable z. Using Equation (4.1) one obtains

$$\frac{\partial f}{\partial \alpha_i} = (e + q\dot{e}) \ (\frac{\partial e}{\partial \alpha_i} + q \ \frac{\partial \dot{e}}{\partial \alpha_i}) = (e + q\dot{e}) \ (\frac{\partial z}{\partial \alpha_i} + q \ \frac{\partial \dot{z}}{\partial \alpha_i}) \tag{4.3}$$

Since the order of differentiation with respect to t and α_i can be interchanged, if z is a continuous and differentiable function of both variables,

$$\frac{\partial}{\partial \alpha_i} (\frac{\partial z}{\partial t}) = \frac{\partial}{\partial t} \ (\frac{\partial z}{\partial \alpha_i}) = \dot{u}_i \tag{4.4}$$

Thus Equations (4.2) and (4.3) can be combined to yield

$$\dot{\alpha}_i = -K \ (e + q\dot{e}) \ (u_i + q \ \dot{u}_i) \tag{4.5}$$

To determine parameter influence coefficients on a continuous basis a set of additional differential equations must be programmed on the computer as follows. By partial differentiation of the model equation (2.17) with respect to α_1 the new equation

$$\frac{\partial}{\partial \alpha_1} (\ddot{z}) + \alpha_1 \frac{\partial}{\partial \alpha_1} (\dot{z}) + \alpha_2 \frac{\partial}{\partial \alpha_1} (z) = -\dot{z} \tag{4.6}$$

is obtained which reduces, by virtue of (4.4), to

$$\ddot{u}_1 + \alpha_1 \dot{u}_1 + \alpha_2 u_1 = -\dot{z} \tag{4.7}$$

where u_1 must satisfy the initial conditions

$$u_1(0) = 0 , \quad \dot{u}_1(0) = 0$$

since the initial values $z(0)$ and $\dot{z}(0)$ are independent of α_1. Equation (4.7) known as sensitivity equation must be solved simultaneously with Equation (2.17) to yield the parameter influence coefficient u_1 and hence the gradient component $\frac{\partial f}{\partial \alpha_1}$.

The forcing terms x and $\dot{x}$ being independent of α_1 do not appear in (4.7). The other components $\frac{\partial f}{\partial \alpha_i}$ are obtained similarly by programming and solving additional sensitivity equations with respect to α_2, α_3, α_4. These equations are given below.

$$\ddot{u}_2 + \alpha_1 \dot{u}_2 + \alpha_2 u_2 = -z \tag{4.8}$$

$$\ddot{u}_3 + \alpha_1 \dot{u}_3 + \alpha_2 u_3 = \dot{x} \tag{4.9}$$

$$\ddot{u}_4 + \alpha_1 \dot{u}_4 + \alpha_2 u_4 = x \tag{4.10}$$

All initial values must satisfy the conditions $u_i(0) = 0$, $\dot{u}_i(0) = 0$. From these equations the following relationships between u_1 and u_2, u_3 and u_4 can be derived as discussed in Section 5.6.

$$\dot{u}_2 = u_1 \tag{4.11}$$

$$\dot{u}_4 = u_3$$

The computer circuits for generating the influence coefficients u_1, u_2, u_3 and u_4 are shown in Figure 4-1. The relations (4.11) simplify the computer implementation. The simulation of the model equation is shown as circuit 1. Circuit 4 representing Equation (4.2) generates the parameter values α_1, α_2, α_3 and α_4.

A mathematical problem inherent in this approach to gradient computation is that the α_i terms were assumed to be time-invariant. Actually, under conditions of continuous adjustment of the coefficients α_i the gradient components can be determined only approximately, where the approximation error depends on the rate of adjustment.

4.2 Determination of Parameter Influence Coefficients of a Nonlinear Model

Linearity and time-invariance of the model differential equation is not a pre-requisite for performing the gradient computation discussed above. However, in the case of time-variant or nonlinear differential equations the structure of the sensitivity equations no longer resembles that of the original differential equation as closely and the computer programming becomes somewhat more complex.

The mathematical model of the pilot used in Task 3 includes three nonlinear terms, a cubic of the input variable, a dead space characteristic acting on the input variable, and a limiter acting on the output variable as discussed in Section 2.6, (see Equation 2.19). Ignoring for the moment the two "non-analytic" second and third nonlinear terms, the parameter influence of the cubic term will first be derived. The system equation then becomes

$$\ddot{y} + a_1\dot{y} + a_2 y = a_3\dot{x} + a_4 x + a_5 x^3 \qquad (4.12)$$

and the model equation with adjustable parameters α_1, α_2, ..., α_5 is given by

$$\ddot{z} + \alpha_1 \dot{z} + \alpha_2 z = \alpha_3\dot{x} + \alpha_4 x + \alpha_5 x^3 \qquad (4.13)$$

To derive the sensitivity equation in α_5, Equation (4.13) is differentiated term by term with respect to α_5. Substituting $u_5 = \frac{\partial z}{\partial \alpha_5}$ one obtains

$$\ddot{u}_5 + \alpha_1\dot{u}_5 + \alpha_2 u_5 = x^3 \qquad (4.14)$$

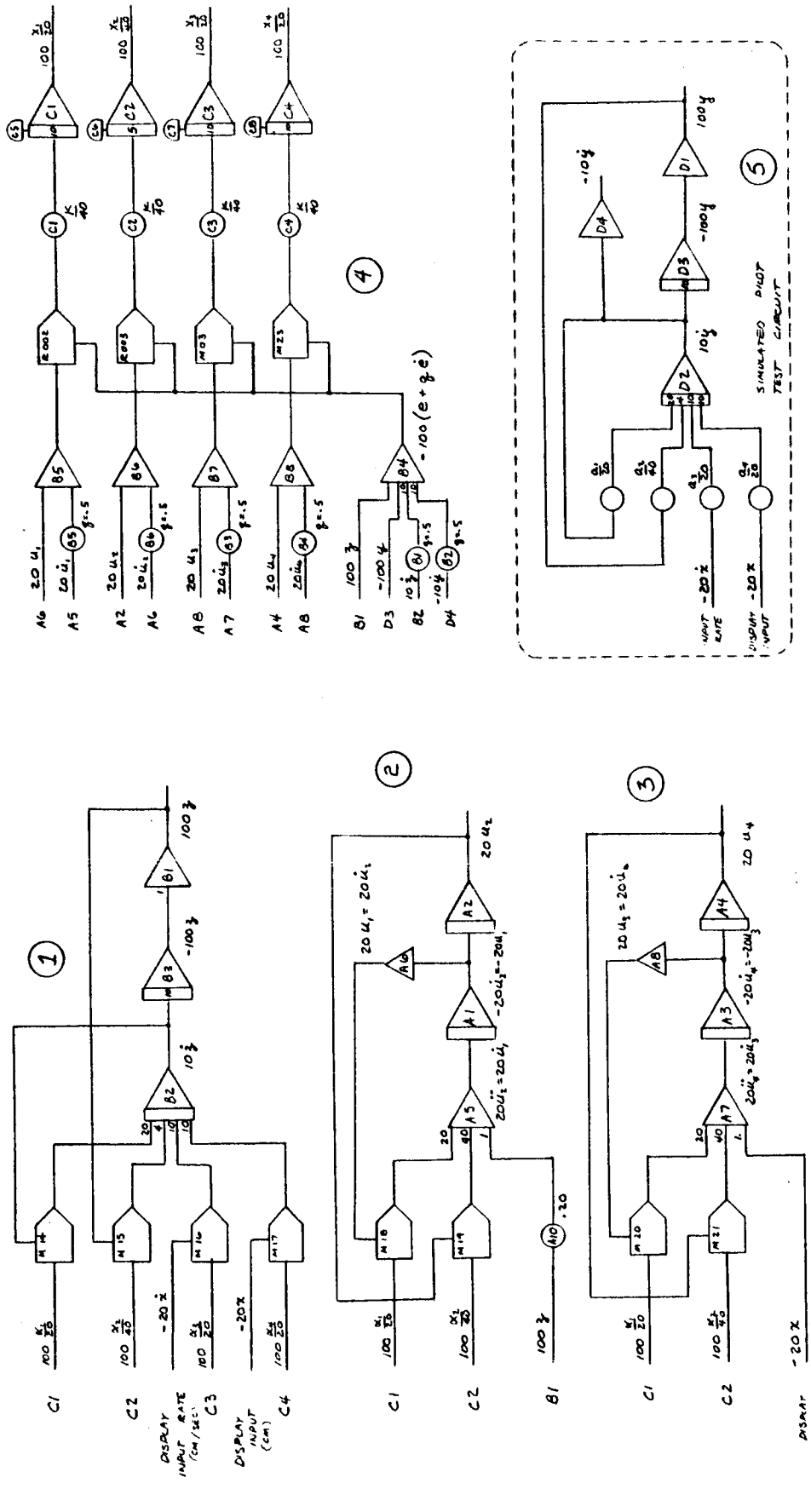

Figure 4-1. Continuous Method Model Matching

This procedure is essentially unchanged from the derivation of the sensitivity equations for α_3 and α_4. The computer implementation of Equation (4.14) and the parameter adjustment circuit for α_5 are illustrated in Figure 4-2a.

The dead space characteristic $x_d = f_2(x; \alpha_6)$ represented by Equation (2.18) will next be considered and the influence of α_6 on z will be derived where α_6 represents half of the adjustable deadspace in x_d. The parameter influence is defined by $u_6 = \frac{\partial z}{\partial \alpha_6}$. Differentiation of Equation (2.19) with respect to α_6 (where the cubic term has been deleted for simplification) yields the sensitivity equation

$$\ddot{u}_6 + \alpha_1 \dot{u}_6 + \alpha_2 u_6 = \alpha_3 \frac{\partial \dot{x}_d}{\partial \alpha_6} + \alpha_4 \frac{\partial x_d}{\partial \alpha_6} + 3\alpha_5 x_d^2 \frac{\partial x_d}{\partial \alpha_6} \qquad (4.15)$$

The term $\frac{\partial x_d}{\partial \alpha_6} = g_d(x)$ poses no problem conceptually, but exhibits jump discontinuities at $x = \pm \alpha_6$.

$$g_d(x) = \frac{\partial x_d}{\partial \alpha_6} \begin{cases} -1 & x > \alpha_6 \\ 0 & \text{if } |x| \leq \alpha_6 \\ +1 & x < -\alpha_6 \end{cases} \qquad (4.16)$$

The term $\frac{\partial x_d}{\partial \alpha_6}$ can be derived by interchanging the order of differentiation with respect to t and α_6, provided the derivatives exist everywhere in the range of interest. This is not the case at the jump discontinuities of $g_d(x)$. To eliminate this difficulty a continuous slope change over a small interval Δx_T of the input variable x at $x = \pm \alpha_6$ is introduced to assure differentiability. The deadzone characteristics with rounded corners shown in Figure 4-3 is a good approximation of the ideal characteristic. It is actually a more realistic representation of many threshold phenomena observed in practice, e.g., the pilot's threshold response. Figure 4-3 also shows the derivative $g_d(x)$ and the term $\frac{\partial \dot{x}_d}{\partial \alpha_6}$ required in Equation (4.15). Interchange

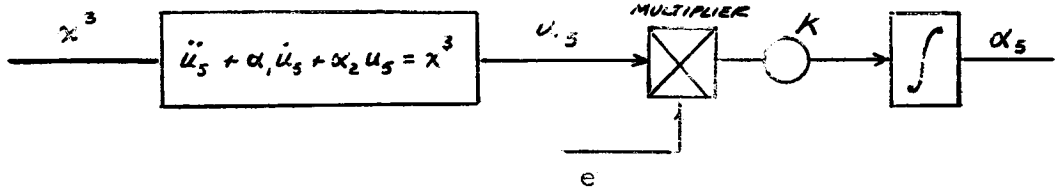

Figure 4-2a

Circuit for Adjustment of Parameter α_5

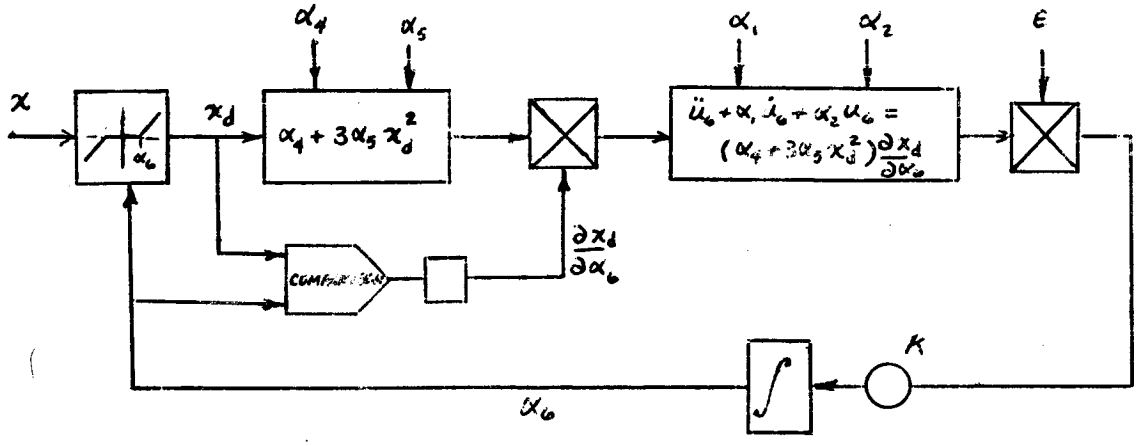

Figure 4-2b

Circuit for Adjustment of Parameter α_6

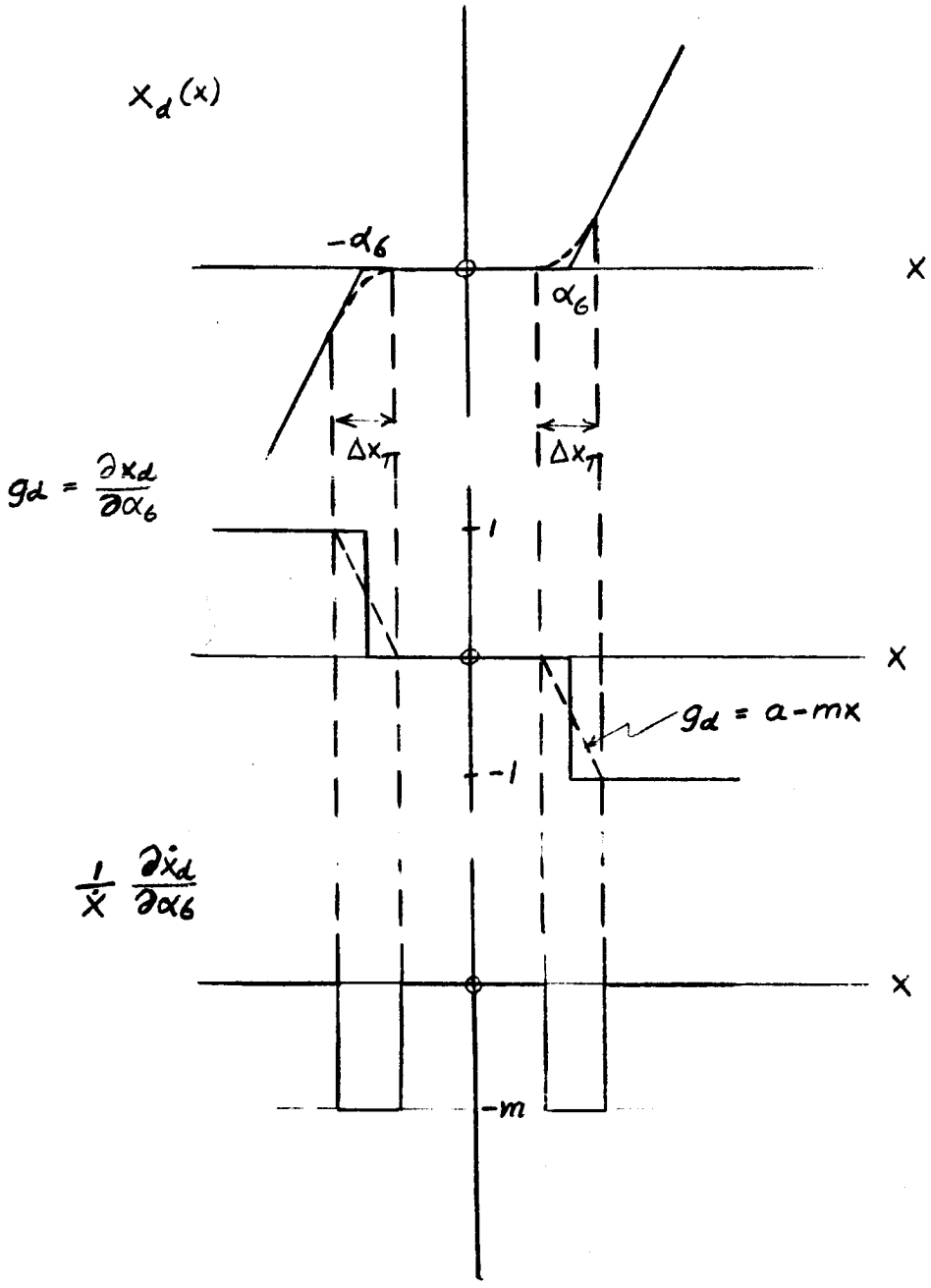

Figure 4-3. Deadspace Characteristics and Derivatives

of the order of differentiation yields

$$\frac{\partial \dot{x}_d}{\partial \alpha_6} = \frac{d}{dt}\left(\frac{\partial x_d}{\partial \alpha_6}\right) = \begin{cases} -m\dot{x} \text{ during transition interval} \\ 0 \quad \text{elsewhere} \end{cases} \tag{4.17}$$

The transition slope is given by

$$m = 1/\Delta x_T \tag{4.18}$$

As $\Delta x_T \rightarrow 0$ this representation of $g_d(x)$ at $x = \alpha_6$ approaches the jump discontinuity. During each transition interval the term $\frac{\partial \dot{x}_d}{\partial \alpha_6}$ introduces an impulse proportional to $\dot{x}$ with a large peak amplitude if Δx_T is short. The effect of such impulses on the output u_6 of a damped second order system, Equation (4.15), is negligible compared to the other input terms. Hence the sensitivity equation (4.15) is in effect approximated by

$$\ddot{u}_6 + \alpha_1 \dot{u}_6 + \alpha_2 u_6 = (\alpha_4 + 3\alpha_5 x_d^2)\, g_d(x) \tag{4.19}$$

and is implemented on the computer in this form. The partial derivative $g_d(x)$ is represented simply by an on-off term controlled by a relay plus dead space α_6. The computer circuit for the adjustable deadspace characteristic is shown in Figure 4-2b.

Similar considerations apply in the derivation of the parameter influence $\frac{\partial z}{\partial \alpha_7} = u_7$ where α_7 is the saturation level of the limiter characteristic used in the nonlinear model.

$$z_L = \begin{cases} \alpha_7 & z > \alpha_7 \\ z \quad \text{if} & |z| \leq \alpha_7 \\ -\alpha_7 & z < -\alpha_7 \end{cases} \tag{4.20}$$

$$\dot{z}_L = \begin{cases} 0 & |z| > \alpha_7 \\ \dot{z} \quad \text{if} & |z| \leq \alpha_7 \end{cases} \tag{4.21}$$

Adjustment by the method of steepest descent requires the formation of u_7 and $\dot{u}_7$. Equations (4.20) and (4.21) yield

$$u_7 = \frac{\partial z_L}{\partial \alpha_7} = \begin{cases} 1 & z > \alpha_7 \\ 0 & \text{if} \quad z \leq \alpha_7 \\ -1 & z < -\alpha_7 \end{cases} \tag{4.22}$$

$$\dot{u}_7 = \frac{\partial \dot{z}_L}{\partial \alpha_7} = 0 \quad \text{except at points } z = \pm \alpha_7 \tag{4.23}$$

As in the case of dead space the derivation of the term $\dot{u}_7$ presupposes differentiability of z_L (a, α_7). The problem is circumvented by defining a transition interval Δz_T in the variable z at $z = \pm \alpha_7$. At each passage of the transition zone a $\dot{z}$ - impulse occurs in $\dot{u}_7$ which can be neglected for practical purposes. A sensitivity equation for u_7 and $\dot{u}_7$ is unnecessary. The generation of u_7 reduces to a simple switching arrangement (See Figure 4-4).

4.3 Extension of the Continuous Method to a Two-axis Model

The coefficients α_i, β_i, γ_i ... of the two-axis model postulated in Section 2.7 can be determined by means of the continuous model matching technique developed for single axis tasks. For the purpose of this study a sequential parameter optimization of two individual "operator channels" provided a reasonable simplification, reducing the number of parallel parameter adjustment circuits from 8 to 4 in the absence of coupling terms in the model.*

To further reduce the number of sensitivity equations required for this task the approximations given by Equation (4.11)were used. This permits the generation of the parameter influences u_1 and u_2 by one computer circuit, and u_3 and u_4 by a second circuit. The second parameter influence circuit can be eliminated entirely since u_3 and u_4 are obtainable from the circuit which generates the output

*Separation into 2 single-axis operations is justifiable since two distinct error criteria

$$f_v = \tfrac{1}{2} (e_v + q\dot{e}_v)^2 \text{ and } f_h = \tfrac{1}{2} (e_h + q\dot{e}_h)^2$$

have to be minimized individually.

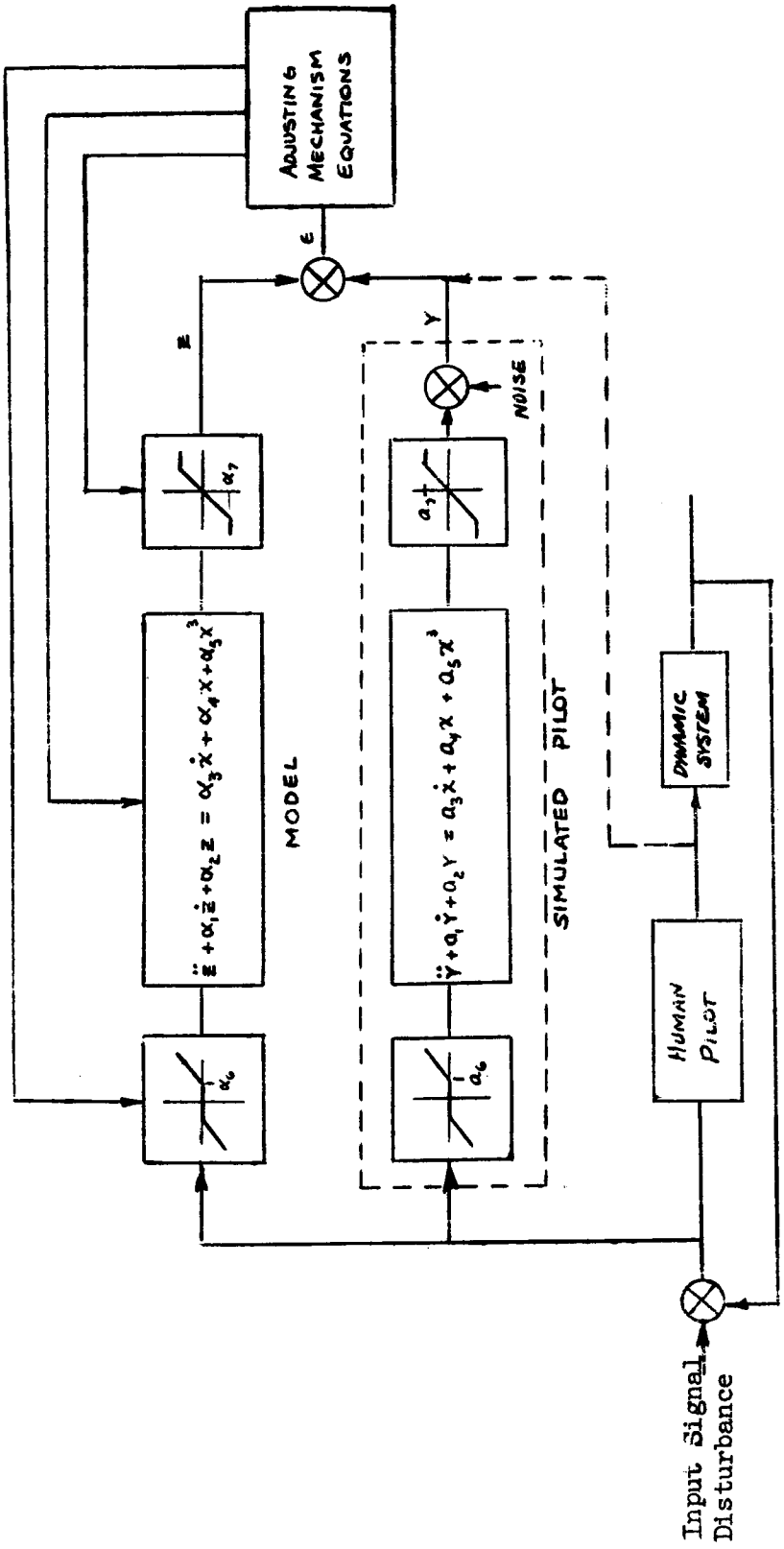

Figure 4-4

Block Diagram of Continuous Nonlinear Parameter Optimization

variable z_1. This requires a modified computer circuit for z similar to that used by Adams (2). According to Equation (2.17) z results from linear super-position of the two terms $\alpha_3 x$ and $\alpha_4 \dot{x}$. On the other hand u_3 and u_4 satisfy the equations

$$\begin{aligned} \ddot{u}_3 + \alpha_1 \dot{u}_3 + \alpha_2 u_3 &= x \\ \ddot{u}_4 + \alpha_1 \dot{u}_4 + \alpha_2 u_4 &= \dot{x} \end{aligned} \tag{4.24}$$

Therefore,

$$z = \alpha_3 u_3 + \alpha_4 \dot{u}_4 \tag{4.25}$$

Equation (4.25) omits the minor effect of initial values in z and $\dot{z}$. The corresponding computer circuit is shown in the Figure 4-5 below.

The computer program for finding the parameter influences of cross-coupling terms β_1, β_2, ... is derived by extension of the above techniques. Using the notation

$$\frac{\partial z}{\partial \beta_3} = u_{\beta 3} \tag{4.26}$$

it follows from Equation (2.24) that $u_{\beta 3}$ must satisfy the sensitivity equation

$$\ddot{u}_{\beta 3} + \alpha_1 \dot{u}_{\beta 3} + \alpha_2 u_{\beta 3} = x_h \tag{4.27}$$

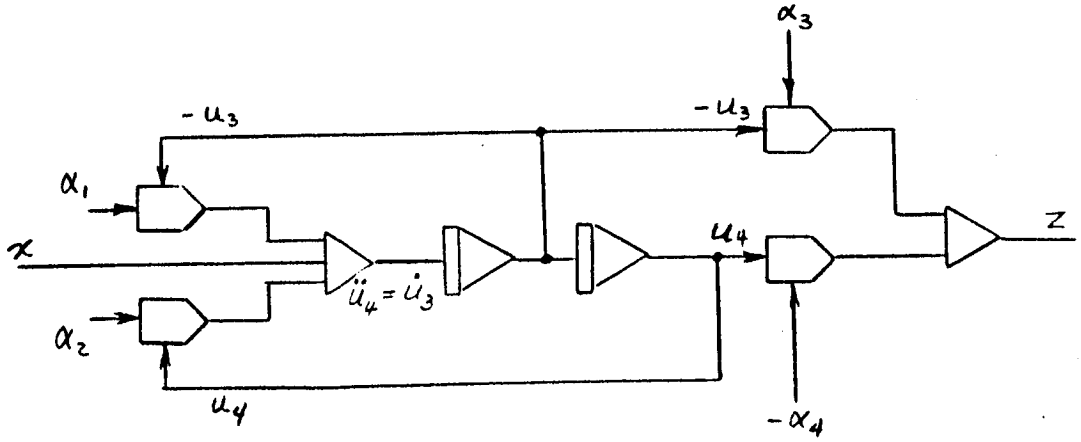

Figure 4-5. Simplified Computer Circuit for z, u_3 and u_4

Similar equations yield the parameter influence coefficients $u_{\beta 1}$, $u_{\beta 2}$, etc. These coefficients can be obtained from the same parameter influence circuit as u_1, u_2, by switching the forcing function in turn from z_v to x_h, $\dot{x}_h$, z_h, ... etc. The sensitivity equation for $u_{\gamma 2}$ requires the product $x_v x_h$, as forcing function while for $u_{\gamma 1}$ a more complicated term $(z_v z_h + \gamma_1 z_h u_{\gamma 1})$ is required.*

4.4 Computer Program for Iterative Parameter Adjustment

The iterative model matching technique was introduced to circumvent the mathematical difficulty associated with gradient computation in the continuous adjustment technique and to minimize stability problems in the adjustment loops. All parameters are held constant during time intervals of gradient computation, and adjustments are made step-by-step during successive reset periods. In addition, the previous computer program for finding partial derivatives $\frac{\partial z}{\partial \alpha_i}$ was replaced by a program of finite difference approximations. The block diagram (Figure 4-6) shows two models operating at slightly different settings of one parameter. The first model yields the output signal z. The second model solves the same equation subject to a variation $\Delta\alpha_i$ of of the parameter α_i yielding the output signal ζ_i. The partial derivative is thus approximated by

$$\frac{\partial z}{\partial \alpha_i} \cong \frac{\Delta z_i}{\Delta \alpha_i} = \frac{z(\alpha_i) - z(\alpha_i + \Delta\alpha_i)}{\Delta \alpha_i} = \frac{z - \zeta_i}{\Delta \alpha_i} \qquad (4.28)$$

This computer program requires separate circuits for each $\Delta\alpha_i$ to generate the finite differences $\Delta z_i = z - \zeta_i$. A considerable amount of computer equipment can be saved by sequential operation which requires implementation of the original unperturbed model equation plus one model equation subject to parameter variations $\Delta\alpha_i$, one at a time.

The iterative method is programmed on the computer as follows. During each iteration the differential equation of the model given by (2.17) is solved with fixed parameters $\alpha_i^{(k)}$, viz.,

$$\ddot{z} + \alpha_1^{(k)} \dot{z} + \alpha_2^{(k)} z = \alpha_3^{(k)} \dot{x} + \alpha_4^{(k)} x \qquad (4.29)$$

---

* The second-order effects of coupling parameters in one channel upon the sensitivities of coupling parameters in the second channel were ignored.

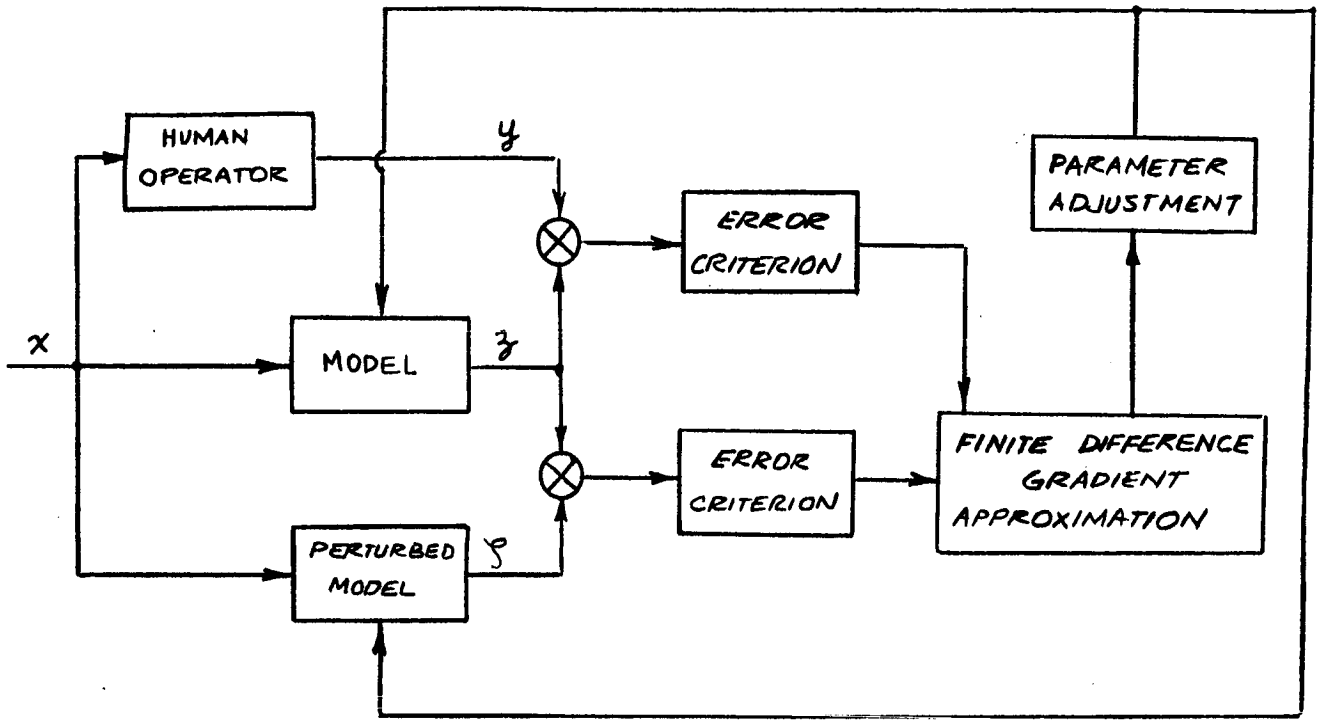

Figure 4-6. Block Diagram of the Iterative Parameter Adjustment Strategy

where the superscript (k) refers to the parameter values reached after the kth iteration. The perturbed model equation is

$$\ddot{\zeta} + \left\{+\alpha_1^{(k)} + \Delta\alpha_1\ \delta_{1,j}\right\}\dot{\zeta} + \left\{\alpha_2^{(k)} + \Delta\alpha_2\ \delta_{2,j}\right\}\zeta = \left\{\alpha_3^{(k)} + \Delta\alpha_3\ \delta_{3,j}\right\}\dot{x} + \left\{\alpha_4^{(k)} + \Delta\alpha_4\ \delta_{4,j}\right\}\ x \qquad (4.30)$$

The symbol $\delta_{i,j} = \begin{cases} 1 & , i = j \\ 0 & , i \neq j \end{cases}$ where i indicates parameter α_i; j indicates the step within the kth iteration

denotes the selection of one out of four variations $\Delta\alpha_i$ in solving (4.30). The computer program is shown in Figures 4-7, 4-8, and 4-9. Circuits (1) and (2) are used to generate input quantities from the tape recorder, the disturbance function, the human operator output, and their derivatives. Circuits (3) and (4) are the model and the perturbed model respectively (see Figure 4-7).

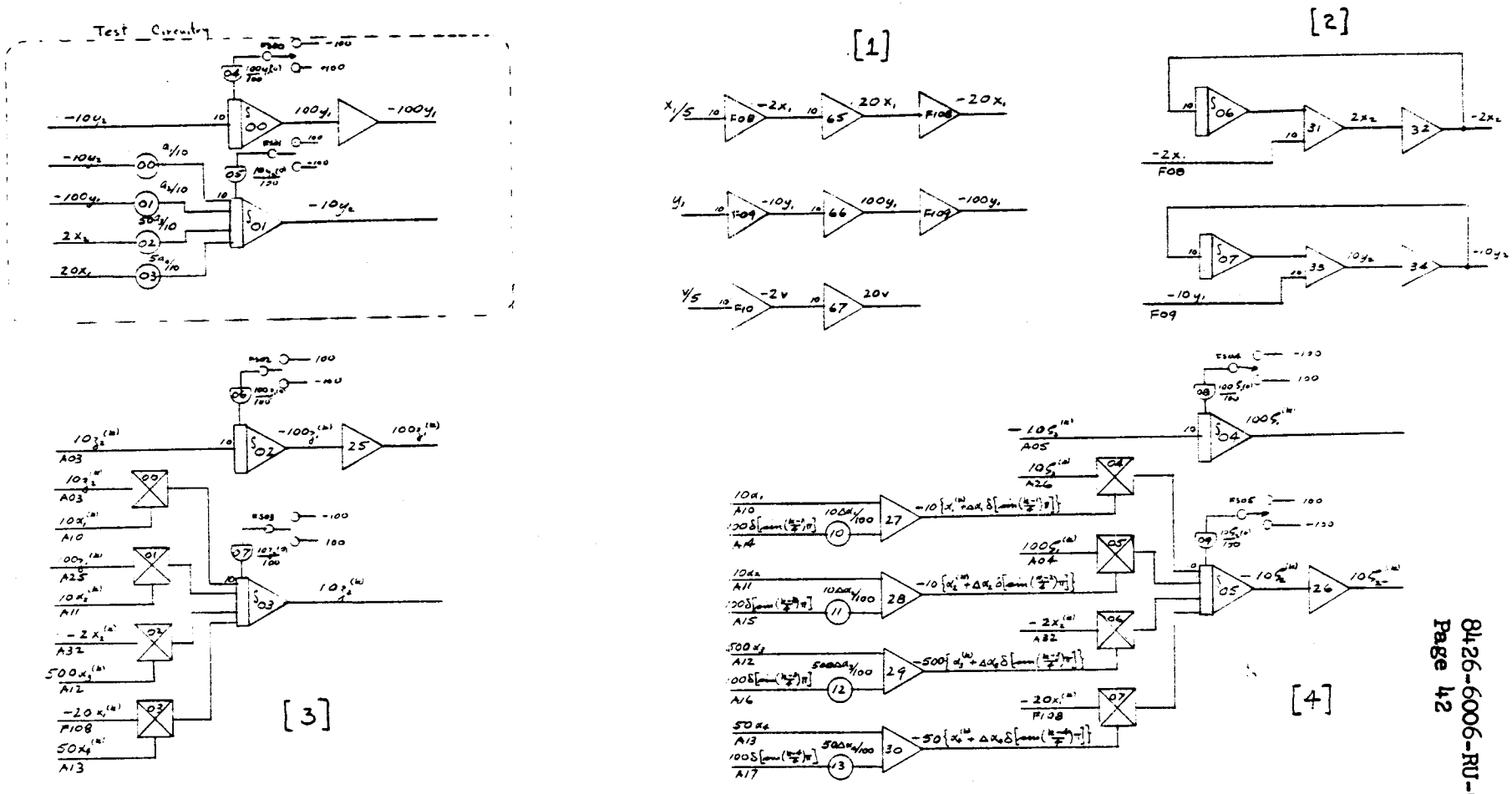

Figure 4-7. Computer Circuits for Iterative Method

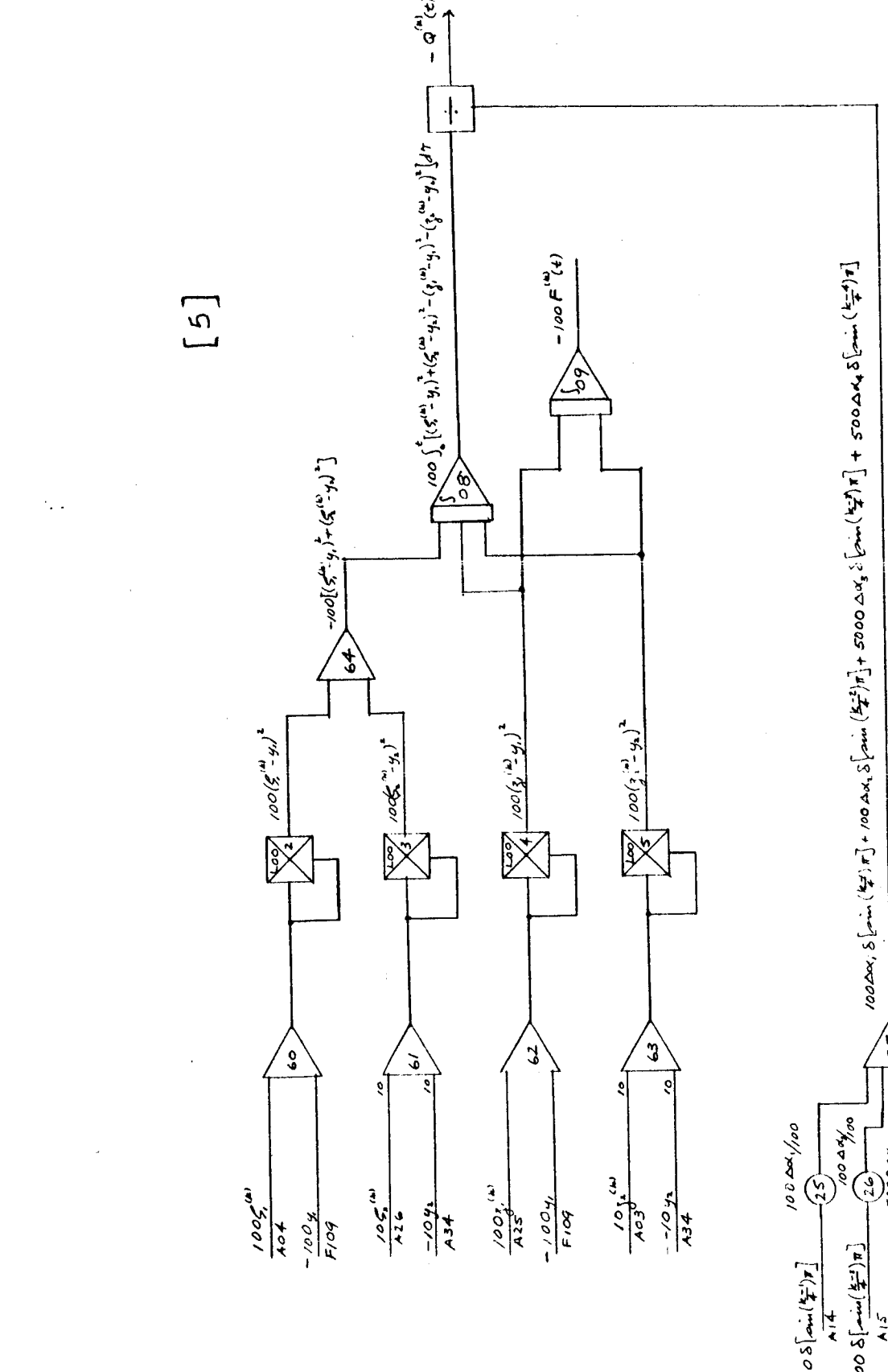

Figure 4-8. Computer Circuits for Iterative Method

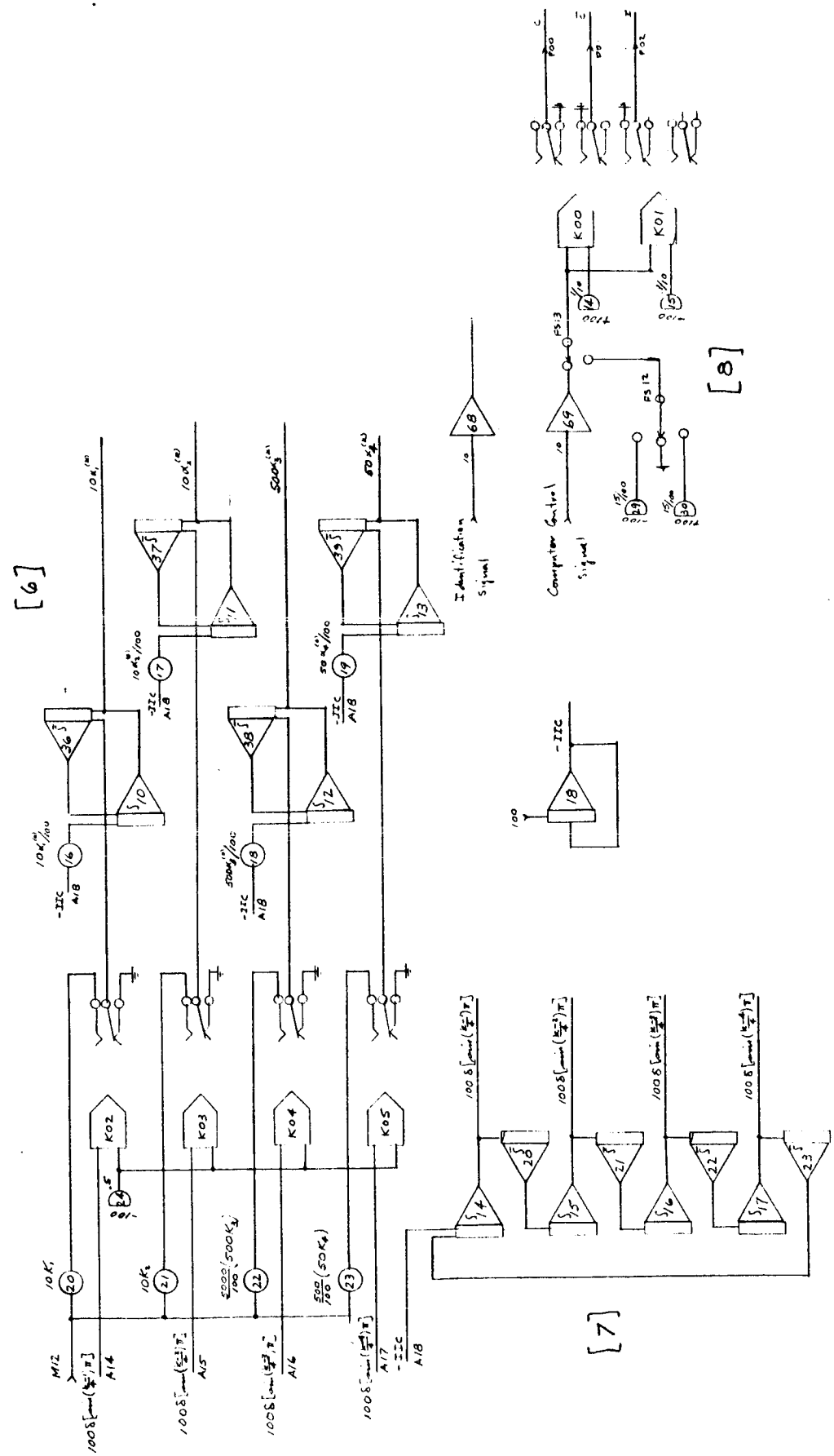

Figure 4-9. Computer Circuits for Iterative Method

The error criterion selected for this program has the form

$$F = \int_0^T (e_2 + \dot{e}^2)\, dt \tag{4.31}$$

In terms of human operator output and model output this may be expressed by

$$F(\alpha_i) = \int_0^T \left[(z - y)^2 + (\dot{z} - \dot{y})^2\right] dt \tag{4.32}$$

On the other hand, the error criterion involving the perturbed model output is

$$F(\alpha_i + \Delta\alpha_i) = \int_0^T \left[(\zeta_i - y)^2 + (\dot{\zeta}_i - \dot{y})^2\right] dt \tag{4.33}$$

Thus the finite difference quotient $\frac{\Delta F}{\Delta \alpha_i}$ is

$$Q^{(k)}(T) = \frac{\int_0^T \left[(\zeta_i - y)^2 + (\dot{\zeta}_i - \dot{y})^2\right] dt - \int_0^T \left[(z-y)^2 + (\dot{z}-\dot{y})^2\right] dt}{\Delta\alpha_i} \tag{4.34}$$

This quantity is computed by circuit (5) (see Figure 4-7). Circuit (6) is a memory circuit which stores successive values of $\alpha_i^{(k)}$, viz.

$$\alpha_i^{(k+1)} = \alpha_i^{(k)} + \Delta\alpha_i^{(k)} = \alpha_i^{(k)} + K\, Q^{(k)}(T) \tag{4.35}$$

A constant step size $\Delta\alpha_i^{(k)}$ was used in all successive computer runs. This step size is equivalent to the adjustment gain K used in the continuous model matching technique. Circuit (7) generates the switching logic for the $\Delta\alpha_i^{(k)}$. The four outputs of the circuit are energized cyclically to adjust the parameters step by step. Circuit (8) controls the computer in accordance with a previously recorded mode control signal (see Figure 4-9).

4.5 Relaxation Technique

The relaxation technique employed in this study was simplified greatly by eliminating the automatic parameter adjustment loop. It only requires the implementation of one model equation and an error criterion function which is minimized by manually adjusting potentiometers. The method employed is described in Section 2.4. The computer diagram is shown in Figure 4-10. Circuits (2), (3), (5) and (6) are input gain circuits and derivatives, respectively. Circuit (7) controls the modes of the computer.

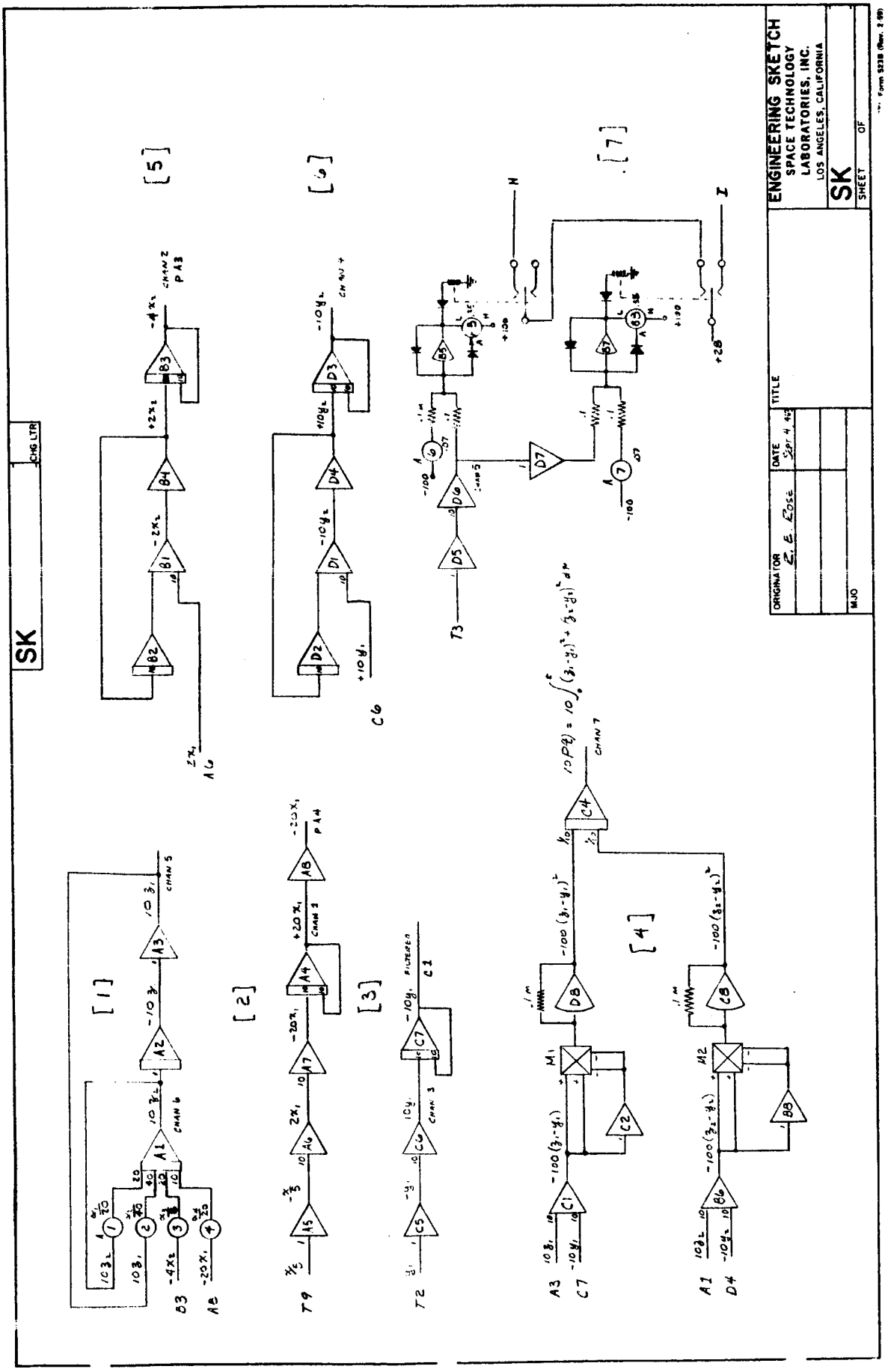

Figure 4-10. Computer Circuits for Relaxation Method

5. ANALYTICAL RESULTS

One of the objectives of this research program has been the clarification of some of the theoretical problems connected with model matching techniques. Among these problems, the following examples can be cited:

1) Ornstein (5,16) has noted that the model parameters do not necessarily converge to correct values, even when a model is matched to a known system, and that iteration may be required to improve the reliability of the computer results.

2) Cross-coupling or interaction among parameter adjustments has been observed by Margolis (8) and by Adams (2), and substantiated by early STL results.

3) The dependence of the parameter adjustments on the choice of criterion function has also been known for some time. Margolis (8) used criterion functions of the form

$$f_1 = e^2 + q\dot{e}^2 + r\ddot{e}^2 \tag{5.1}$$

and

$$f_2 = (e + q\dot{e} + r\ddot{e})^2 \tag{5.2}$$

(where e is the output error or model-matching error and q and r are constants) and he observed significant differences in parameter adjustments when f_2 was used instead of f_1 and when q and r were given non-zero values. Ornstein (5) used an absolute value error criterion of the form:

$$f_3 = |e|$$

with considerable success. However, this criterion function was not suitable for models with certain nonlinearities, and Humphrey and Bekey (10) were forced to abandon it and return to a quadratic form.

4) Iterative techniques of parameter optimization generally use integrated error criteria, such as

$$F_1 = \int_0^T e^2 \, dt \tag{5.3}$$

where T is a time interval during which the parameters remain constant. It has been shown (13) that criteria such as F_1 make possible a discrete steepest descent process. However, the use of instantaneous error criteria such as f_1, f_2 or f_3 with the output error method raise fundamental problems regarding the definition of the local gradient.

The four problems cited above have been considered under the theoretical portion of the present study. Considerable effort was devoted to studying the nature of the criterion surface, the interaction among parameters during the adjustment process, and the effects of the choice of criterion function on the convergence and stability of the model matching process. The major results of these investigations are summarized in the following paragraphs.

5.1 The Nature of the Criterion Surface for Iterative Parameter Optimization

Consider an iterative parameter optimization process with

$$F = \int_0^T (e^2 + \dot{e}^2) \, dt \tag{5.4}$$

where the parameters α_1, α_2, α_3 and α_4 of Equation (2.17) are held constant for intervals of T seconds. Under these conditions F is an ordinary function of the parameters, i.e.,

$$F = F(\alpha_1, \alpha_2, \alpha_3, \alpha_4) \tag{5.4a}$$

and profiles of F as a function of any parameter α_i can be plotted by holding the other three parameters constant, and evaluating F for a sufficiently large number of values of α_i to obtain a curve.

An inspection of the characteristics of the criterion function in the neighborhood of its minimum helps to explain the behavior of the adjustment process at the approach to steady state. Figures 5-1 to 5-4 show profiles of $F(\alpha_1, \alpha_2, \alpha_3, \alpha_4)$ plotted versus one parameter at a time exhibiting the minimum, with the other parameters held fixed at the respective minimizing values. The curves pertain to the case of an analog model of known parameters, rather than to a human operator and hence have a deterministic character. One observes that the minimum with respect to parameters α_2 and α_4 is quite flat, whereas the minimum is sharper in the case of parameters α_1 and α_3. This explains why the minimum-seeking process yields well-defined parameters α_1 and α_3 and poorly defined values α_2 and α_4, and hence partly explains the difference in the statistical variation of solutions exhibited in the scatter plots of experimental data obtained in Phase 1 (Figures 6-1 to 6-3).

It should be noted that the profiles of Figures 5-1 to 5-4 are based on a known transfer function and not on actual human operators. Similar contours can be obtained for human tracking data.

5.2 The Nature of the Criterion Surface for Continuous Parameter Optimization Methods

In the iterative technique discussed in the preceding paragraph it is possible to obtain contours where F = constant in the parameter space. For example, Figure 2-2 in Section 2 shows a typical set of contour lines in a parameter plane defined by two parameters α_1 and α_2. Such contours could be constructed by taking corresponding F values from the criterion function profiles of Figure 5-1 (F vs. α_1) and Figure 5-2 (F vs. α_2) and plotting the respective values of α_1 and α_2. In the case of continuous parameter optimization a different approach will be used to analyze the criterion function and its contours in the parameter space. The output error $e = z - y$ in the vicinity of the minimum is expanded in a power series* in terms of the deviations $\Delta\alpha_i, \Delta\alpha_j$ of the parameters α_i, α_j

*The discussion will be restricted initially to parameter adjustment in two dimensions, assuming that all but two of n parameters have been adjusted to, and are held fixed at their correct values.

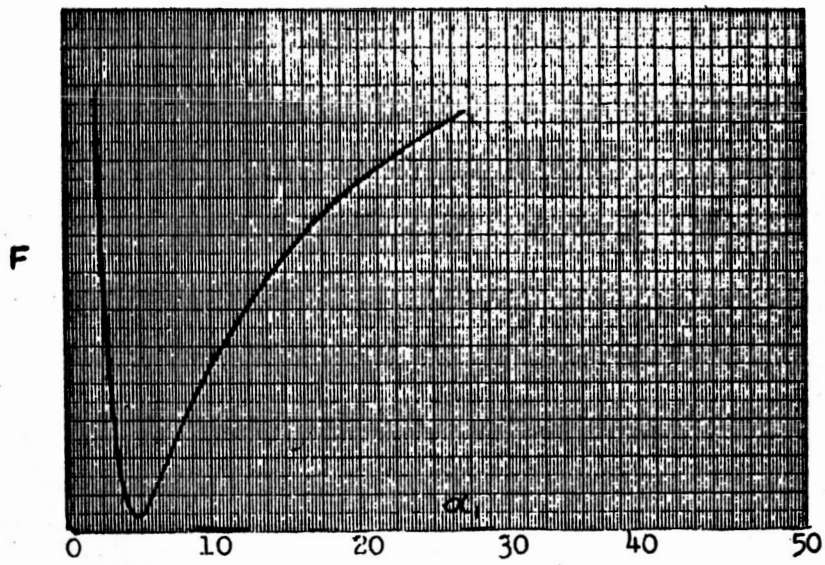

Figure 5-2. Profile of the Criterion Function $F(\alpha_1, \alpha_2, \alpha_3, \alpha_4)$

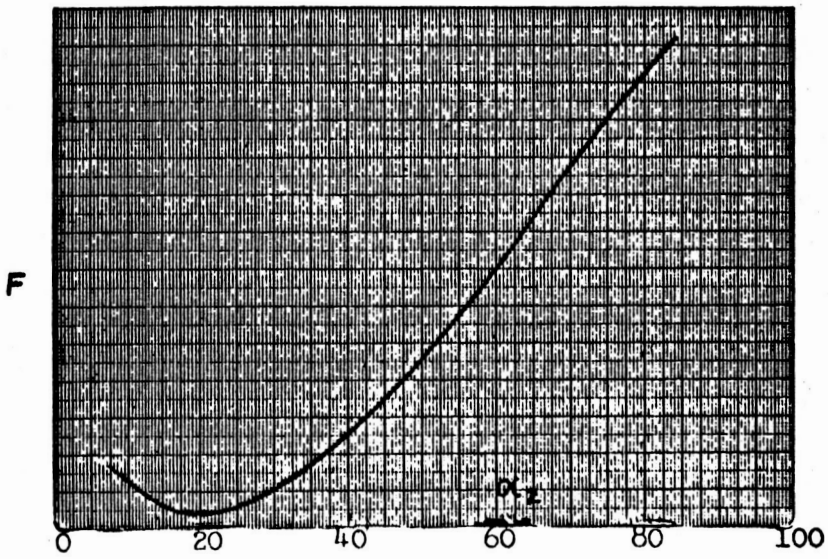

Figure 5-1. Profile of the Criterion Function $F(\alpha_1, \alpha_2, \alpha_3, \alpha_4)$

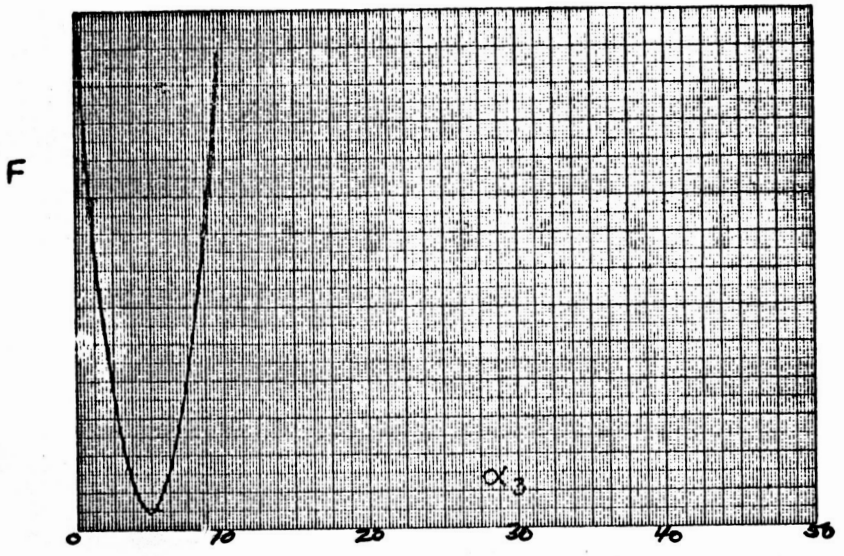

Figure 5-3. Profile of the Criterion Function $F(\alpha_1, \alpha_2, \alpha_3, \alpha_4)$

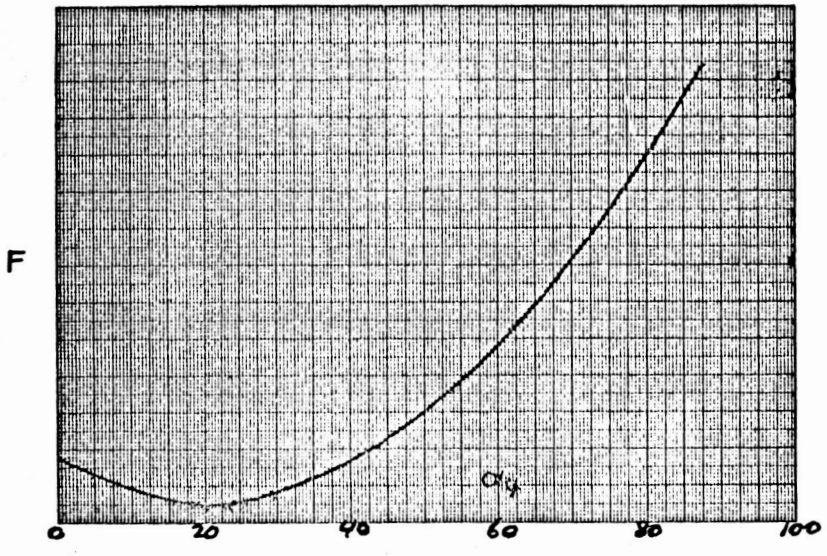

Figure 5-4. Profile of the Criterion Function $F(\alpha_1, \alpha_2, \alpha_3, \alpha_4)$

from their correct values, viz.,

$$e \cong \frac{\partial e}{\partial \alpha_i} \Delta\alpha_i + \frac{\partial e}{\partial \alpha_i} \Delta\alpha_j + \ldots + e_{res} \tag{5.5}$$

and since

$$\frac{\partial e}{\partial \alpha_i} = \frac{\partial z}{\partial \alpha_i} = u_i \,,$$

$$e \cong u_i \Delta\alpha_i + u_j \Delta\alpha_j + \ldots + e_{res} \tag{5.5a}$$

Higher than first order terms are neglected.

The term e_{res} includes a collection of terms not dependent on $\Delta\alpha$ which contribute to the instantaneous model matching error, such as uncertainty in the structure of the unknown system equation, random perturbations, computer inaccuracy, etc.

Using the expansion of e by Equation (5.5), one obtains for the error criterion

$$f = \tfrac{1}{2}(u_i \Delta\alpha_i + u_j \Delta\alpha_j + e_{res})^2 \tag{5.6}$$

Therefore the contour lines f = const. are described by

$$(u_i \Delta\alpha_i + u_j \Delta\alpha_j + e_{res}) = \pm C \tag{5.7}$$

which is the equation of a pair of parallel straight lines in the $\Delta\alpha_i, \Delta\alpha_j$ plane, (see Figure 5-5). A similar result was obtained by Clymer et al, (16). The effect of e_{res} will be ignored for the moment. The contour lines intersect the axes $\Delta\alpha_i$, $\Delta\alpha_j$ at the points

$$A_i = \pm \frac{C}{u_i}$$

$$A_j = \pm \frac{C}{u_j} \tag{5.8}$$

and have the slope

$$m_c = -\frac{u_i}{u_j} \tag{5.9}$$

Due to time-variation of u_i and u_j the position and orientation of the contour lines vary. Conditions of zero or infinite slope occur whenever u_i or u_j, respectively, change sign. The criterion function is zero when C = 0. In this case the two contour lines merge into a single line passing through the point $\Delta\alpha_i = 0$, $\Delta\alpha_j = 0$. The residual error term produces a parallel shift of the contour lines without altering their distance; the contour C = 0 is shifted from the origin by a distance

$$p = \frac{e_{res}}{\sqrt{u_i^2 + u_j^2}} \tag{5.10}$$

Since the criterion function is generated by the family of parallel lines and since f increases in proportion with C^2 it is represented geometrically by a cylindrical surface with a parabolic cross-section. This cylinder is tangential to the $\Delta\alpha_i$ - $\Delta\alpha_j$ plane along the contour line C = 0 (see Figure 5-6). The time-variation of u_i, u_j causes the cylinder to change orientation in accordance with the rotation of the tangential line C = 0. In the absence of residual errors the axis of rotation remains fixed being the f-axis of the 3-axis system shown in Figure 5-6. With non-zero residual errors the instantaneous axis of rotation is shifted randomly but always remains parallel to the f-axis.

The fact that the instantaneous criterion function f (α_i, α_2...) does not form a bowl-shaped surface with closed contour-lines must be noted here to avoid misconceptions as to the manner in which the descent path is formed. If the criterion surface were time-invariant a descent to the proper end condition $\Delta\alpha_i = 0$, $\Delta\alpha_j = 0$ would not be assured. Instead, all descent paths would terminate on points along the line

$$u_i \Delta\alpha_i + u_j \Delta\alpha_j = 0 \tag{5.11}$$

(or on a shifted line for $e_{res} \neq 0$). Time variation of u_i, u_j and

Figure 5-5

Contours F = const in $\Delta\alpha_i - \Delta\alpha_j$ - Plane

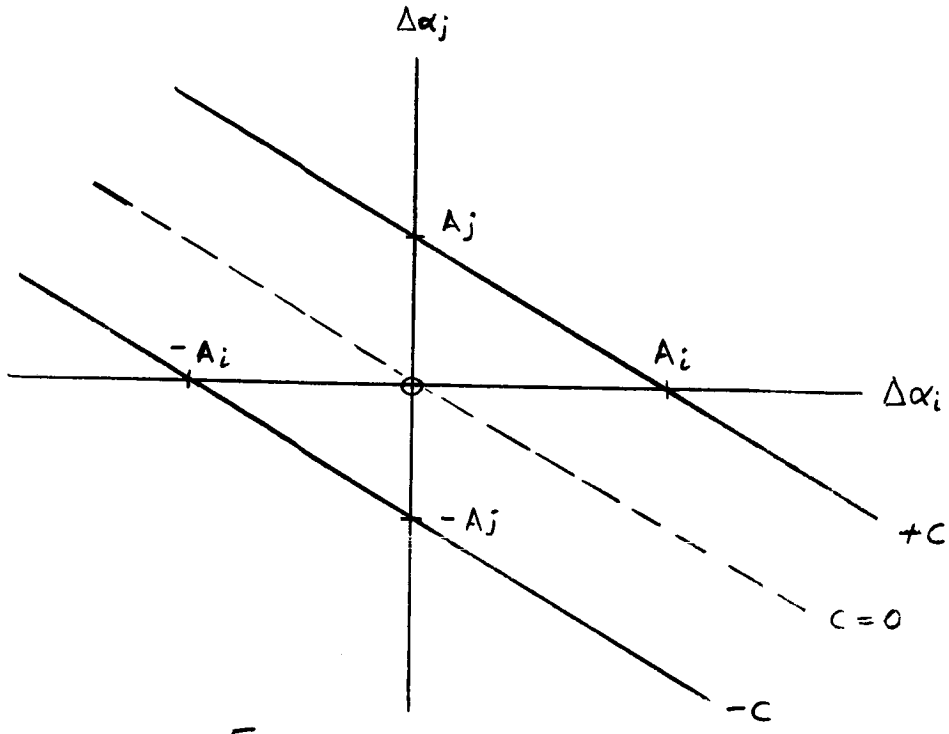

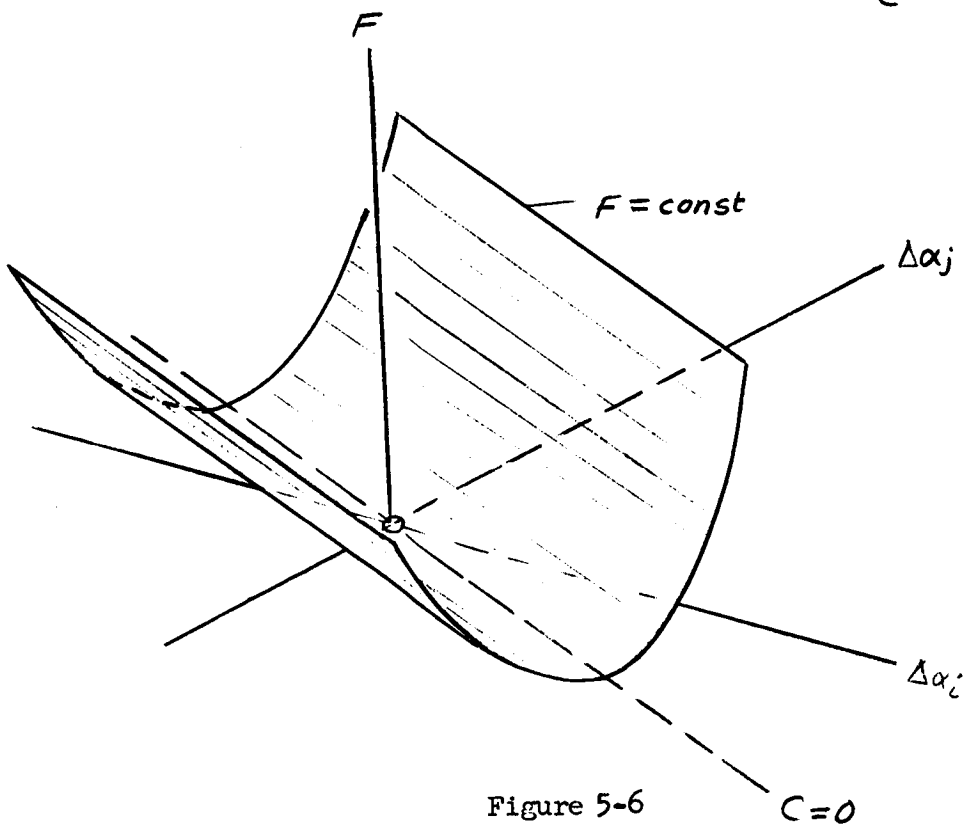

Figure 5-6

Criterion Function F Versus $\Delta\alpha_i - \Delta\alpha_j$

the resulting rotation of the contour line C = 0 around the point $\Delta\alpha_i = 0$, $\Delta\alpha_j = 0$ assures convergence to the proper end condition. With non-zero values of e_{res} the intersection of successive contour lines C = 0 shifts continuously, causing the descent path to move randomly about the origin at distances which depend, of course, on the magnitude of e_{res}.

It is interesting to note that the rotating cylindrical criterion surface may, under certain conditions, define a closed, bowl-shaped envelope surface, such that in effect the steepest descent on the cylinder becomes, in the average, a descent on the envelope surface.

This effect can best be illustrated in two dimensions by deriving the envelope curves for the family of rotating contour lines in terms of $\Delta\alpha_i, \Delta\alpha_j$ coordinates. The envelope of the contour lines is obtained from

$$\begin{aligned} H = f - \text{const.} = 0: &\quad u_i \Delta\alpha_i + u_j \Delta\alpha_j \mp C = 0 \\ \frac{\partial H}{\partial t} = 0: &\quad \dot{u}_i \Delta\alpha_i + \dot{u}_j \Delta\alpha_j = 0 \end{aligned} \tag{5.12}$$

This yields the coordinates of the envelope

$$\begin{aligned} \Delta\alpha_{i_E} &= \mp C \frac{\dot{u}_j}{u_i \dot{u}_j - u_j \dot{u}_i} \\ \Delta\alpha_{j_E} &= \mp C \frac{\dot{u}_i}{u_i \dot{u}_j - u_j \dot{u}_i} \end{aligned} \tag{5.13}$$

Consider for example the parameter adjustment of α_3, α_4 in the case of sinusoidal excitation, which is characterized by influence coefficients $u_4 = A \sin \omega t$ and $u_3 = \dot{u}_4 = A\,\omega \cos \omega t$*. Introducing these terms into Equation (5.13) yields:

$$\begin{aligned} \Delta\alpha_{3_E} &= \frac{C}{A\omega} \cos \omega t \\ \Delta\alpha_{4_E} &= \frac{C}{A} \sin \omega t \\ \text{where} \quad C^2 &= 2f \end{aligned} \tag{5.14}$$

*The functional relation $u_3 = \dot{u}_4$ will be further discussed in Section 5.6.

The envelope surface represented by Equations (5.14) has elliptic cross-sections (contours), as illustrated in Figure 5-7 with semi-major axes increasing in proportion with C. For the special case $\omega = 1.0$ the contours are circles with radius $\frac{C}{A}$.

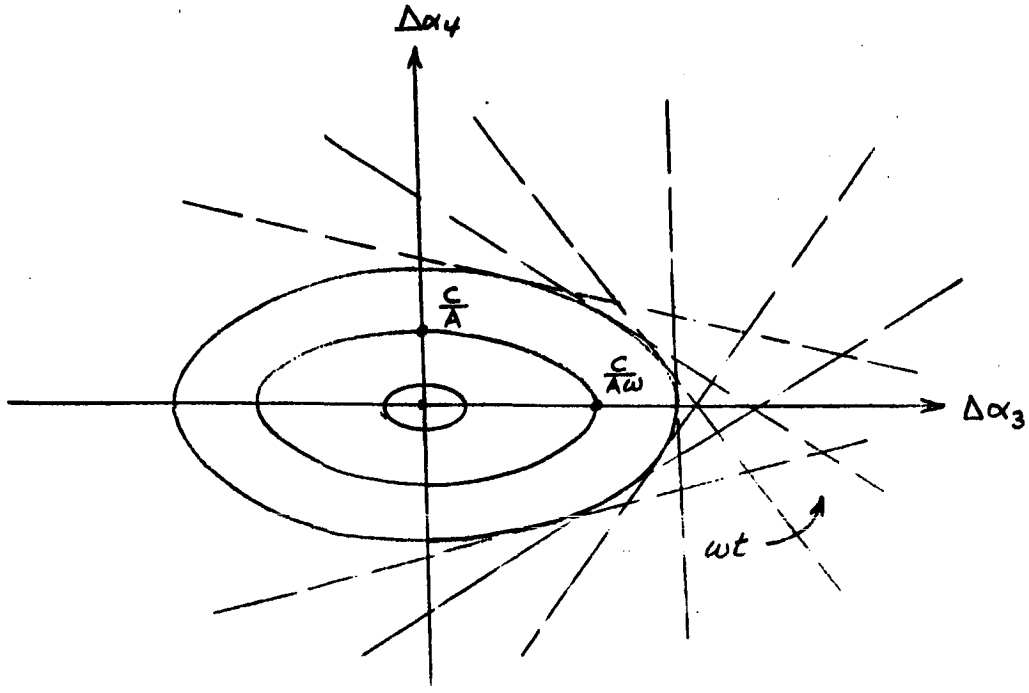

Figure 5-7

Envelopes of Contour Lines f = const. in the $\Delta\alpha_3$, $\Delta\alpha_4$ Plane

These results derived for two parameters may be extended to higher dimensions. In the three-dimensional case the F-contours are characterized by a pair of parallel planes which intersect the parameter axes at

$$A_1 = \pm \frac{C}{u_1} \quad , A_2 = \pm \frac{C}{u_2} \quad , A_3 = \pm \frac{C}{u_3} \tag{5.15}$$

and are separated by the distance $2C/\sqrt{u_1^2 + u_2^2 + u_3^2}$. Time-variation of the u_i cause the contour planes to envelop a set of nested contour surfaces. The descent paths must penetrate these contour surfaces orthogonally in converging to the center at C = 0. In the four-dimensional case the contour planes become hyperplanes enveloping a set of 3-dimensional closed hypersurfaces.

It is interesting to consider the possibility of uncontrolled, large excursion of the descent paths in the directions left open between parallel contour planes or hyperplanes. The simultaneous adjustment of more than two or three parameters at a time can become quite problematic, as indicated by some of the parameter tracking records, and more research is needed to establish sufficient assurance of convergence.

The above results explaining the character of the criterion function raise some questions as to the nature of the parameter adjustment paths and make it mandatory to examine the behavior of the time-varying gradient vector. These questions will be considered in the following section.

5.3 The Nature of the Gradient in Continuous Model Matching

The gradient vector in the iterative adjustment process is defined by

$$\overline{\nabla} F\,(\bar{\alpha}) = \left[\frac{\partial F}{\partial \alpha_1}, \frac{\partial F}{\partial \alpha_2}, \frac{\partial F}{\partial \alpha_3}, \cdots \frac{\partial F}{\partial \alpha_n} \right]$$

where n refers to the number of adjustable parameters. An analogous definition is not possible for the continuous method since the parameters are varying and the partial derivatives are not defined. The partial derivatives generated by the computer in terms of the variables u_i are, at best, approximate gradient components if the parameter adjustment is a slow process. In order to circumvent this difficulty and gain some insight into the nature of the gradient, it is possible to compute the partial derivatives u_i (influence coefficients) by opening the adjustment loops, thus keeping the parameters constant.

The previous section showed that for the criterion $f = \frac{1}{2} e^2$, the contours for f = const. are pairs of straight lines. The gradient vector always intersects the contour f = const. at right angles, and the rotation of the contour surface results in a time variation of both the direction and magnitude of the gradient vector.

Let the criterion function be $f = \frac{1}{2} e^2$. Then, the orientation of the gradient in a two-parameter space defined by α_i and α_j is given by

$$m_g = \frac{\partial f/\partial \alpha_j}{\partial f/\partial \alpha_i} = \frac{e\, u_j}{e\, u_i} = \frac{u_j}{u_i} \qquad (5.16)$$

Consider now a specific case. Let the system be defined by Equation (2.17) with α_1 and α_2 being held fixed, and assume a sinusoidal excitation signal

$$x(t) = D \sin \omega t \ .$$

The influence coefficients u_3 and u_4 are obtained as solution of the sensitivity equations

$$\begin{aligned} \ddot{u}_3 + \alpha_1 \dot{u}_3 + \alpha_2 u_3 &= \dot{x} \\ \ddot{u}_4 + \alpha_1 \dot{u}_4 + \alpha_2 u_4 &= x \end{aligned} \tag{5.17}$$

and consequently they may be written as

$$\begin{aligned} u_4 &= B \sin (\omega t + \varphi) \\ u_3 &= B \omega \cos (\omega t + \varphi) \end{aligned} \tag{5.18}$$

where B/D is the amplitude ratio obtained from solution of the second order systems of Equation (5.18) and φ is the resulting phase shift.

Hence

$$\text{tau } \Theta = m_g = \frac{u_4}{u_3} = \frac{1}{\omega} \tan (\omega t + \varphi) \tag{5.19}$$

where Θ is the orientation angle of the gradient vector relative to the α_3-axis. Θ thus becomes a periodic function of time. For the care $\omega = 1.0$ Equation (5.19) yields

$$\Theta = \omega t + \varphi \pm k\pi \tag{5.20}$$

The gradient vector oscillates both in direction and magnitude, as indicated graphically in Figure 5-8. This result agrees with the previous findings, discussed in Section 5.2, regarding rotation of the contour lines. Note that the parameters α_3 and α_4 are being held fixed at the point where $\overline{\nabla} F$ is evaluated.

Experimental verification of these results was obtained by using the computer to plot the loci of the open loop gradient in the α_3-α_4 plane with a sinusoidal input. Figure 5-9 shows these loci at various trial points. The parameters α_1 and α_2 were set at their correct values, i.e., they were equal, respectively, to the system parameters a_1 and a_2.

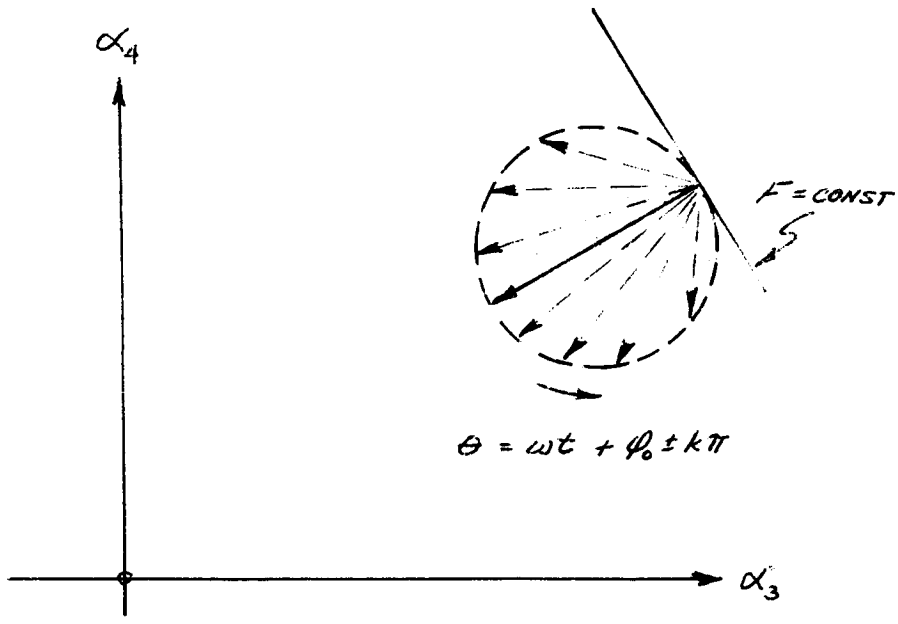

Figure 5-8

Time Varying Gradient in α_3, α_4 Plane

As expected, the α_3, α_4 loci of the time-variant gradient vector $\left[\frac{\partial f}{\partial \alpha_3} , \frac{\partial f}{\partial \alpha_4} \right]$ are nearly circular, describing two full rotations for every period of the sinusoidal excitation signal. The loci pass through the trial point during every full rotation. At these instances the gradient has the magnitude zero. For random excitation of the model matching system the loci have irregular shape with varying time-intervals per full rotation, i.e., between passages through the trial point. The implications of this result are significant. It can be observed that the gradient sweeps an angular domain of 180 degrees in the α_3, α_4 plane and that only the mean orientation of the gradient vector points in the desired direction. In other words, the criterion function forms the time-varying surface discussed in the previous section. This suggests low-pass filtering of the gradient components $\frac{\partial f}{\partial \alpha_i}$ in order to emphasize the preferred mean gradient orientation. Figure 5-10 is a sketch of different open-loop gradient loci obtained with and without low pass filtering.

Open Loop Gradient Loci in the α_3, α_4, Plane

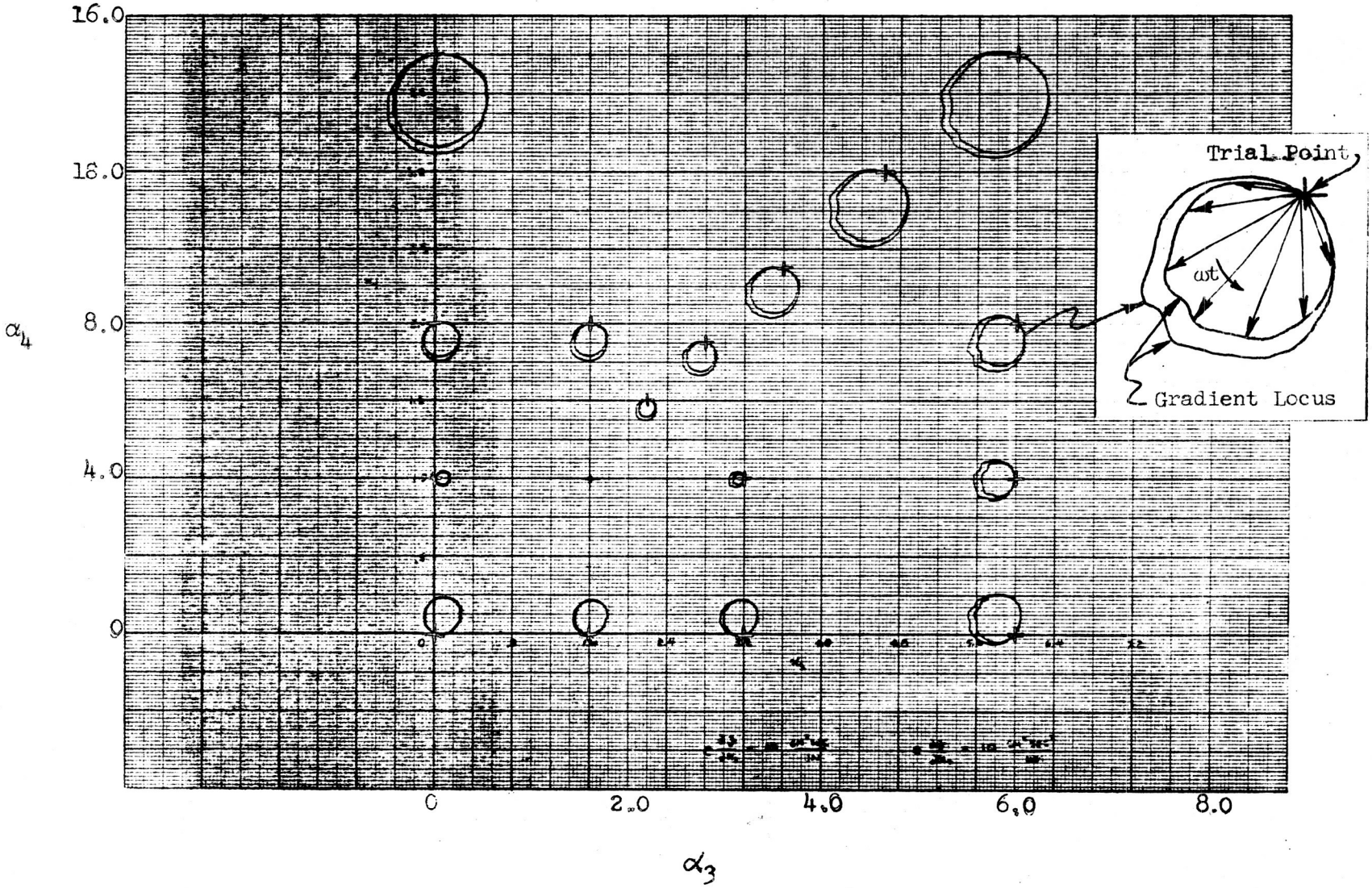

Figure 5-9

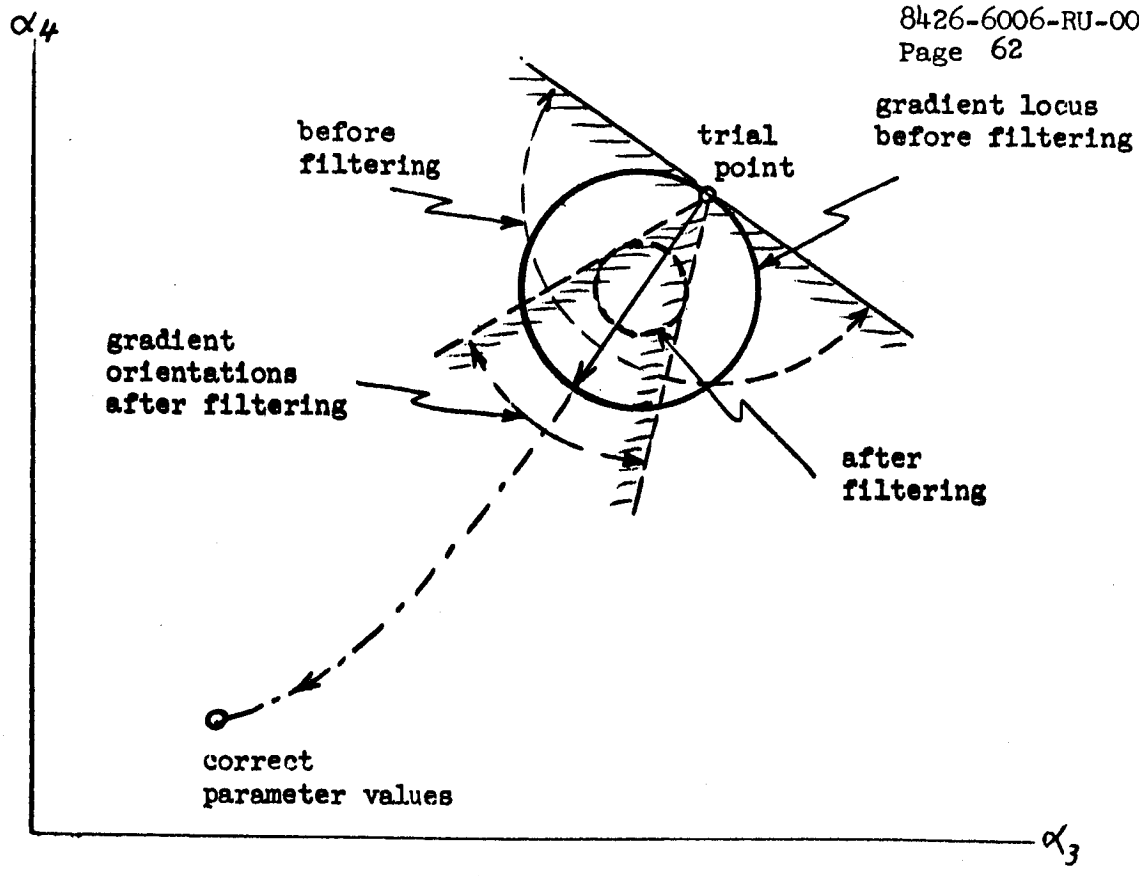

Open-Loop Gradient Loci in α_3, α_4 Plane before and after Filtering of Output Signals
Figure 5-10

The time-variation of the gradient leads to an interesting observation regarding the speed of convergence for a model matching problem with many parameters. The probability of the gradient being oriented within the desired angular range is less than 1 inasmuch as the vector points in other directions part of the time. If, for example, the vector points in the desired direction only 50% of the time in a two-parameter adjustment problem, this probability is reduced further in a three-parameter problem, and still further in a four-parameter problem, since the desired direction encompasses less and less of the total spatial angle over which the gradient vector can sweep. As a result, the settling time increases at least in proportion with the number of parameters to be adjusted simultaneously. On theoretical grounds the time would tend to increase with powers of 2^n where n is the number of parameters, considering the geometry of angular sectors in a hyper-space.

5.4 The Adjustment Path in Parameter Space

The time-variation of the gradient vector examined above suggests that when the loop is closed to allow continuous parameter adjustment, the rate of adjustment will also be time-varying. The

continuous adjustment method is based on the steepest-descent principle expressed by

$$\dot{\bar{p}} = -K\,\bar{G}\,(p) = -K\,\overline{\nabla f}(\bar{p}) \qquad (5.21)$$

where $\bar{G}\,(\bar{p})$ is a vector approximately equal to the gradient of f and $\bar{p}$ is the parameter vector. The degree of approximation inherent in Equation (5.21) improves as the rate of adjustment decreases. Therefore, at points where $\overline{\nabla f}(\bar{p}) = 0$, the rate of adjustment $\dot{\bar{p}}$ will also be zero. The adjustment path resulting from a sinusoidal input is shown in Figure 5-11 for several values of adjustment gain K.

The nature of the envelope curves discussed in Section 5.2 above is inferred by reference to Figure 5-12 which shows the adjustment paths from different initial conditions. The envelope curves were shown previously in Figure 5-7 to be ellipses. Consequently, the gradient descent paths are seen to approximate the radii of ellipses when the rate of descent has decreased sufficiently. The adjustment paths for random excitation for several values of adjustment gain is illustrated in Figure 5-13.

An important result of this analysis is the confirmation of the original conjecture that for sufficiently low adjustment rates a gradient descent path is being followed. Serious questions regarding the nature of the gradient approximation used only arise at instances of maximum adjustment rate. Although the descent path is confined within the closed contours of the envelope surface if the rate of adjustment is sufficiently slow, it can be seen in Figures 5-11 and 5-12 that for large values of adjustment gain K a path may develop which at a subsequent time increment leads in a direction nearly parallel to the generator lines of the instantaneous cylindrical contour surface so that large and uncontrolled excursions from the desired end point may occur. This can be expected if the excitation frequency ω, for sinusoidal excitation or the bandwidth of excitation frequencies in random excitation is too small in comparison with K. Additional study of the desired relationship between K and bandwidth of the excitation signal will be necessary.

Descent Trajectories in α_3, α_4 Plane - Sinusoidal Excitation

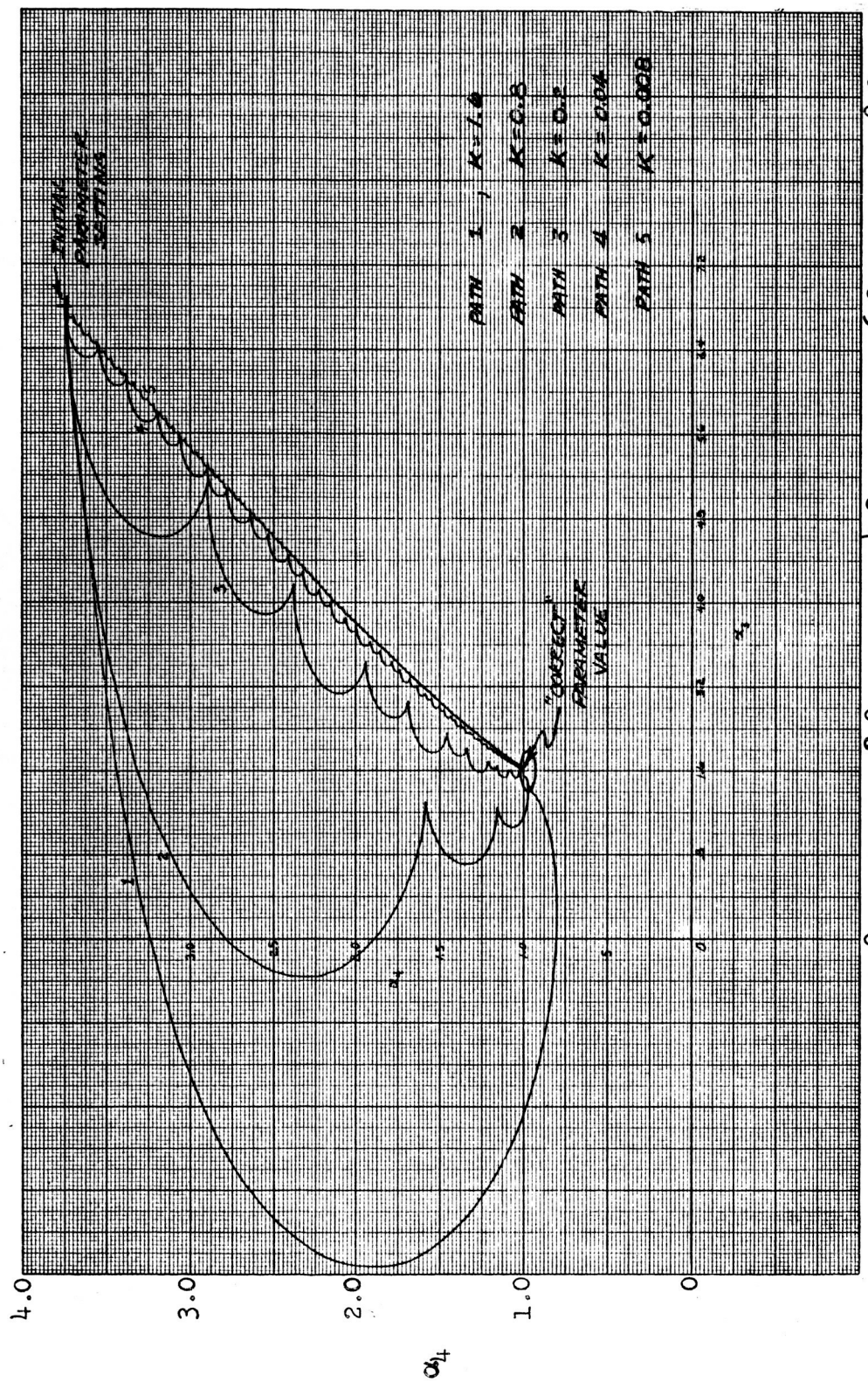

Figure 5-11

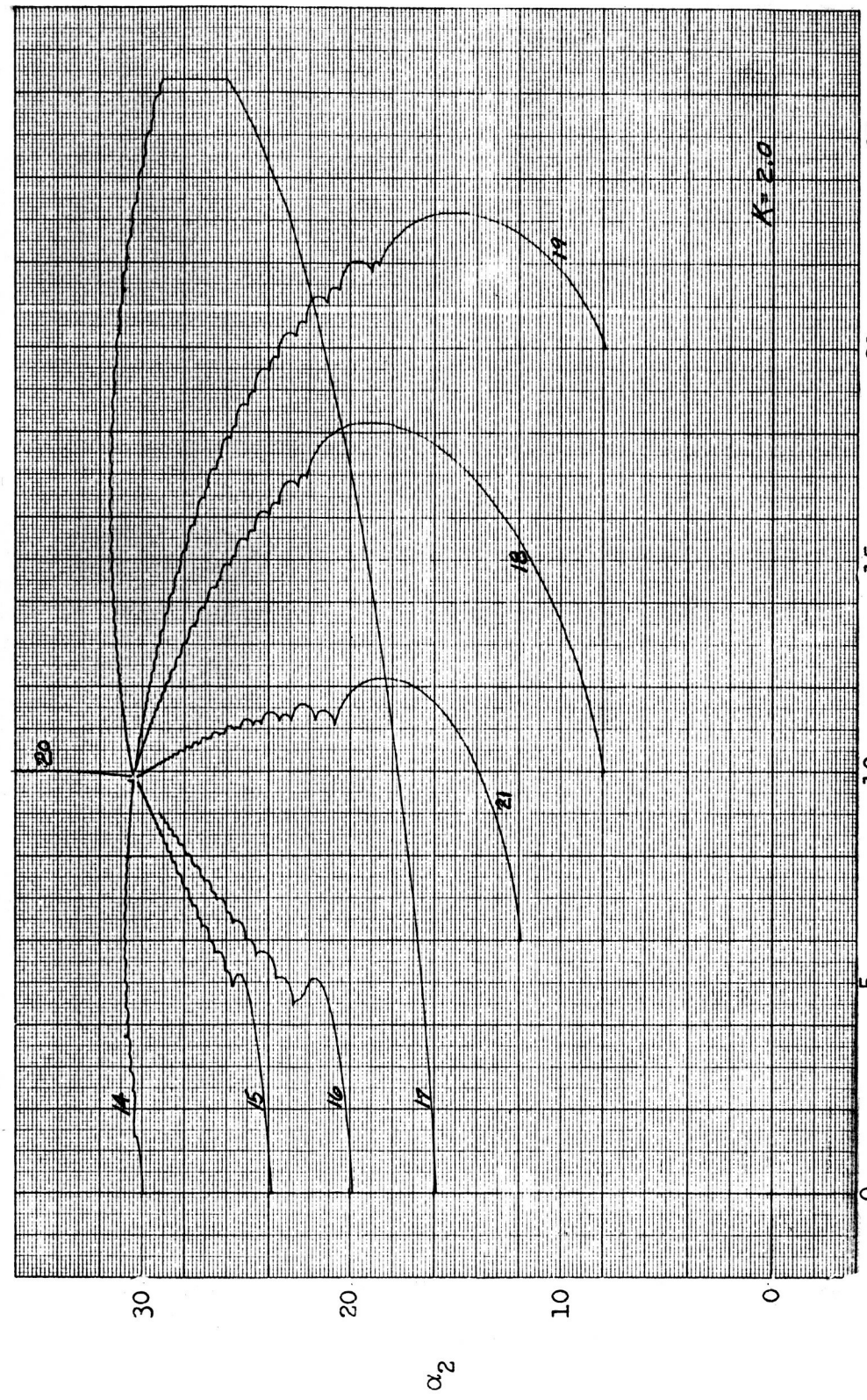

Effect of Parameter Initial Conditions on Trajectories in α_1, α_2 Plane
Sinusoidal Excitation

Figure 5-12

Descent Trajectories in α_3, α_4 Plane - Random Excitation

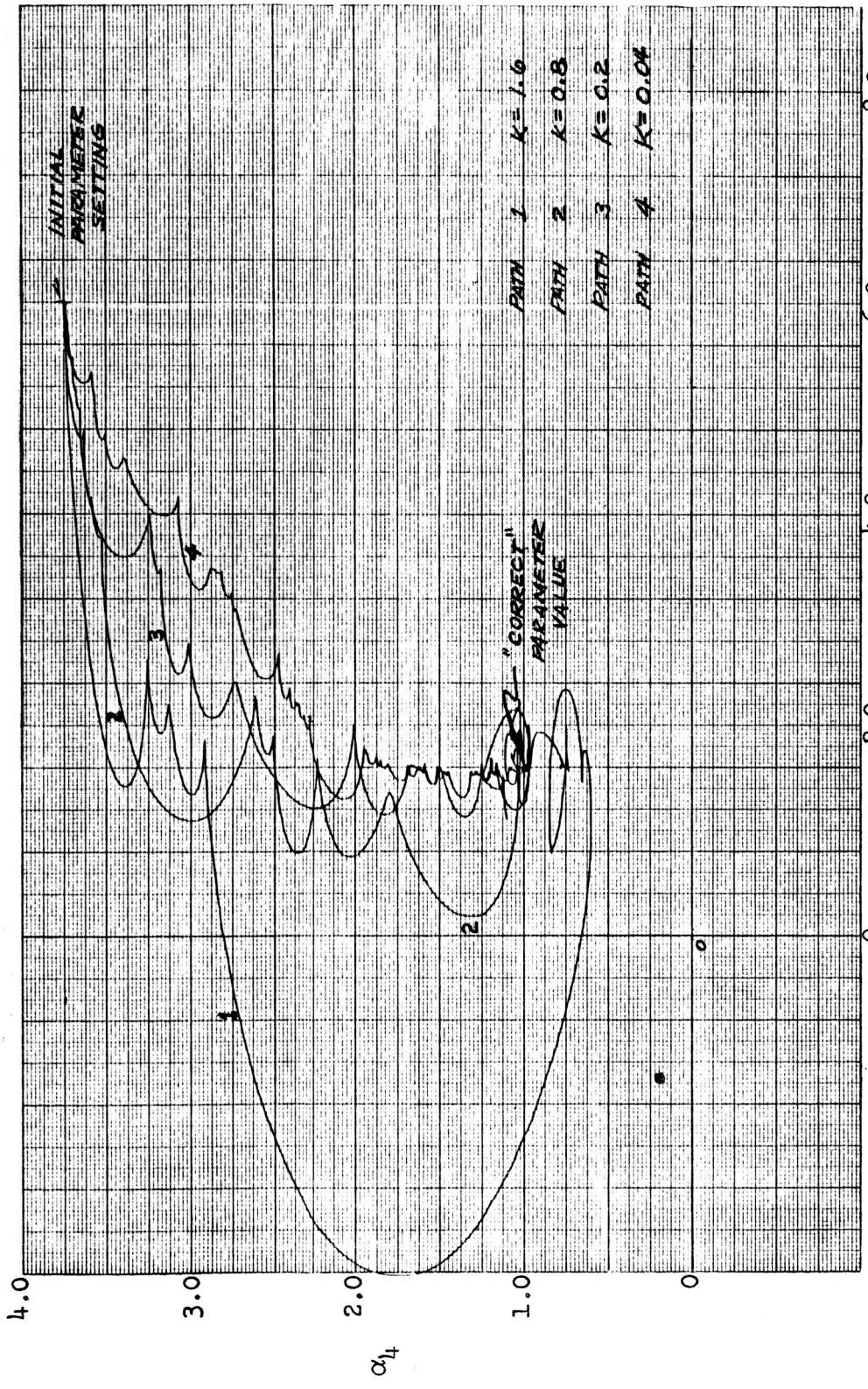

Figure 5-13

5.5 Effect of the Choice of Adjustment Gain K

The role of the gain factor K in the parameter adjustment process and the question of whether equal or unequal values of K should be selected in the different adjustment loops is of major interest from a standpoint of optimizing the overall performance of multi-parameter adjustment. The following discussion is concerned with those characteristics of the descent path which depend on the choice of K and on the scale of presentation in the parameter space.

Steepest descent requires that the adjustment path always be tangential to the local gradient vector $\overline{\nabla} f$. The components $d\alpha_i$ and $d\alpha_j$ of a path element ds in the 2-dimensional case must therefore be chosen in the same ratio as the gradient components $\frac{\partial f}{\partial \alpha_i}$ and $\frac{\partial f}{\partial \alpha_j}$, thus requiring equal gain factors K in both dimensions. If the gain factors K_i and K_j are chosen unequal a path other than steepest descent will result. Different paths obtainable by different ratios $K_i : K_j$ will all converge to the desired end point, but from different directions. These paths are illustrated in Figure 5-14.

Using the concept of effective closed f-contours established in Section 5.2, one finds that for circular contours the steepest descent paths are radial, whereas for elliptic contours the steepest descent paths are curved, tending on approach to the minimum to become tangential to the larger of the two major axes (see Figure 5-15).

It is noted that a choice of unequal scale factors for the coordinate axes in the parameter space does not alter the character of the descent paths, but only has the apparent effect of changing orthogonality of contour crossings. This effect is illustrated in the lower half of Figure 5-15.

The question arises here what normalized scaling must be used for the various α_i in a plot of the descent path in order to show orthogonality with respect to the f-contours if all adjustment gains are equal. To resolve this question it will be necessary to consider the implications of parameter adjustment in accordance with

$$\dot{\alpha}_i = -K \frac{\partial f}{\partial \alpha_i} \qquad (5.22)$$

Figure 5-14

Dependence of Descent Path on Choice of K_i, K_j

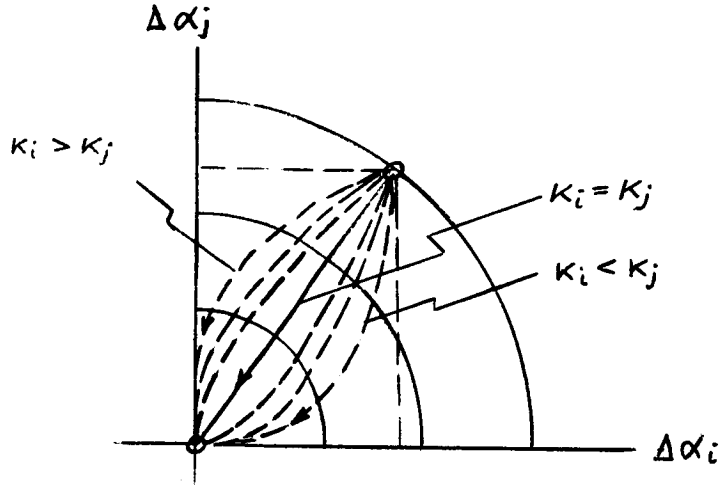

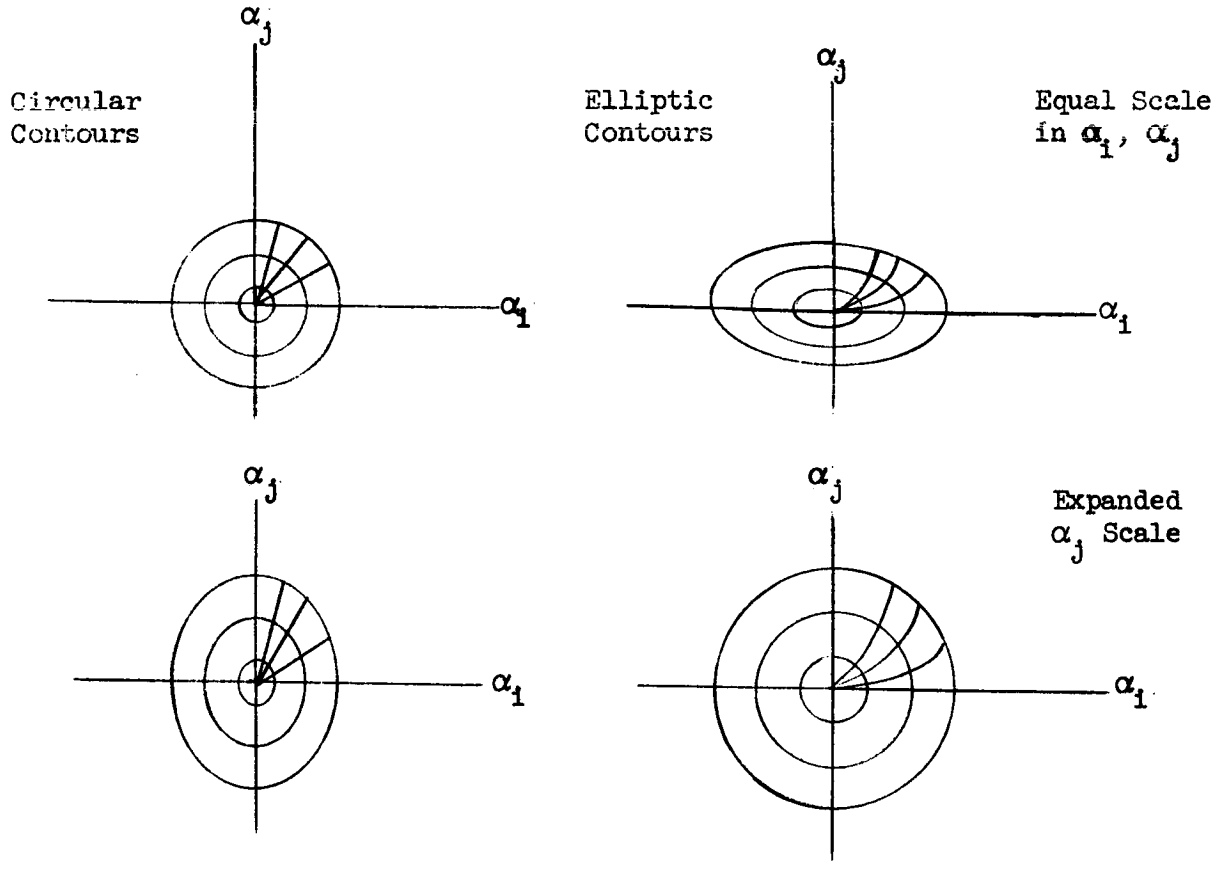

Figure 5-15

Descent Paths in the α_i, α_j Plane

Only the numerical value of each parameter α_i, regardless of physical significance, physical dimension, or computer scaling, is controlled by the adjustment loop on the basis of the numerical value of $\frac{\partial f}{\partial \alpha_i}$. The parameters implemented on the computer may be considered as non-dimensional quantities (potentiometer setting times associated amplifier input gain). The gradient components also are non-dimensional; consequently all adjustment gains K must have the dimension sec^{-1} to assure dimensional agreement on both sides of the adjustment equation (5.22). Different physical dimensions of the various system parameters can thus be ignored from the standpoint of parameter adjustment. For a rigorous treatment of parameters and their physical dimensions it is appropriate to express each (physical) coefficient α_k as the product of a pure number $\bar{\alpha}_k$ and a dimensional factor of unit magnitude ℓ_k,

$$\alpha_k = \bar{\alpha}_k \ell_k \tag{5.23}$$

The normalized plotting scale of the parameter $\bar{\alpha}_i$ as programmed on the computer is in the same non-dimensional units as those of $\bar{\alpha}_j$. This procedure has been followed in this study, the parameter plots being consistently labeled in non-dimensional units. However, different axis scales were adopted for convenience in some of the plots shown.

5.6 Cross-coupling or Interaction Among Parameters

Interaction effects can be observed during simultaneous adjustment of several parameters in many of the figures shown in Appendix A. This section analyzes these effects and the underlying mathematical relationships.

5.6.1 Functional Relation Between Sensitivity Coefficients

Consider the sensitivity equations for u_1 and u_2 for invariant α_1, α_2

$$\ddot{u}_1 + \alpha_1 \dot{u}_1 + \alpha_2 u_1 = -\dot{z} \tag{5.24}$$

$$\ddot{u}_2 + \alpha_1 \dot{u}_2 + \alpha_2 u_2 = -z \tag{5.25}$$

The initial values must satisfy the condition $u_1(0) = \dot{u}_1(0) = u_2(0) = \dot{u}_2(0) = 0$. Time-differentiation of Equation (5.25) yields the approximate relation

$$u_1 \cong \dot{u}_2 \tag{5.26}$$

Transient differences between u_1 and $\dot{u}_2$ are caused by a non-zero initial value

$$\ddot{u}_2(0) = -z(0)$$

Note that $\dot{u}_1(0)$ equals zero by definition but $\ddot{u}_2(0)$ in general does not equal zero.

Similarly, the corresponding two sensitivity equations for u_3 and u_4

$$\ddot{u}_3 + \alpha_1 \dot{u}_3 + \alpha_2 u_3 = \dot{x} \tag{5.27}$$

$$\ddot{u}_4 + \alpha_1 \dot{u}_4 + \alpha_2 u_4 = x \tag{5.28}$$

with initial values $u_3(0) = \dot{u}_3(0) = u_4(0) = \dot{u}_4(0) = 0$
yield the approximate relation

$$u_3 \cong \dot{u}_4 \tag{5.29}$$

which is valid after transient differences between u_3 and $\dot{u}_4$ due to $x(0) \neq 0$ have subsided.

Combination of the sensitivity equations (5.25), (5.28) and the original model equation

$$\ddot{z} + \alpha_1 \dot{z} + \alpha_2 z = \alpha_3 \dot{x} + \alpha_4 x \tag{5.30}$$

yields the approximate relation

$$u_2 x = -u_4 z \tag{5.31}$$

which is applicable after transients due to $z(0)$ and $\dot{z}(0)$ have disappeared.

It is important to note that Equations (5.26), (5.29) and (5.31) imply time-invariant coefficients. If α_1 and α_2 are time-variant,

a time-differentiation of Equation (5.25) would yield

$$\dddot{u}_2 + \alpha_1 \ddot{u}_2 + \alpha_2 \dot{u}_2 = -z - \dot{\alpha}_1 \dot{u}_2 - \dot{\alpha}_2 u_2 \qquad (5.32)$$

In this case Equation (5.26) implies an approximation other than the initial condition effect previously noted. For sufficiently small adjustment rates $\dot{\alpha}_1$, $\dot{\alpha}_2$, the approximations (5.26) and (5.29) are useful in providing estimates of the relative magnitudes of the u_i terms. They also permit a very considerable simplification in implementing the parameter adjustment system on the computer. This computer program includes only Equations (5.25) and (5.28) to generate u_1, u_2 and u_3, u_4, respectively. The approximation has been used successfully in several phases of the study to save computer channels, as explained in the Computer Implementation Section. Similar formulations have been used by Klenk (17) and Adams (2,18) to simplify the computer program.

5.6.2 Precision of Parameter Matching

As will be noted in the discussion of the computer results, different parameters of the system are matched with different degrees of precision. The relative magnitude of the sensitivities u_i helps to explain this fact. Equation (5.5) shows that the instantaneous model matching error constitutes a weighted average of the individual adjustment errors $\Delta\alpha_i$ where u_i are the weighting factors. Clearly those adjustment errors which have dominant weighting factors will be adjusted with the greatest precision. Since u_3 dominates in many of the cases examined, the precision of the α_3 adjustment is generally quite high. By contrast, u_2 is dominated by the other sensitivities and hence α_2 is poorly defined. These results are also borne out by Figures 6-1 to 6-3 of Section 6.

An investigation of the underlying mathematical relations will clarify the picture. The following discussion applies rigorously only to the linear time-invariant case, but serves to explain basic trends in the time-variant and nonlinear cases as well.

It is first observed that the random excitation signal x(t) includes frequencies up to 5 rad/sec due to human tracking behavior. Therefore $\dot{x}$ has higher amplitudes in the upper frequency band than x, and causes u_3 to dominate u_4 (see Equations (5.27), (5.28), (5.29)). Similarly, since z and $\dot{z}$ follow x and $\dot{x}$, respectively, it is expected that u_1 will dominate u_2, depending on the filtering characteristics of the model equation (5.30). Typical values of transfer function gain for the time-invariant system over the range of input frequencies are

$$\left|\frac{Z}{X}\right| = 0.15 \ldots 0.25$$

where X and Z are Laplace transforms of x, z. An estimate of u_2 and u_4 magnitudes can be obtained on the basis of Equation (5.31), viz.,

$$\left|\frac{U_2}{U_4}\right| = \left|\frac{Z}{X}\right|$$

Therefore, the sensitivity term u_4 dominates u_2 at least by a ratio of 3:1. This result is confirmed by many of the time histories obtained (see Appendix A). For the conditions under which the model matching system was operated it may be seen that u_3 dominates u_4 which in turn dominates u_2. Also, u_1 dominates u_2, hence the poor definition of α_2 and the generally good definition of α_3 observed in many of the computer runs. The relatively larger values of u_3 also tend to make the α_3 adjustment loop the most critical in terms of stability.

5.6.3 Analysis of Cross-coupling Effects

Considering the steepest descent equation

$$\dot{\alpha}_i = -K \frac{\partial f}{\partial \alpha_i} = -K\, e\, u_i \qquad i = 1, 2, 3, 4. \tag{5.33}$$

it can be seen that the adjustment rate is proportional to the model matching error e and the sensitivity u_i. The error term e may again be expanded, in first order approximation, in terms of individual parameter errors $\Delta\alpha_i$, viz.,

$$e \cong u_1 \Delta\alpha_1 + \ldots + u_4 \Delta\alpha_4 \tag{5.34}$$

where higher order effects, noise, and uncertainty in the structure of the mathematical model are omitted. This equation implies e = 0 when all parameters α_i have been adjusted to the desired values a_i, such that $\Delta\alpha_i = 0$. (This restriction will be removed later.) Combining Equations (5.33) and (5.34) one obtains

$$\dot{\alpha}_i \cong -K\, u_i \sum_{j=1}^{4} u_j \Delta\alpha_j \qquad i = 1, 2, 3, 4. \tag{5.35}$$

Hence each parameter adjustment rate $\dot{\alpha}_i$ is sensitive, to a varying degree, to all of the instantaneous parameter adjustment errors $\Delta\alpha_j$. This sensitivity is expressed by the (approximate) symmetrical square matrix (S) with time-varying elements

$$S_{ij} = u_i\, u_j \tag{5.36}$$

such that

$$\dot{\bar{\alpha}} = -K\,(S)\,\overline{\Delta\alpha} \tag{5.35a}$$

where $\dot{\bar{\alpha}}$ is the rate of change of the parameter vector $\bar{\alpha}$. K may be a scalar if the same adjustment gain is used for all parameters; otherwise it becomes a constant matrix.

If the adjustment of each parameter were independent of all the other parameter-offsets, (S) would be a diagonal matrix. Actually, the various parameter-offsets interact dynamically, the off-diagonal elements of the matrix being the cross-coupling coefficients. Under random excitation x(t) the cross-coupling terms may have small average values, provided the u_i and u_j terms are statistically independent. The diagonal terms u_i^2 are non-negative and their average values tend to be larger than those of the cross-coupling terms.

It was previously noted that the sensitivity terms u_1 and u_3 dominate u_2 and u_4, respectively. This is explained by the fact that u_1 and u_3 are obtained as solutions of sensitivity equations in which the time-derivatives $\dot{z}$ and $\dot{x}$ rather than z and x are the forcing functions of Equations (5.24),(5.26). Considering the frequency content of the excitation signal x and the dependent variable z it follows that $\dot{x}$ and $\dot{z}$ have larger maximum excursions than x and z, respectively.

These facts explain the prevalence of cross-coupling effects between errors in the α_1 and α_3 adjustments which were observed in Figures A-10 and A-15. In Figure A-10, the variation in α_1 which was introduced by a sinusoidal perturbation of the corresponding system parameter a_1 also caused sinusoidal variations in α_3. This effect in turn caused secondary cross-coupling in α_1.

Cross-coupling effects are also noticed when all but one model parameter are initially set at their correct values. During the adjustment of the initially incorrect parameter some transients will occur in the remaining parameters α_i as a result of cross-coupling, according to Equation (5.35) because the sensitivities u_i corresponding to these parameters are non-zero.

Equation (5.34) in the above analysis is based on the assumption that residual modeling errors due to model structure uncertainty, random noise, etc. can be ignored. However, in the presence of residual error this equation must be augmented by forcing terms proportional to e_{res}

$$\dot{\bar{\alpha}} = -K(S)\,\overline{\Delta\alpha} - K\,e_{res}\,\bar{u} \qquad (5.37)$$

Actually, since the u_i, u_j depend to some degree on all α_k settings, the equations (5.35), (5.37) are not strictly linear.

In summary, the following properties of the adjustment process are derived from this mathematical formulation:

1) Cross-coupling effects are introduced by the off-diagonal terms $u_i\,u_j$. The magnitude of mean values as well as instantaneous excursions of $u_i\,u_j$ relative to those of the diagonal elements u_i^2 indicate the extent of cross-coupling in the adjustment process.

2) In the case of random excitation signals $x(t)$ with zero mean the influence coefficients u_i are also random with zero mean but u_i and u_j may be correlated so as to form a non-zero mean product. In the case where one influence coefficient is the derivative of another, e.g. $u_i = \dot{u}_2$, $u_3 = \dot{u}_4$ in linear invariant systems the mean product tends to be zero.

3) The instantaneous products may be large even for zero mean, and integration may yield large disturbances in α_i adjustment. This is possible particularly with low frequency of excitation which allows the products $u_i\ u_j$ to maintain positive or negative values for extended periods of time.

5.7 Analysis of Model Matching Using a Sinusoidal Excitation Signal

5.7.1 Indeterminacy of Model Parameters

The use of a purely sinusoidal excitation signal x(t) in some portion of the analytical and experimental studies helped to clarify fundamental properties of the parameter adjustment process. However, from a practical standpoint such an excitation signal is unsuitable since, in general, it does not yield unique parameter values if more than two parameters are being adjusted simultaneously. This fact has been observed experimentally during the computer study and can be easily explained.

Let the system be described again by

$$\ddot{y} + a_1 \dot{y} + a_2 y = a_3 \dot{x} + a_4 x \tag{5.38}$$

and the model by

$$\ddot{z} + \alpha_1 \dot{z} + \alpha_2 z = \alpha_3 \dot{x} + \alpha_4 x \tag{5.39}$$

This case permits exact model matching if all $\alpha_i = a_i$. The question considered here is concerned with the uniqueness of this solution for the α's. If individual parameter errors $\Delta\alpha_i$ are assumed to exist such that

$$a_i = \alpha_i + \Delta\alpha_i$$

then for uniqueness of parameter definition an exact model match $e = z - y \equiv 0$ must imply zero values of all $\Delta\alpha_i$ and vice versa.

In order to examine the behavior of the $\Delta\alpha$'s Equation (5.38) is subtracted from (5.39) yielding

$$(\ddot{y} - \ddot{z}) + (a_1\dot{y} - \alpha_1\dot{z}) + (a_2 y - \alpha_2 z) = \Delta\alpha_3 \dot{x} + \Delta\alpha_4 x \tag{5.40}$$

For the case of ideal model matching, z-y ≡ 0, this equation reduces to

$$\Delta\alpha_1 \dot{y} + \Delta\alpha_2 y - \Delta\alpha_3 \dot{x} - \Delta\alpha_4 x = 0 \qquad (5.41)$$

This linear algebraic equation is satisfied by

$$\Delta\alpha_1 = \Delta\alpha_2 = \Delta\alpha_3 = \Delta\alpha_4 = 0$$

which is the correct solution to the problem, regardless of the nature of the excitation x(t). Clearly, if the excitation is a random signal or a composite of sinusoids no other solution is possible, hence the correct solution is unique. For the pure sinusoidal case

$$x(t) = A \sin \omega t$$

which yields a steady state output

$$y(t) = B \sin (\omega t + \varphi)$$

The equation (5.41) is equivalent to two equations derived by separating since and cosine terms:

$$\begin{aligned} B\,\omega \cos\varphi\,\Delta\alpha_1 + B \sin\varphi\,\Delta\alpha_2 - A\omega\,\Delta\alpha_3 &= 0 \\ B\,\omega \sin\varphi\,\Delta\alpha_1 - B \cos\varphi\,\Delta\alpha_2 + A\,\Delta\alpha_4 &= 0 \end{aligned} \qquad (5.42)$$

In addition to the solution $\Delta\alpha_i = 0$ there exist infinitely many other solutions making the parameter values indeterminate. By assuming fixed non-zero values for two of the parameters the two remaining parameters are uniquely determined. This result agrees with observations during parameter adjustments performed on the computer: The indeterminacy of two of the parameters appeared as drift or by settling on incorrect terminal values (see Figure A-4).

In the more realistic case of matching an unknown system the two equations corresponding to (5.38) and (5.39) do not have exactly the same form, hence residual terms will appear in Equation (5.40) and (5.41) even for a very close agreement of the output variables of y and z. Therefore the condition of optimum match becomes an inhomogeneous algebraic equation in $\Delta\alpha_i$ equivalent to (5.41) having unique solutions for $\Delta\alpha_i$ for random or random-appearing excitation signals.

5.7.2 Model Matching With Low Frequency Input

It is interesting to consider the special condition of very low frequency input signals where the human operator can follow the displayed excursions with negligible phase shift. A reasonable approximation of human response is given by

$$z \cong k\, x \tag{5.43}$$

where k is the low-frequency gain (assumed constant under the given conditions). This yields the derivatives

$$\begin{aligned} \dot{z} &\cong k\, \dot{x} \\ \ddot{z} &\cong k\, \ddot{x} \end{aligned} \tag{5.44}$$

Substitution of these terms into Equation (5.39) results in

$$\dddot{z} + \left(\alpha_1 - \frac{\alpha_3}{k}\right) \ddot{z} + \left(\alpha_2 - \frac{\alpha_4}{k}\right) \dot{z} = 0 \tag{5.45}$$

For arbitrary input signals no direct conclusion can be drawn from this statement. However, if the input is a sinusoid of low frequency, the output will be proportional. But for sinusoidal signals z it can be concluded that the coefficient of z must vanish, and the coefficient of z equals ω^2 where ω is the excitation frequency. Therefore,

$$\begin{aligned} \alpha_3 &= k\alpha_1 \\ \alpha_4 &= k\alpha_2 + k\omega^2 \cong k\alpha_2 \end{aligned} \tag{5.46}$$

It is again seen that two parameters in the set of four are indeterminate, i.e. only the combinations $(\alpha_3 - k\alpha_1)$ and $(\alpha_4 - k\alpha_2)$ are determined in this case.

The coupling effects present in α_1, α_3 and in α_2, α_4 can also be obtained by consideration of the sensitivity matrix $[S_{ij}]$ previously introduced in this section. Since all sensitivities u_i are sinusoids and are in phase with either x or $\dot{x}$ one obtains

$$\begin{aligned} u_1 &= k_1\, \dot{x} \\ u_2 &= k_2\, x \\ u_3 &= k_3\, \dot{x} \\ u_4 &= k_4\, x \end{aligned}$$

where the k's are constants. Consequently, the sensitivity matrix has the form

$$S = \begin{bmatrix} k_1^2 (\dot{x})^2 & k_1 k2\ x\ \dot{x} & k_1 k3\ (\dot{x})^2 & k_1 k_4\ x\ \dot{x} \\ k_2 k_1\ x\ \dot{x} & k_2^2\ x^2 & k_2 k_3\ x\ \dot{x} & k_2 k_4\ x^2 \\ k_3 k_1\ (\dot{x})^2 & k_2 k_3\ x\ \dot{x} & k_3^2\ (\dot{x})^2 & k_3 k_4\ x\ \dot{x} \\ k_4 k_1\ x\ \dot{x} & k_4 k_2\ x^2 & k_4 k_3\ x\ \dot{x} & k_4^2\ x^2 \end{bmatrix}$$

It can be noted that only three types of terms appear in this matrix: namely, x^2, $\dot{x}^2$ and $x\ \dot{x}$. The average or expected value of x^2 and $\dot{x}^2$ is clearly positive, since they each represented squared sinusoids. However, the average value of $x\ \dot{x}$ is zero. Therefore, on the average, the $x\ \dot{x}$ terms do not contribute to their respective equations. Hence the equation for $\dot{\alpha}_1$ has strong coupling from $\Delta\alpha_3$. Likewise, $\dot{\alpha}_3$ has strong coupling from $\Delta\alpha_1$. A similar effect exists for α_2 and α_4.

6. EXPERIMENTAL RESULTS

The experimental work has been divided into two portions, as follows:

a) Computer experiments designed to explore and improve model matching techniques and to determine their limitations. These tests were performed by matching the output of a known system (a linear or nonlinear second-order differential equation) with that of a mathematical model of the same form, whose parameters were to be adjusted.

b) Application of the model matching techniques to actual human pilot tracking data, recorded on magnetic tape. The form of mathematical model used here was similar to that examined during development of the techniques.

The results will be presented in two major portions in accordance with classifications (a) and (b).

6.1 Experiments with Model Matching Techniques

In order to optimize the convergence time in the case where the system to be identified has fixed parameters, the behavior of the continuous model matching technique was examined for both sinusoidal and random inputs. In both cases the effect of adjustment gain, initial conditions, and criterion function on the adjustment path was examined. This study was initiated with sinusoidal inputs to facilitate analysis of the adjustment process.

6.1.1 Effect of Adjustment Gain

Consider first the effect of the adjustment gain on the time history of the parameters. The theoretical aspects of this problem were discussed in Section 5, and descent trajectories in the α_3-α_4 plane are shown in Figure 5-11 (for sinusoidal inputs) and Figure 5-13 (for random inputs). Corresponding time traces of the parameters α_3 and α_4 are shown in Appendix A in Figures A-2 and A-3. The behavior of the parameter traces in these figures is due to the nature of the gradient and the characteristics of the forcing function. The local variations of the parameters noticeable in Figures A-2 and A-3 therefore are characteristic of the process. Where they occur in subsequent examples they should be viewed with caution

since they do not necessarily indicate local time variations in the parameters being matched.

Referring again to the adjustment trajectories displayed in Figures 5-11 and 5-13 the effect of increased gain (K) is strongly noticed by comparison to low-gain trajectories. For K = 0.008 and 0.04 the adjustment rate is extremely small and the almost monotonic trajectories approximate a nearly ideal descent path. This behavior clearly shows the validity as well as the limitation of the basic assumption inherent in this approach to model matching, regarding the nature of gradient descent paths. A direct observation of units of time along the trajectory, and hence of the descent rate, is possible by counting the successive scallops formed by the oscillating gradient vector. Each scallop corresponds to a half-period (3.14 sec) of the sinusoidal excitation signal.

6.1.2 The Effect of Parameter Initial Values

The results obtained from this experiment are given in Figure 5-12 and have been discussed in Section 5.

6.1.3 Effects of Rate Terms in the Criterion Function

Margolis (8) has shown that improvement in stability and convergence time of continuous model matching processes is achieved if a term proportional to the rate of change of the matching error is added to the criterion function. To study this effect the criterion function

$$f = \tfrac{1}{2}\,(e + q\dot{e})^2 \qquad (6.1)$$

was adopted with q = const. Different values of q were used in the study to find optimum conditions.

In order to obtain rapid convergence (which is desirable for the tracking of time-varying parameters) it is necessary to increase the adjustment loop gain. However, the parameter adjusting loop becomes unstable when gain is increased. This effect is illustrated in Appendix A in Figures A-4 and A-7 for q = 0, that is, when no rate term is present in the criterion function. These figures illustrate the behavior of the four parameters for sinusoidal excitation at a frequency of 1.0 rad/sec.

The effect of increasing the contribution of the rate term is seen in Figures A-4, A-5, and A-6 for q equal to zero, 0.5, and 1.0, respectively.* The adjustment gain in each of these three figures is held at K = 8.0, that is, the value of gain is selected sufficiently high to cause oscillatory behavior of the parameter adjusting circuits in the absence of the rate term. As q is increased from zero a dramatic improvement in performance is evident. For q = 0.5, most of the oscillation in α_3 and α_4 disappears and the criterion function is essentially zero throughout the duration of the run. As q is increased to 1.0 the oscillation in parameter α_4 disappears entirely while that in α_3 is reduced to less than 5 percent of its maximum value. Convergence of the parameters to within 5 percent of the desired values occurs in approximately 3 seconds. These results show that high gain values yielding rapid convergence can be tolerated by the parameter adjustment circuits without instability only when the criterion function is augmented by a sufficiently large error rate term. It is interesting to note that in Figures A-4 and A-5 the oscillatory behavior of the parameters is not revealed by a mismatch of model output and system output.

The effect of the rate term q on parameter adjustment in the case of random excitation is illustrated in Figures A-7 and A-8. These results were obtained under the following conditions: The random input signal obtained from a Gaussian noise generator was filtered by a third order lag circuit with a break frequency of 1.0 rad/sec. Parameters α_1 and α_2 were held constant in order to minimize the interaction between parameters. The adjustment loop gain for parameters α_3 and α_4 was set at K = 16. This gain value resulted in instability for a sinusoidal input. The values of q used in Figures A-7 and A-8 were 0 and 0.5 respectively.

Figure A-7 shows instability of the parameter adjusting circuits in the absence of the rate term. It is interesting to note that due to the nature of the excitation signal there are portions of the tracking run when the parameters remain approximately constant and the matching error approaches zero. However, at times when the excitation makes large excursions the equilibrium is disturbed and the parameters begin to oscillate.

*Attempts at adjustment of four parameters under sinusoidal system excitation normally lead to indeterminacy of two of the parameters if q = 0. It was observed here that a sufficiently large rate term (q = 1.0) eliminates this condition, but an analytical explanation has not been found.

Figure A-8 shows the behavior of the system with q = 0.5. Parameters α_3 and α_4 converge to within approximately 5 percent of their correct values within one second but continue to exhibit small random oscillations ($\pm$ 5 percent from the correct value) during the entire run. The improved convergence time, as compared to the 3 second adjustment with the sinusoidal input, is probably due to the presence of higher frequencies within the excitation signal. It can also be noted that the system output and the model output are essentially equal, i.e., the matching error is nearly zero. Increasing the rate term to q = 1.0 does not result in further improvement of the parameter adjustment process.

6.1.4 Sinusoidal Variation of Parameter α_1

Results obtained when attempting to track a sinusoidal variation of parameter a_1 are shown in Figures A-9 and A-10. The experimental conditions imposed in each case were as follows:

Figure A-9: The system parameter a_1 was perturbed sinusoidally at a frequency of .1 radians per second. Model parameters α_2, α_3, and α_4 were held constant.

Figure A-10: Same perturbation of system parameter a_1 as in Figure A-9 but all four model parameters allowed to adjust.

The criterion function did not include a rate term in this instance. The results obtained are summarized as follows:

1) When only the model parameter is allowed to adjust which corresponds to the perturbed system parameter (in this case a_1), an acceptable parameter tracking performance is observed. Superimposed on the sinusoidal parameter variation of α_1 are random components which are introduced by the random excitation signal. Disturbances in the time history of parameter α_1 correspond to large excursions in the system and model output quantities.

2) When all four circuits are activated some undesirable side effects are observed (see Figure A-10): The sinusoidal perturbation of system parameter a_1 reflects not only in the model parameter α_1 but also in parameter α_3. Secondary cross-coupling effects are caused in turn by α_3 variation and tend to reduce the amplitude of oscillation in parameter α_1 to a new and incorrect value. Parameters α_2 and α_4 exhibit some

drift from their correct values, but their effect upon the criterion function is negligible. These phenomena have been adequately explained in Section 5.6 by the analysis of cross-coupling and relative accuracy of parameter determination.

6.1.5 Sinusoidal Variation of Parameter a_3

Attempts to track a sinusoidal variation of parameter a_3 are illustrated in Figures A-11, A-12, and A-13. During this experiment only model parameters α_3 and α_4 were allowed to vary, while parameters α_1 and α_2 were held fixed. The results are summarized as follows:

1) Attempting to track parameter a_3 with a low value of gain (K = 2.0) and q = 0 results in the curves of Figure A-11. It is apparent that parameter α_3 does not follow the sinusoidal perturbation of a_3. Furthermore, parameter α_4 drifts from its correct value to a new incorrect equilibrium position. The matching error, which is given in trace 8 of Figure A-11 is quite small when the corresponding scale is taken into account.

2) Increasing the gain to K = 16 with q = 0 results in the curves shown in Figure A-12. Evidently both parameters α_3 and α_4 become unstable and the match between system and model becomes considerably worse. As observed in previous results, there are periods of time during which the match is rather good, followed by periods of time when the random excitation signal causes uncontrolled parameter oscillations.

3) Figure A-13 shows the improvement obtained by adding a rate term (q = 0.5) to the criterion function while all other experimental conditions remain the same as in Figure A-12. The match between system and model outputs is excellent, and α_3 approximately tracks the sinusoidal oscillation in a_3. However, the effect of random excitation peaks is reflected again in random disturbances superimposed on the oscillation of parameter α_3.

6.1.6 Step Variations in Parameter a_3

Figures A-14 and A-15 show the behavior of the parameter tracking system when parameter a_3 is perturbed by step changes at a low and high frequency, respectively. The adjustment gain is K = 16, and q = 1.0. All four parameters are allowed to track. Consider first Figure A-14 which in effect corresponds to the behavior of the model matching technique

for fixed parameters since adequate time for parameter adjustment elapses before the values are changed. The match between system output and model output is excellent but a switching transient is observed in the matching error. Trace 8 which includes the effect of error rate exhibits this effect clearly.

In Figure A-15 parameter a_3 is perturbed by a square wave signal. It can be seen that the system and model outputs contain significant energy at frequencies approximately equal to the fundamental frequency of the square wave. Consequently, the behavior of parameter α_3 in the model varies from cycle to cycle, dependong on the corresponding initial conditions present in the random excitation signal. Cross-coupling of parameters is again evident, both in α_1 and in α_4.

6.1.7 Adjustment of Parameters in Nonlinear Models

The nonlinear system described was simulated on the analog computer. The adjustable model was identical in form to this system, and had seven adjustable parameters $\alpha_1, \alpha_2, \ldots\alpha_7$. Of particular interest in this portion of the study are the parameters characterizing the nonlinear terms of the model equation:

α_5 : coefficient of the cubic term x^3

α_6 : coefficient representing dead space

α_7 : coefficient representing saturation level.

The criterion function included the rate term $q\dot{e}$, where $q = 0.5$. The adjustment process of each parameter α_5, α_6, and α_7 was first studied separately.

1) The results of adjusting parameter α_5 are shown in Figure A-16. The presence of the cubic term in the system cannot become noticeable until the output variable y becomes large. Consequently, α_5 does not deviate substantially from its initial value until the random excitation causes large excursions in the system and model outputs. Total adjustment time is of the order of 5 seconds.

2) Adjustment of the deadzone parameter (α_6) is shown in Figure A-17. When the model deadzone is set to an initial value of zero, the initial excursions in the model output z are clearly too large. The adjustment process requires approximately three seconds to increase α_6 to its correct value.

3) The saturation level α_7 was adjusted manually due to a lack of computing channels required to perform automatic adjustment. The results of this manual adjustment process are shown in Figure A-18.

4) Figure A-19 shows the effect of simultaneous adjustment of the deadzone and the cubic term. The behavior exhibited here is typical of a number of runs performed. A relatively rapid initial adjustment of the deadzone is followed by a gradual adjustment of the cubic term. This effect can be expected: after adjustment of the deadzone the matching error becomes extremely small and relatively large excursions of the model output are required to further actuate the adjustment circuitry. The final adjustment of parameter α_5 to its correct value occurs at the point indicated by an arrow in Figure A-19, approximately 37 seconds after the beginning of the run, at a time when the matching error becomes sufficiently large to cause parameter adjustment. A slight cross-coupling between the parameters is also evident at this time. Since at this point the model output is too large this error can be corrected either by a decrease in the cubic term or by an increase in the deadzone width. Both effects are noticeable. Such interactions are typical under conditions where different parameters have a comparable effect on the output signal.

6.1.8 Effect of Additive Noise on the Parameter Adjustment Process

Random noise perturbations were added to the output of the system equation to simulate unmatched random fluctuations of the human operator's output in order to observe the effect of this disturbance on the model adjustment process. The additive noise can also be interpreted as measurement error occurring in the process of data handling, e.g., signal transmission, recording and playback of pilot output data.

The effect of the noise on the adjustment of one linear and one nonlinear parameter is illustrated in Figures A-20, A-21, and A-22. The parameters being adjusted are the coefficient α_3 of the input rate term, and the deadzone α_6. Figure A-20 shows the adjustment process with no additive noise. It can be seen that the rate term adjusts rapidly with the occurrence of peaks in the system output and that the adjustment is essentially complete for both parameters in approximately 10 seconds. The matching error is essentially zero after this time.

The effect of low frequency additive noise is illustrated in Figure A-21. It can be seen that both parameters deviate substantially from their correct values, due to the low disturbance frequencies (the noise signal input gain used here is c = 8).

A vastly different result obtained with wideband noise input having a bandwidth of 30 cps and an input gain c = 1 is shown in Figure A-22. The disturbances at high frequency observed in the system output and the error signal are very large but are filtered effectively by the parameter adjustment circuits. The two parameters α_3 and α_6 converge as rapidly as in the undisturbed case (Figure A-20) and reach their correct values. It must be noted that the gain of the noise disturbance is much lower than in the case shown for low frequency noise (Figure A-21). Noise signals with the same zero frequency spectral density were used in both cases.

6.2 Matching of Human Tracking Data

Model matching techniques were applied to human tracking data in each of the four main parts of the study and the results will be presented separately for each part.

6.2.1 Linear Invariant Models of Human Operators

The three methods (continuous, iterative, and relaxation) discussed in Section 4 were employed to determine the coefficients α_1, α_2, α_3, and α_4 by matching the solution of the linear equation (2.17) to human tracking data.

All three of the techniques employed can be considered successful in the sense that all converge to steady-state values of the four parameters in the model. The values of the parameters α_1, α_2, α_3, α_4, obtained are presented in graphical form in Figures 6-1, 6-2, and 6-3. These figures correspond to three different controlled element dynamics as indicated in the legend. The following observations are made:

1) The mean values of parameters obtained by the three adjustment strategies are not equal but the scattered data usually overlap. For parameter α_1 the continuous method yields smaller values than the other two. For parameter α_2 the iterative method yields the smallest value of the parameter. Parameter α_3 yields approximately equal values with

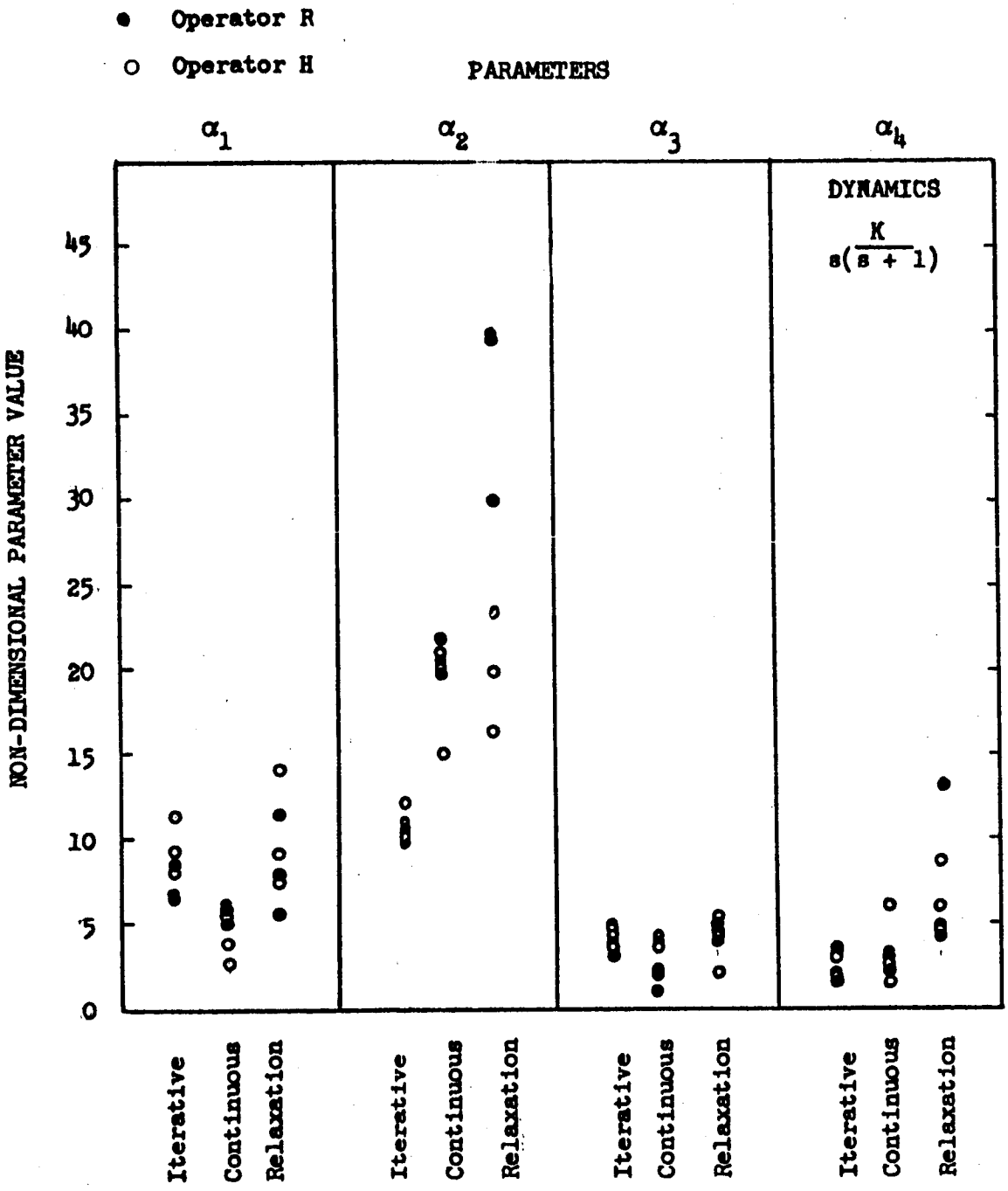

Scatter Graph of Experimentally Determined Parameter Values Using Three Adjustment Techniques

Figure 6-1

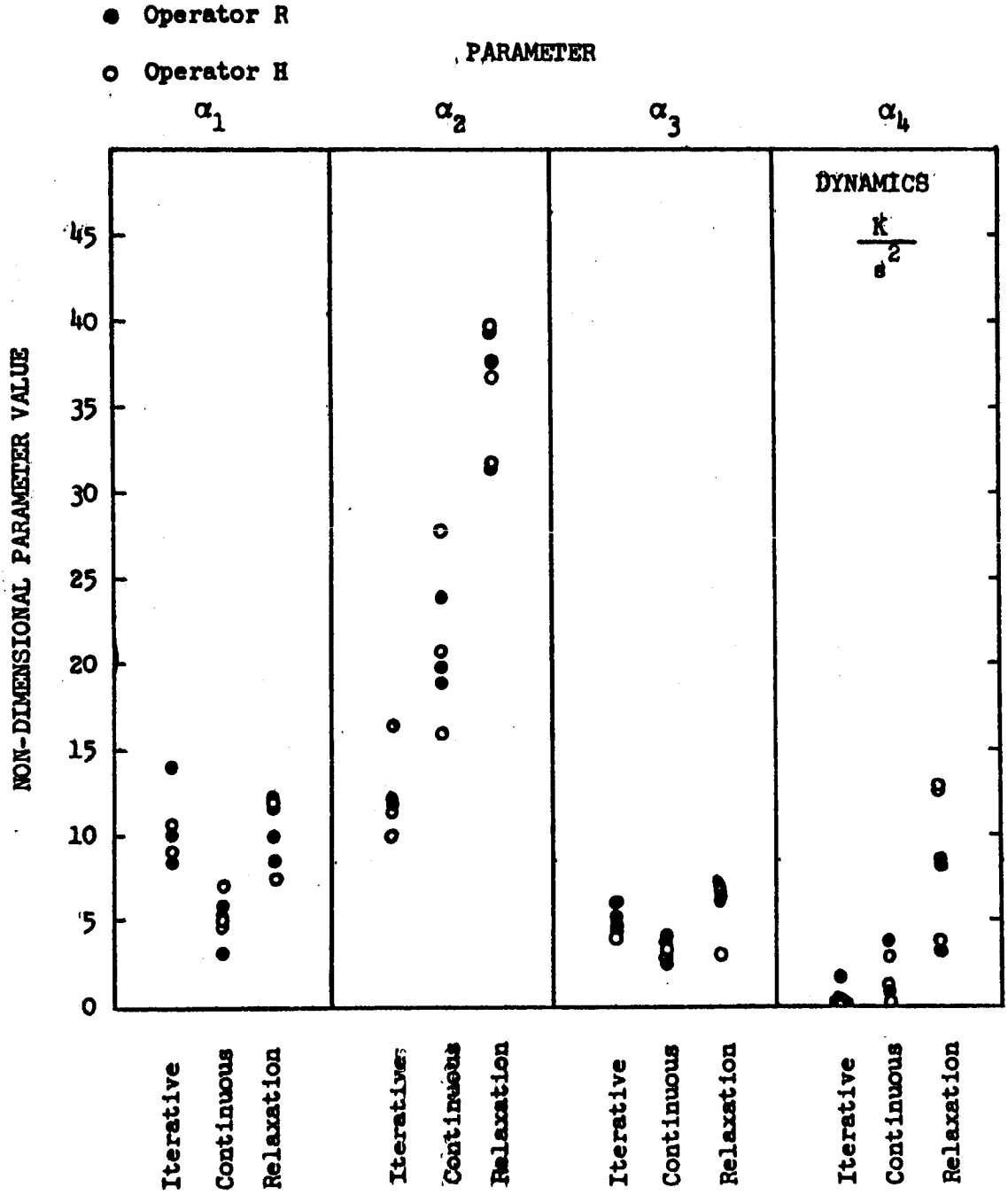

Scatter Graph of Experimentally Determined Parameter Values
Using Three Adjustment Techniques

Figure 6-2

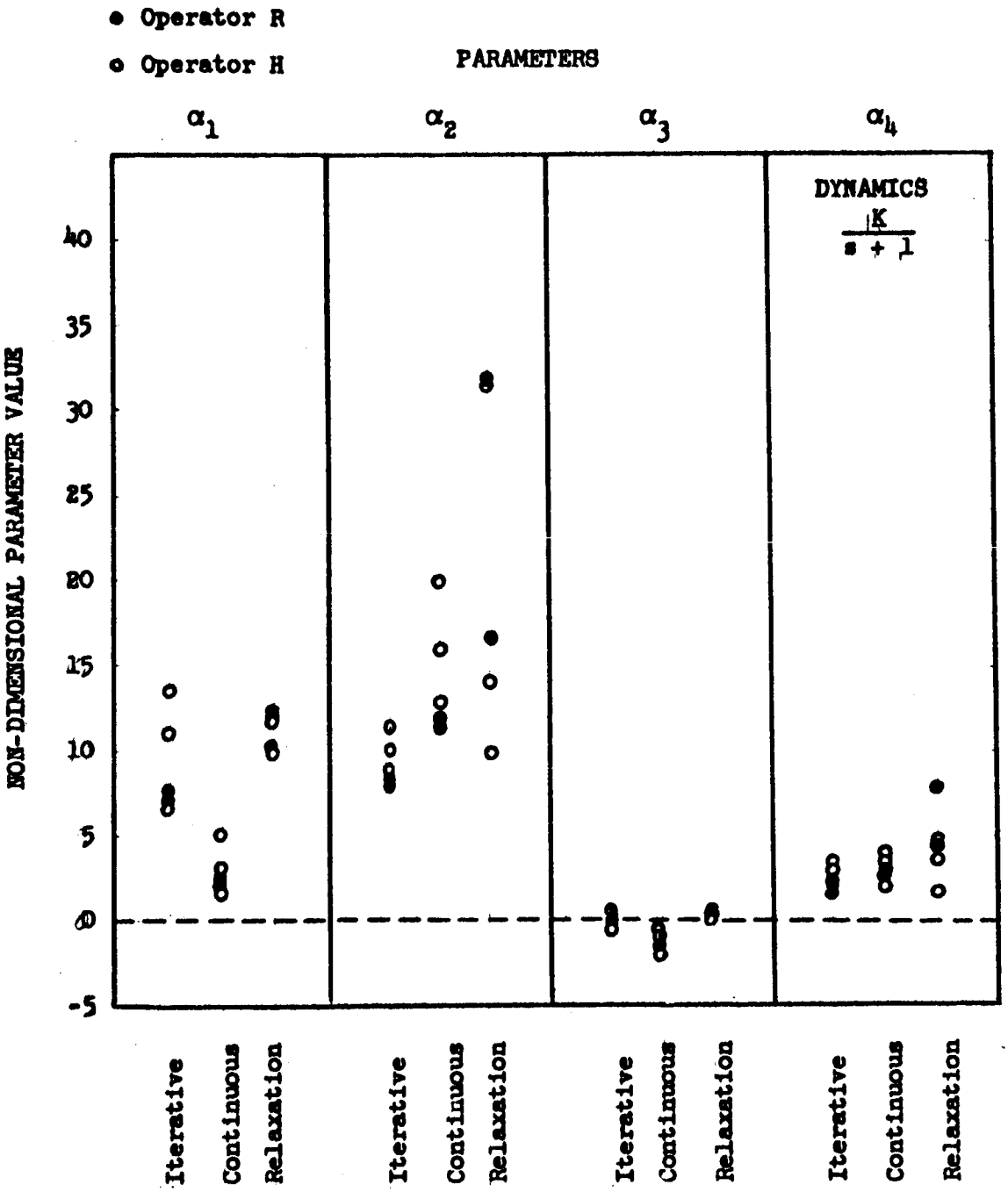

Scatter Graph of Experimentally Determined Parameter Values Using Three Adjustment Techniques

Figure 6-3

all three methods. A slightly higher value for parameter α_4 is obtained by the relaxation method. These differences have been partly explained in Section 5 in terms of the sensitivity of the error criterion to individual parameter deviations. It should be recalled here that the sensitivity u_3 exceeds all other sensitivities and u_2 is the smallest sensitivity, in terms of mean absolute values. The variances in α_3 and α_2 reflect this property.

2) The values of the parameters obtained with any one adjustment strategy vary from run to run and between operators. This variation is of the same order of magnitude as the variation between strategies. However, insufficient data are available to determine the statistical significance of the variations.

3) The values of parameters obtained with the two second-order dynamics (Figures 6-1, 6-2) are approximately equal. There is an apparently significant difference between these parameters and those obtained with first order dynamics (Figure 6-3). Intuitively one would expect that the easier first order task requires smaller lead compensation values α_3, on the average. This expectation is clearly confirmed by the data.

4) Parameter values for six typical runs, averaged over the three methods, have been tabulated and are shown in Table 6-1. Equivalent values of gain and time constants in the corresponding transfer function are also listed. The majority of the data yield complex roots in the denominator of the transfer function. However, at least two of these exhibit very small imaginary parts. The significance of these complex roots will be discussed in Subsection 6.2.3. The results from any two runs with the same dynamics are quite consistent. Greater consistency is found in the values of gain K obtained from any two runs than in the values of the time constants.

An interesting general conclusion regarding the sensitivity and ease of determination of the transfer function characteristics can be derived from the data obtained in this study. The numerator terms α_3, α_4 (and hence K_1 and T_1) can be determined with high accuracy. They are also very sensitive to the dynamics of the task, i.e., the human operator alters his responses readily to adapt his performance to the task. Conversely the denominator terms are difficult to determine but they do not

TABLE 6-1

AVERAGED PARAMETER VALUES OBTAINED FOR THREE CONTROLLED ELEMENT DYNAMICS

Controlled Element Dynamics	Run No.	Coefficients α_1	α_2	α_3	α_4	Elements of Transfer Function K_1	T_1	T_2	T_3
$\frac{12.5}{S(S+1)}$	1	6.3	19.0	3.67	5.8	.30	.63	.17+.15j	.17-.15j
	5	6.8	14.0	4.15	3.7	.26	1.1	.24+.11j	.24-.11j
$\frac{K}{S^2}$	7	8.3	23.0	3.4	2.3	.10	1.48	.18+.1j	.18-.1j
	12	9.5	23.0	5.5	1.8	.078	3.0	.21+.03j	.21-.03j
$\frac{K}{S+1}$	15	8.0	13.2	-.73	3.4	.26	-.21	.18	.42
	17	6.6	12.2	.067	3.0	.25	.022	.27+.082j	.27-.082j

change much as the control task is altered. These conclusions should have a major influence on the experimental design of future model matching studies.

6.2.2 Comparison with Previously Published Data

A comparison of these results with data published by Adams (2) is indicated in Table 6-2. The results are comparable. The restriction to real roots in Adams' study is due to the model transfer function format adopted by him. In comparing the data the following factors must be noted:

a) The excitation signal break frequency was 1 rad/sec in both studies. However, the STL study used a third-order filter while Adams presumably used a first-order filter.

b) The gain term in the definition of the dynamics cannot be compared without additional data. The STL gain includes the oscilloscope gain in volt/cm, thus yielding units of cm^{-1}. In Adams' notation the gain refers to the controlled element dynamics only thus yielding units of $volts^{-1}$.

TABLE 6-2

COMPARISON OF EXPERIMENTAL RESULTS WITH PUBLISHED RESULTS

Controlled Dynamics (CM^{-1})	Disturbance Break Frequency (rad/sec)	STL RESULTS (Operator H)				Controlled Dynamics (IN^{-1})	Published Results (Adams, (2), Pilots F & H)		
		K_1	T_1	T_2	T_3		K	T_1	$T_2=T_3$
$\frac{12.5}{s(s+1)}$	1	.26	1.1	2.4+.11j	2.4-.11j	$\frac{10}{s(s+1)}$	.25	2.0	.33
$\frac{12.5}{s(s+1)}$	1	.30	.63	.17+.15j	.17-.15	$\frac{10}{s(s+1)}$	.77	.85	.15
$\frac{12.5}{s^2}$	1	.078	3.0	.21+.03j	.21-.03j	$\frac{10}{s^2}$	.167	1.78	.22
$\frac{12.5}{s^2}$	1	.10	1.48	.18+.1j	.18-.1j	$\frac{10}{s^2}$	.62	1.0	.125

In STL's notation the α's are related to transfer function gain and time constants as follows:

$$K_1 = \frac{\alpha_4}{\alpha_2} \quad , \quad T_1 = \frac{\alpha_2}{\alpha_4}$$

T_2, T_3 are derived from the roots of the quadratic

$$\frac{1}{\alpha_2} s^2 + \frac{\alpha_1}{\alpha_2} s + 1$$

6.2.3 Occurrence of Complex Roots

Table 6-2 shows the occurrence of complex values of the parameters T_2, T_3 in the human operator transfer function that are derived from the coefficients α_1, α_2. On the other hand, Adams' results (2) are obtained from a transfer function model with denominator $(1 + \tau s)^2$. This formulation excludes the possibility of complex roots but postulates real-valued double roots. The following mathematical aspects are of interest and must be considered when comparing these data:

1) The complex roots T_2, T_3 are obtained from the characteristic equation of the human operator model expressed in terms of α_1, α_2

$$\frac{1}{\alpha_2} s^2 + \frac{\alpha_1}{\alpha_2} s + 1 = 0$$

Inaccuracy in the determination of α_1, α_2 therefore reflects strongly in the roots T_2, T_3, particularly if these roots are approximately equal.

2) The correspondence of the coefficients α_1, α_2 and the character of roots $s_2 = 1/T_2$, $s_3 = 1/T_3$ of the characteristic equation is shown in the α_1, α_2 plane (see Figure 6-4a) which delineates regions of real and complex roots as well as regions of instability. The stable quadrant ($\alpha_1 > 0$, $\alpha_2 > 0$) is mapped into a plane of real-valued and a plane of complex-valued roots s_2, s_3, as shown in Figure 6-4b and c. Curves of constant α_1 and α_2 values are plotted in these graphs; their intersections show the corresponding values of s_2, s_3. At the locus of double roots the α_1, α_2 curves intersect in cusps, making the location of the roots extremely sensitive to small α-variations.

3) The characteristics of the pilot model and the relative magnitudes of parameter influences analyzed in Section 5 explain the limited accuracy inherent in the determination of α_1 and α_2 which was confirmed experimentally as shown by the scatter plots (Figures 6-1, 6-2, and 6-3).

The combined effect of the above factors explains the apparent discrepancy in the denominator terms in the STL model and in Adams' model.

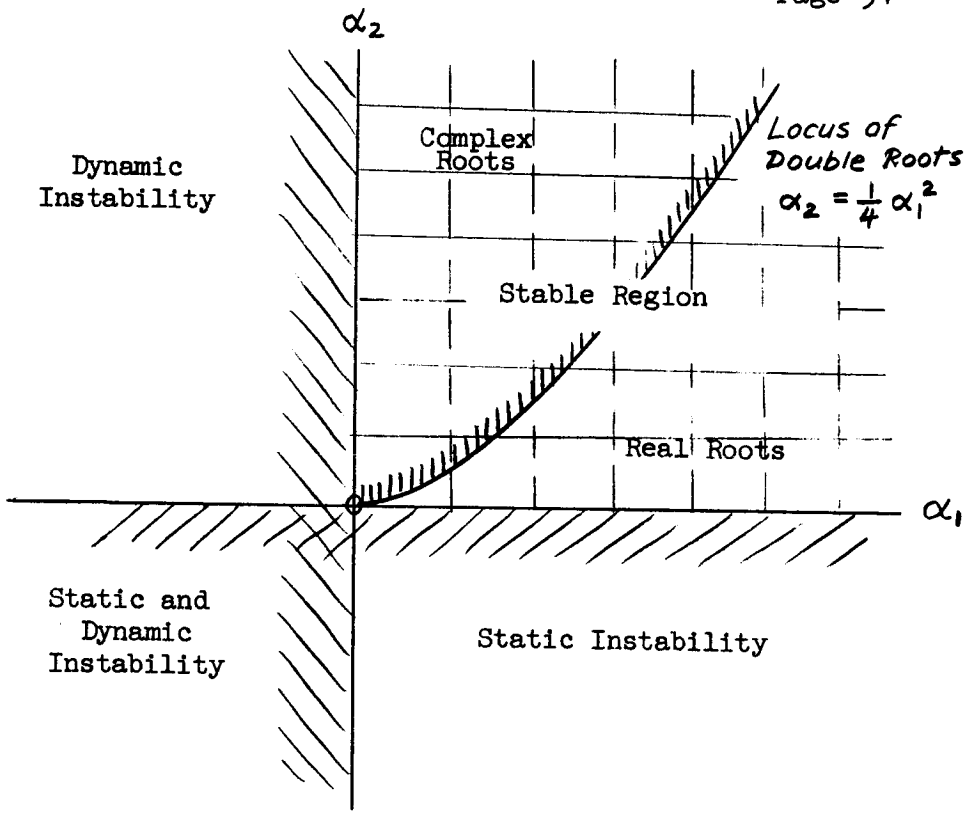

Figure 6-4a

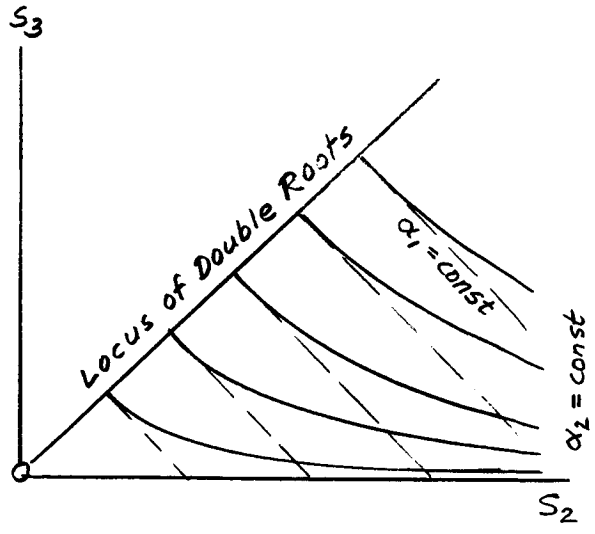

Real Roots

Figure 6-4b

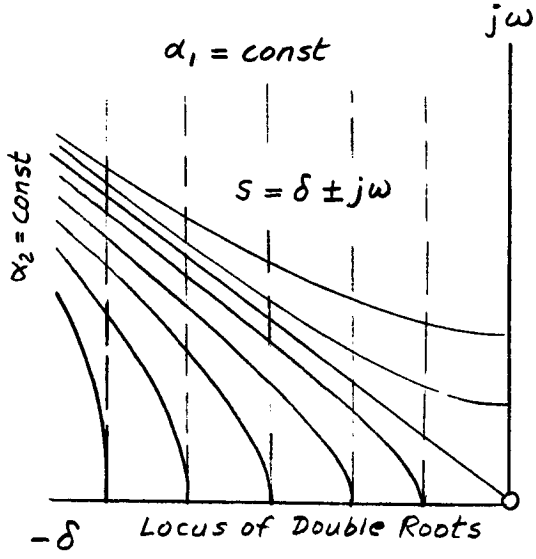

Complex Roots

Figure 6-4c

Figure 6-4

Regions of Real and Complex Roots
of Characteristic Equation

Time Recordings

The actual performance of each of the three methods can be examined more directly from the strip chart recordings obtained during typical runs; see Appendix A, Figures A-23 to A-27. The recordings contain the time history of the four parameters as well as inputs and outputs of model and human operator and the criterion function.

The iterative method is illustrated in Figures A-23a, 23b, and 24. Figure A-23a shows a computer run performed during one iterative cycle with all parameters held fixed. The corresponding iterative sequence is shown on a different time scale in Figure A-23. An essentially monotonic decrease of the criterion function F is exhibited by the envelope of the sawtooth curve, trace 5. The total time of convergence in this example is quite large since each iterative cycle required approximately 160 seconds, composed of four subcycles resulting in step adjustment of one parameter at a time. This time sequence is noticeable in Figures 23b and 24. In practical uses of the method a time compression of at least 50:1 would be possible with high-speed iterative analog computers.

Figure A-24 shows an iterative run where terminal limit cycle oscillations are observable in all parameters, but most notably in α_3 and α_4 which have the highest adjustment loop gain as previously discussed. In this case the finite step size $\Delta\alpha_i^{(k)}$ being maintained throughout the sequence was obviously too large. A refined technique would require a reduction of step size when the occurrence of limit cycles is registered by the computer. The oscillation may also be due in part to the fact that the gradient was computed using the finite difference approximation

$$\frac{\Delta F}{\Delta \alpha_j} = \frac{F(\alpha_1,\alpha_2,\ldots\alpha_j+\Delta\alpha_j,\alpha_n) - F(\alpha_1,\alpha_2,\ldots\alpha_j,\ldots\alpha_n)}{\Delta\alpha_j}$$

$$j = 1,2,\ldots n$$

rather than the influence coefficient method.

Typical results using the continuous method are shown in Figures A-25 and A-26.

The relaxation method was based on finding the minimum of the criterion function (on a digital voltmeter) and manual adjustment of the parameters. No attempt was made to improve the resolution of the voltmeter near the minimum, which explains a somewhat uncertain convergence to the final parameter values, as shown in Figure A-27.

Validity of the Results

The results show that all three methods considered yield parameter values which are approximately equal. However, the final values of the performance criterion function (in the iterative and relaxation methods) was seldom smaller than 30% of the values obtained with arbitrary initial parameter values. Furthermore, while the model output, after parameter adjustment, does resemble the human pilot's output, this resemblance is not sufficiently close to make the criterion function approach zero. The differences could be due to:

a) Omission of the time-delay (reaction-time) term known to exist in the human

b) Inadequate complexity of the model

c) Inadequate training and, hence, lack of consistency in tracking on the part of the operators.

6.2.4 Identification of Time-variant Human Operator Parameters

The continuous model matching technique was used to identify the parameters of a human operator in a tracking task so constructed that the operator's behavior became time-varying. The operator is expected to adjust his response to changes in the dynamics of the controlled elements. The controlled element gain and "time constants" were varied as functions of time as outlined in Section 3. The results for two different operators performing the same time-varying tasks are shown in Figures A-28 and A-29.

Consider Figures A-28a and b. Parameter α_1 does not reveal any well-defined pattern and can be considered approximately constant for the five-minute duration of the run. Parameter α_2 exhibits what appear to be significant changes. As the plant gain is increased parameter α_2 likewise increases while parameter α_4 decreases. As the plant is transformed into a double integrator, parameter α_2 further increases while parameter α_4 further decreases. The trend observed in parameter α_2 is essentially reversed in α_3 in the course of these plant variations. Effects of these changes manifest themselves in the tracking behavior: The operator's output, the second trace of Figure A-28b, shows that during the portions of the run when the loop gain was high the amplitude

of the operator's corrections was correspondingly lower. This behavior is to be expected since the same magnitude of correction can be obtained with a smaller stick displacement when the plant gain increases.

The effect of the observed time variations in parameters α_2, α_3 and α_4 is most clearly discernible in terms of the gain and lead time constant in the operator's mathematical model. It is assumed that at the end of each phase in the tracking run the model parameters are stationary. Average values of the parameters α_1 through α_4 were read at the times indicated in Figure A-28b as listed in Table 6-3.

TABLE 6-3

Indicated Time	Model Gain K_1	Lead Time Const. τ_n
t_1	.437	1.5
t_2	.278	1.9
t_3	.150	2.8
t_4	.443	1.5

As the difficulty of the task increases, i.e., as the plant gain increases and the dynamics is changed to a double integration, the operator's gain decreases and his lead time constant increases. In other words, the operator increases his effort of input prediction at the expense of output gain. As the plant is once again adjusted to its original condition the model parameters return to approximately their original values and the matching error again approaches its original value.

A similar pattern of behavior is observable in the records of Figures A-29a and b, except that the operator performing the task in this case exhibits a considerably greater variation in response than the previous one as is indicated by larger excursions in the parameter values. It is expected that longer training times would have resulted in smoother performance for both operators.

The results show the feasibility of using continuous parameter tracking techniques for the identification of time-varying human pilot parameters. However, considerable caution must be exercised in interpreting the parameter values in a time-varying model since these values are also influenced by such factors as the excitation signal, transients caused by particular initial conditions, and parameter interaction.

6.2.5 Matching a Nonlinear Model to Human Pilot Data

The continuous method was used to match the nonlinear model discussed in Section 3 against human operator tracking data. In order to minimize cross-coupling effects, only two parameters were adjusted simultaneously during one run. Following this parameter adjustment, a mean value for these parameters was obtained from the traces and used in following runs. The results of this process are shown in Figures A-30, A-31 and A-32. The input and output were obtained from approximately 30 seconds of human tracking data recorded on a magnetic tape loop. The following observations are made:

1) The addition of nonlinear terms α_5 and α_6 to the model reduces the model matching error. Evaluation of the integrated absolute error,

$$F_1 = \int_{t_1}^{t_1+T} \left| e + q\dot{e} \right| dt$$

over the last 30 seconds of each of the three runs yields

$$F_1 \hat{=} 2.2 \text{ cm}^2 \text{ from Figure A-30}$$

$$F_1 \hat{=} 1.9 \text{ cm}^2 \text{ from Figure A-31}$$

$$F_1 \hat{=} 1.5 \text{ cm}^2 \text{ from Figure A-32}$$

During the run shown in Figure A-32 the four linear parameters were held fixed at the mean values determined from the runs of Figures A-30 and A-31. The reduction in the error measure is taken as an indication that nonlinear effects in the pilot's response are at least partially taken into account by the nonlinear terms added to the model.

2) The role of the parameter associated with the cubic term α_5 in the model output is not sufficiently clear. In Figure A-32 α_5 is a small negative value for a portion of the run, then zero, and then a small positive value. Whether or not this variation represents in fact a change in human pilot characteristics cannot be determined without additional supporting data.

3) The deadzone term α_6 also varies both positively and negatively. A "negative deadzone" corresponds to a nonlinear characteristic known as "negative deficiency" (Figure 6-5). The adjustment of α_6 has the following effect: When the model output is too small, α_6 tends to become negative, thus causing in effect an amplification of the model output by increasing the magnitude of the input term x_d. When the model output is too large α_6 becomes positive thus causing a decrease in the magnitude of the input term and a corresponding attenuation of the output.

The results shown in these three figures indicate that continuous model-matching techniques can be used for the determination of parameters in nonlinear models of human pilots. The tracking records used in this portion of the study were obtained during an earlier phase of the program, where no attempt was made to induce or accentuate nonlinear behavior. The human operators would probably show clearer evidence of nonlinear behavior if the task had included nonlinear dynamics.

Block Diagram of Continuous Computation Scheme

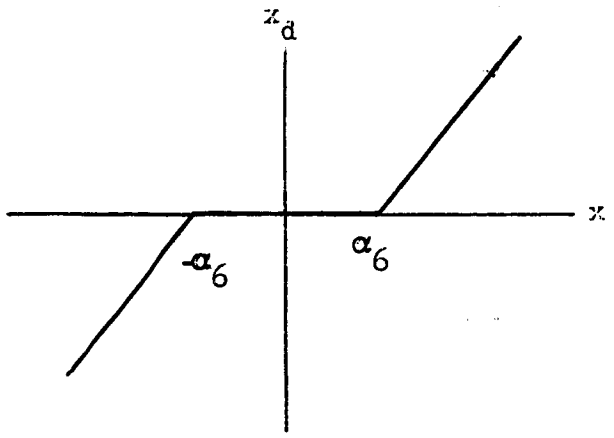

Dead Zone, $\alpha_6 > 0$

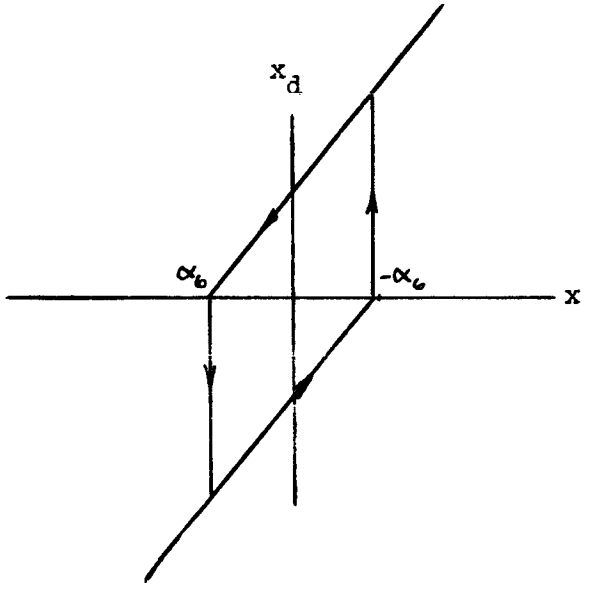

Negative Deficiency $\alpha_6 < 0$

Figure 6-5

6.2.6 Two-Axis Model Matching Results

As outlined in Section 3, the computer simultaneously adjusts the four parameters of a single-channel linear model which represents the input-output characteristics of the human operator in each axis of the two-axis task in the absence of cross-coupling. Figure A-33 shows the parameter values obtained when this model is matched to the horizontal tracking response. The parameters obtained from matching vertical axis tracking responses are shown in Figure A-34. The displayed error appears on channel 1, the pilot's output on channel 3 of these figures. The two traces exhibit a highly consistent tracking behavior, with the frequency and amplitudes of the operator's output not varying significantly during the run. Consequently, it is expected to find that the model parameters maintain approximately constant values. This result can indeed be observed in both figures on channels 4 through 8.

The validity of the model matching results presented in this section will be evaluated by examining the mean squared residual matching error defined by

$$\overline{e_h^2} = \frac{1}{T}\int_0^T e_h^2\, dt$$

where e_h is the error obtained by subtracting the model output for the horizontal axis from the pilot's horizontal axis output and T is the run length. Similarly, $\overline{e_v^2}$ represents the mean squared residual matching error in the vertical axis. The values of $\overline{e_v^2}$ abd $\overline{e_h^2}$ obtained for the runs of Figures A-33 and A-34 are given in Table 6-4.

TABLE 6-4

Values of Mean Squared Matching Accuracy in Horizontal & Vertical Axes

	Matching Accuracy		% of Human Power Output Accounted for by Model	
	$\overline{e_h^2}$	$\overline{e_v^2}$	Horizontal	Vertical
Variable Parameters	0.0115	0.0167	-	-
Fixed Parameters	0.0112	0.0180	63.0	82.7

The resulting residual error is approximately the same for fixed settings of the parameters at their approximate mean values and for parameters which are allowed to vary about the mean value. The percentage of human operator output power accounted for by the model is also listed. Since the model accounts for 82.7 percent of the total output power in the vertical case, and for 63.0 percent in the horizontal case, it can be considered a reasonably good representation of the human pilot's tracking characteristics in the two-axis case.

The effects of adjustment gain and error rate term on the mean squared error $\overline{e_v^2}$ are given in Table 6-5.

TABLE 6-5

Effect of K and q on Model Matching Accuracy

Gain, K	q	$\overline{e_v^2}$
0	0	0.0095
0.5	0	0.0092
1	0	0.0098
2	0	0.0122
0.5	0	0.0092
0.5	0.5	0.0088
0.5	1.0	0.0098

An increase in adjustment gain produces a poorer match to the human pilot's output than that obtained with low values of gain. This result probably is due to the larger parameter excursions from the optimum which result from increases in adjustment gain. The integrated effect of the parameter excursions results in an overall mean residual error which is larger than the one obtained with small parameter excursions. For comparison the result of a run made with fixed parameter values is included (K = 0) which shows a low value of residual error. The mean parameter values used in this run were determined by visual inspection of the tracking record and are not necessarily the true optimum.

Table 6-5 also shows the effect of the rate term $q\dot{e}$ on model matching accuracy. The results indicate a small improvement by selecting $q = 0.5$ which had been the optimum in previous portions of the study from a standpoint of stabilization of the adjustment process.

6.2.7 Comparison of Tracking Performance and Model Matching in One and Two Axes

An extensive number of measures of tracking performance were taken during the model matching runs in order to evaluate quantitatively the differences between operator performance in single-axis and in two-axis tasks. As discussed previously, two subjects were first asked to perform single axis tracking of horizontal and vertical motions of the display dot on the oscilloscope screen. The same subjects subsequently performed two-axis tracking tasks, and a comparison of the performance between these two situations was highly desirable. In addition, the following measures defining model matching accuracy were determined:

1. Mean square horizontal disturbance input $\overline{r_h^2}$
2. Mean squared vertical disturbance input $\overline{r_v^2}$
3. Mean squared horizontal tracking error $\overline{x_h^2}$
4. Mean squared vertical tracking error $\overline{x_v^2}$
5. Mean squared horizontal controller output $\overline{y_h^2}$
6. Mean squared vertical controller output $\overline{y_v^2}$
7. Mean squared residual matching errors $\overline{e_h^2}$ and $\overline{e_v^2}$

The mean squared tracking error in each axis can be used to evaluate the ability of the operator to perform the tracking task, while the mean squared residual matching error can be used to evaluate the degree to which the mathematical model serves to represent the pilot's performance. A tabulation of these measures and of the values of the four parameters obtained for each tracking run is given in Table 6-6.

The differences between performance in the one and two-axis tasks respectively can be seen most clearly by averaging mean squared tracking error values obtained in Table 6-6. The tabulation of these averaged values

TABLE 6-6

Flight No.	Operator	Run Length T	$\overline{x_H^2}$	$\overline{x_V^2}$	$\overline{r_H^2}$	$\overline{r_V^2}$	$\overline{e^2}$	$\overline{y_H^2}$	$\overline{y_V^2}$	Match %	a1	a2	a3	a4
1	H	305	0	0.258	0	19.2	0.0196	0	0.0805	75.6	6.40	26.00	4.40	6.40
2	R	300	0	0.223	0	23.2	0.0107	0	0.0825	87	6.00	26.00	4.00	8.00
3	H	308	0	0.279	0	16.4	0.0212	0	0.0971	78	6.00	28.00	4.00	8.00
4	R	303	0	0.187	0	16.5	0.0111	0	0.0915	87	6.00	28.00	5.60	10.40
5	H	308	0	0.213	0	19.6	0.0190	0	0.0972	80.5	5.00	28.80	5.00	10.00
6	R	304	0	0.191	0	21.3	0.0132	0	0.0997	86.7	5.00	26.00	5.00	10.40
7	H	304	0.104	0	10.8	0	0.0167	0.0390	0	57	5.60	28.80	4.00	10.40
8	H	306	0.100	0	11.1	0	0.0170	0.0448	0	62	4.80	30.00	4.00	10.80
9	H	305	0.080	0	12.3	0	0.0205	0.0487	0	58	6.00	34.00	6.00	12.40
10	R	303	0.150	0	8.1	0	0.0113	0.0485	0	76.8	4.00	30.00	3.00	12.40
11	R	301	0.114	0	11.9	0	0.0127	0.0460	0	72.4	5.00	28.80	4.40	11.20
12	R	302	0.084	0	11.6	0	0.0151	0.0521	0	71.1	5.60	32.00	5.00	12.00
13	H	297	-	0.316	-	11.6	0.0122	-	0.0600	79.6	4.00	34.00	2.00	9.00
13	H	-	0.153	-	11.0	-	0.0190	0.0594	-	68	3.60	36.00	2.40	14.00
14	R	301	-	0.237	-	10.9	0.0141	-	0.0613	77	3.40	32.80	1.60	9.00
14	R	-	0.131	-	7.20	-	0.0199	0.0461	-	57	2.80	26.00	2.40	14.00
15	H	305	-	0.176	-	15.9	0.0176	-	0.0735	76	7.00	28.00	5.00	14.00
15	H	-	0.113	-	8.7	-	0.0233	0.0880	-	73.5	5.00	36.00	5.00	20.00
16	R	301	-	0.25	-	11.2	0.0112	-	0.0650	82.7	4.00	26.00	2.00	7.00
16	R	-	0.115	-	5.95	-	0.0180	0.0486	-	63.0	3.00	40.00	3.00	16.00
17	H	301	-	0.179	-	13.8	0.0145	-	0.0718	79.8	5.00	32.00	4.00	9.00
17 *	H	-	0.101	-	10.2	-	-	0.0860	-	-	—	—	—	—
18	R	300	-	0.284	-	24.5	0.0197	-	0.0858	77	4.00	32.00	2.00	9.00
18	R	-	0.113	-	11.5	-	0.0170	0.0687	-	75.2	4.00	36.00	5.00	15.00

* Parameters fluctuate

Mean Squared Values for Single and Two-axis Tracking

is given in Table 6-7. A significant increase in normalized mean squared tracking error is observed for both operators in the two-axis task as compared with single axis tracking. Normalized performance measures

$$\left[\overline{x_h^2}\right]_n = \frac{\overline{x_h^2}}{\overline{r_h^2}} \qquad \left[\overline{x_v^2}\right]_n = \frac{\overline{x_v^2}}{\overline{r_v^2}}$$

are obtained by using the total power in the input signal as a normalizing factor. The use of such a normalizing factor is consistent with previous work published in the literature. The increase in normalized mean squared tracking error ranges from 20 to 67 percent, and reflects the increase in the difficulty of the task when the second axis is added.

Table 6-7 shows average values of the parameters obtained for both axes and both operators. The parameters values obtained in a particular axis are remarkably consistent, i.e., the α's obtained for the vertical axis from both operators H and R are approximately equal. Likewise, the horizontal axis results for both operators are in close agreement. In view of the rather wide differences in normalized mean squared tracking error between the operators this consistency in the models indicates that variations in tracking performance cannot be described completely by the linear time-varying mathematical model assumed here.

Asymmetry between performance in the two axes is revealed by the degree to which a mathematical model is capable of representing a pilot's performance in each axis. Table 6-8 lists $(\overline{e_h^2})$ and $(\overline{e_v^2})$ obtained for both operators normalized with respect to the mean squared tracking error in each case. Input mean squared tracking error rather than the disturbance input were used as normalizing factors in this case since the tracking error is in fact the input signal to both pilot and model in the model matching configuration of Figure 2-1. Table 6-8 lists values of $(\overline{e_h^2})_n$ and $(\overline{e_v^2})_n$ averaged among all runs for both operators in the respective axes. It is observed that $(\overline{e^2})_n$ is considerably smaller in the vertical axis than in the horizontal axis, both in single axis tasks and for the

TABLE 6-7

Comparison of Mean Squared Matching Accuracy
for One and Two-axis Tasks

	Operator	Normalized Mean Square Tracking Error		Mean Parameter Values				Axis	K_1
		Horiz.	Vert.	α_1	α_2	α_3	α_4		
Single Axis	H	.0083	.0136	5.8	27.6	4.2	8.0	v	.29
				5.4	30.8	4.6	11.2	h	.36
	R	.011	.0099	5.6	26.0	4.8	9.6	v	.37
				4.8	30.0	4.2	11.8	h	.39
Two-axis	H	.0122	.0163	5.3	31.4	3.68	8.6	v	.27
				4.3	36.0	4.7	17.0	h	.47
	R	.0146	.0166	3.8	30.3	1.9	8.4	v	.28
				3.27	36.3	3.5	15.0	h	.41
Percent Increase	H	47%	20%						
	R	33%	67%						

TABLE 6-8

Comparison of Normalized Matching Accuracy for Two Operators

Operator	$\overline{(e_h^2)}_n$	$\overline{(e_v^2)}_n$	
H	.19	.080	One-axis
R	.112	.060	One-axis
H	.172	.067	Two-axis
R	.150	.058	Two-axis
$\overline{(e^2)}_n$ Average of Two Operators			
One-axis	.150	.070	
Two-axis	.160	.062	
Percent of Total Operator Output Power Not Matched by Model $\frac{\overline{e^2}}{\overline{y^2}}$			
Operator	Horiz.	Vertical	
H	41.0	21.7	One-axis
R	27.0	12.7	One-axis
H	27.2	21.6	Two-axis
R	33.6	21.2	Two-axis

vertical axis of the two-axis task. In other words the mathematical model represents the operator's performance in the vertical axis more satisfactorily than in the horizontal axis. The cause of this lack of symmetry in the performance of the two tasks requires further investigation. A controlled experiment may be required in order to isolate pertinen effects such as mismatch between design characteristics of the two axes of the hand controller which might contribute to the asymmetry. This result is confirmed also by a comparison of the values $\frac{\overline{e^2}}{\overline{y_h^2}}$ and

$\frac{\overline{e_v^2}}{\overline{y_v^2}}$ which represent the fraction of the total operator's output which is not matched by the model (bottom of Table 6-8).

6.2.8 Cross Coupling Between Axes

As discussed in Section 3, two types of cross-coupling between axes were considered: perceptual (or input) cross coupling and motor (or output) cross coupling. An extensive visual search of the tracking records for each run of the two-axis task was made to identify possible cross-coupling effects between the perceptual input in the vertical axis on the motor output in the horizontal axis (and vice versa). Such an examination of the tracking record should reveal disturbances in the horizontal output resulting from a disturbance in the vertical input when no such disturbance appears in the horizontal input. After finding tracking records which show this type of cross-coupling, the corresponding terms were introduced into the model, and parameter matching was performed over the entire length of the tracking run. The resulting values of $\overline{e_h^2}$ were compared with the value of $\overline{e_h^2}$ obtained when no cross-coupling terms were employed. It was anticipated that this comparison would yield evidence of the existence of cross-coupling terms of the form

$$\beta_1 y_v,\ \beta_3 x_v,\ \text{and}\ \beta_4 \dot{x}_v$$

in the horizontal model. However, the resulting tracking records did not show clearly defined or consistent values of the cross-coupling terms for the entire length of the tracking record. The corresponding value of the mean squared residual error actually shows a slight increase as a result of introducing the β_3 cross-coupling term into the mathematical model. Similar results were observed for the β_1 and β_4 cross coupling terms. In general, the introduction of the cross-coupling terms appeared to be detrimental to overall model matching in terms of residual mean square error. During the search for cross-coupling terms, the α parameters were held fixed at their average values in order to eliminate possible interaction of the adjustment loops.

Some of the tracking records indicated values of β_3 which remained approximately constant for periods ranging from 20 to 60 seconds. A typical run showing this effect is given in Figure A-35. The cross-coupling coefficient β_3 has a reasonably constant value extending from $t_1 \cong 130$ seconds to $t_2 \cong 204$ seconds at values between 1.2 and 1.6 units. The effect of introducing the cross-coupling term into the model of the human operator during this interval results in approximately 10% reduction in $\overline{e^2}$ as shown in Table 6-9. This decrease of $\overline{e^2}$ indicates the existence of cross-coupling for short periods of time. Similar reductions of $\overline{e^2}$ were observed for other short duration runs.

TABLE 6-9

Effect of Cross-Coupling Term βx_v
on Model of Horizontal Axis Response

Run	β_3	$10\int_{t_1}^{t_2} e^2\,dt$	t_2-t_1	$\frac{10}{t_2-t_1}\int_{t_1}^{t_2} e^2\,dt$	Ave.	Dif.	%
1	0	14.59	74	.1972			
2	0	14.49	74	.1958	.1961	.0180	9.2
3	0	13.69	70	.1955			
4	1.6	12.79	72	.1776			
5	1.6	12.60	73	.1726	.1781		
6	1.6	13.63	74	.1841			

$t_1 \cong 131$ sec $t_2 \cong 204$ sec

In summary, the model matching technique used in this study is suitable for detection and quantitative determination of cross-coupling which occurs in the responses of the human operator in two-axis tracking. Additional research is required to determine human cross-coupling effects in realistic tracking situations which may be caused by the dynamic characteristics of the controlled element. The task studied here did not include conditions which would evoke a more consistent coupling in operator responses.

6.2.9 Closed-Loop Characteristics of Human Dynamic Response

The closed-loop stability of the model was examined for a single axis task and one axis of the two-axis task. Results showed only a minor shift in the closed-loop poles with little effect on system stability.

The human dynamic response equation obtained from a typical single-axis tracking run is given by

$$G_1(s) = \frac{Z}{X} = \frac{.29\ (.525\ s + 1)}{(.036\ s^2 + .21s + 1)}$$

whereas a typical case of two-axis tracking yielded

$$G_1(s) = \frac{Z}{X} = \frac{.269\ (.286\ s + 1)}{(.0385\ s^2 + .154\ s + 1)} .$$

In both tasks the controlled element dynamics was characterized by

$$G_2(s) = \frac{10}{s\ (s + 1)} .$$

The resulting characteristic equations of the closed-loop system are

$$.036s^4 + .246\ s^3 + 1.21\ s^2 + 1.52\ s + 3.9 = 0$$

for the single axis case, and

$$.0385\ s^4 + .1925\ s^3 + 1.154\ s^2 + 1.769\ s + 2.69 = 0$$

for the two-axis case.

The closed loop poles obtained from these characteristic equations are given below:

Single-axis Task (vertical)	Two-axis Task (vertical axis)
$s_1 = -1.55 + 4.0j$	$s_1 = -1.67 + 4.29j$
$s_2 = -1.55 - 4.0j$	$s_2 = -1.67 - 4.29j$
$s_3 = -.315 + 2.04j$	$s_3 = -.83 + 1.62j$
$s_4 = -.315 - 2.04j$	$s_4 = -.83 - 1.62j$

These data signify stable closed-loop operation, in agreement with the stable performance observed in all single and two-axis human tracking experiments performed in this study. Other researchers in the field have obtained unstable roots from parameter identification studies of two-axis tracking data that appeared stable on inspection.* A more comprehensive investigation of this point should be desirable.

* Verbal communication by Mr. M. Sadoff of NASA Ames Research Center.

7. CONCLUSIONS AND RECOMMENDATIONS FOR FURTHER STUDY

Automatic adjustment techniques for determining the parameters of dynamic models of the human operator have been investigated experimentally and analytically with emphasis on developing practical computer methods for this task. These techniques operate in the time domain and determine the parameters of linear or nonlinear differential equations which match human operator output data by minimizing a selected error criterion by a gradient or steepest descent process. This approach avoids any constraints of linearity and time-invariance of the dynamic model which are frequently found in methods used by other researchers. The use of transfer functions or describing functions to characterize the human operator's input-output relationship has been included only where it was strictly applicable: in such cases the differential equation parameters and the transfer function parameters obtained in similar tracking tasks were found comparable.

The study proceeded from parameter matching of linear time-invariant and time-variant models (Parts 1 and 2) of the human operator in a single-axis tracking situation to nonlinear models (Part 3). In each case the necessary confidence in the model matching technique was developed by first applying the technique successfully to a system with known parameters before attempting the more exacting task of matching human operators' data. The final part consisted in matching human output data in a two-axis tracking situation characterized by symmetrical and uncoupled dynamics of the controlled element. In all situations considered in this study the operator performed a compensatory tracking task by observing tracking errors displayed on an oscilloscope screen and by manipulating a 2-axis fingertip control stick to null the error.

This study was primarily concerned with methods development rather than with obtaining and cataloguing human operator performance data. Inasmuch as the method of automatic model matching has been developed to the point of providing consistent human operator parameters with small residual model matching errors it will be desirable in further studies

to apply the method to an evaluation of human performance data in a systematic manner in tracking and control problems of practical interest.

Significant experimental results obtained in this study include: the improvement of stability characteristics of the parameter adjustment loops by introducing an error rate term into the criterion function; the demonstration of parameter tracking in time-variant dynamic models; the ability to determine parameters of nonlinear models; and the development of techniques for determining cross-coupling coefficients in two-axis tracking data. The most important theoretical results include the explanation of the continuous gradient adjustment process and of fluctuation of the local gradient vector in the parameter space. The influence of excitation frequencies and adjustment gain on the dynamics of the adjustment process was analyzed. This clarified the source of transient peaks in the time histories of individual parameters. In addition, the nature of dynamic interaction of individual adjustment loops and the differences in relative adjustment gain were analyzed and expressed in terms of the sensitivity matrix which governs the adjustment rate of each of the parameters being simultaneously optimized.

Results of primary interest regarding computer programming included the simplification of computer channels which yield the influence coefficients u_i (e. g., only one sensitivity equation and one model equation is needed to yield the four influence coefficients of the basic linear model); computer techniques for iterative and sequential model matching; computer techniques for detecting and measuring cross-coupling phenomena; and computer programming for determining the parameters of analytic and nonanalytic nonlinear characteristics which may be present in the model structure, such as deadspace, limiting, relay switching, and hysteresis effects.

It is recommended that future research into model matching of human operators be addressed to two areas in general:

1) the study of advanced methods of model matching including methods which were outside the scope of the above investigations.

2) the study of human tracking performance in tasks of practical importance, including multi-axis tasks with essential cross-coupling.

The results of the above investigations permit the use of continuous and iterative model matching techniques with increased confidence in manual control and tracking situations which can conveniently be described in terms of differential equations rather than by transfer functions. This removes the restrictions on linearity and time-invariance of the model imposed by other techniques currently in use and simplifies the manipulation of model equations in deriving influence coefficients.

The mean-square tracking error as well as the parameters of the operator's mathematical model yield important measures of tracking performance and should be considered as related aspects in the description of human tracking capability. Determination of quantitative relations between these measures should be of great theoretical and practical interest. The tracking error also yields quantitative information on the stationarity of the operator's tracking behavior as well as on the stationarity of the controlled system dynamics. It can, for example, provide important cues on the state of training of the operator which in turn may explain fluctuations occurring in the parameters of the mathematical model.

A second measure of importance which should be the subject of further research is the model matching error itself. This error term can yield much information on missing elements in the mathematical model in addition to registering the quality of model matching performance. The relative power in the model matching error as compared to that of the tracking error provides a quantitative measure of model matching accuracy which is often more significant than the absolute power. This relationship was briefly explored in the 2-axis tracking results of Phase 4 but should be further investigated in any subsequent studies.

An aspect of great significance which should also be studied for a better understanding of human tracking performance in multi-axis tasks is the reception and interpretation of displayed stimuli by the operator. Clearly, the presentation of specific stimuli such as vertical and horizontal dot excursions on an integrated display instrument is an idealization

seldom encountered in practice. The stimuli received may be more diffuse, including visual cues from flight instruments, visual cues from the extra-vehicular scene, plus kinesthetic and proprioceptive feedback stimuli. The significant effect of additional motion cues on pilot tracking performance has been demonstrated by the interesting results of Adams' study (19). Practical considerations of vehicle control and of the controller characteristics should also be included in plans for further studies with emphasis on clear definition of pilot input stimuli.

APPENDIX A

Model Matching Time-Histories

The sample time-histories presented in this Appendix were selected to exhibit significant characteristics of the parameter optimization processes studied experimentally. These specimens serve to illustrate the analytical results discussed in Section 5 of this report and support the conclusions derived from the experimental study presented in Section 6. The reader will find detailed explanations in the latter section. Symbols used to designate output variables in the oscillograph records can be identified by reference to the block diagram, shown in Figure A-1.

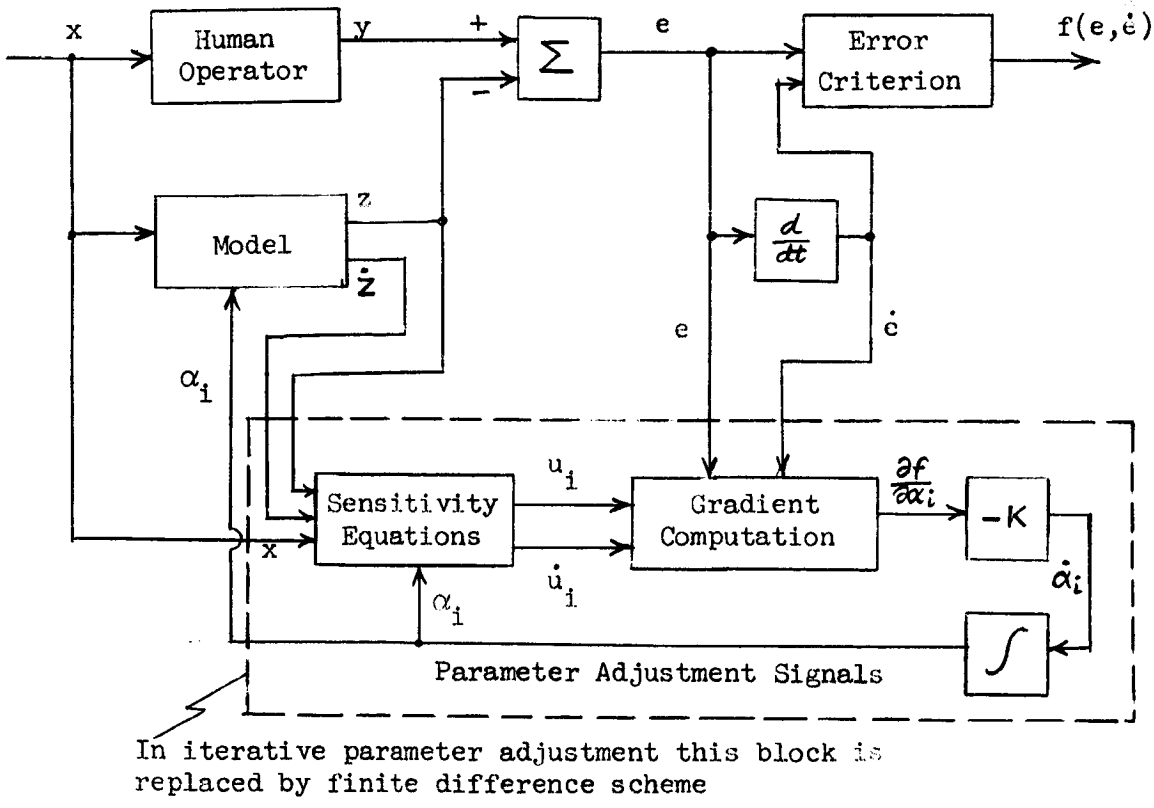

Figure A-1

Elements of Model Matching Technique

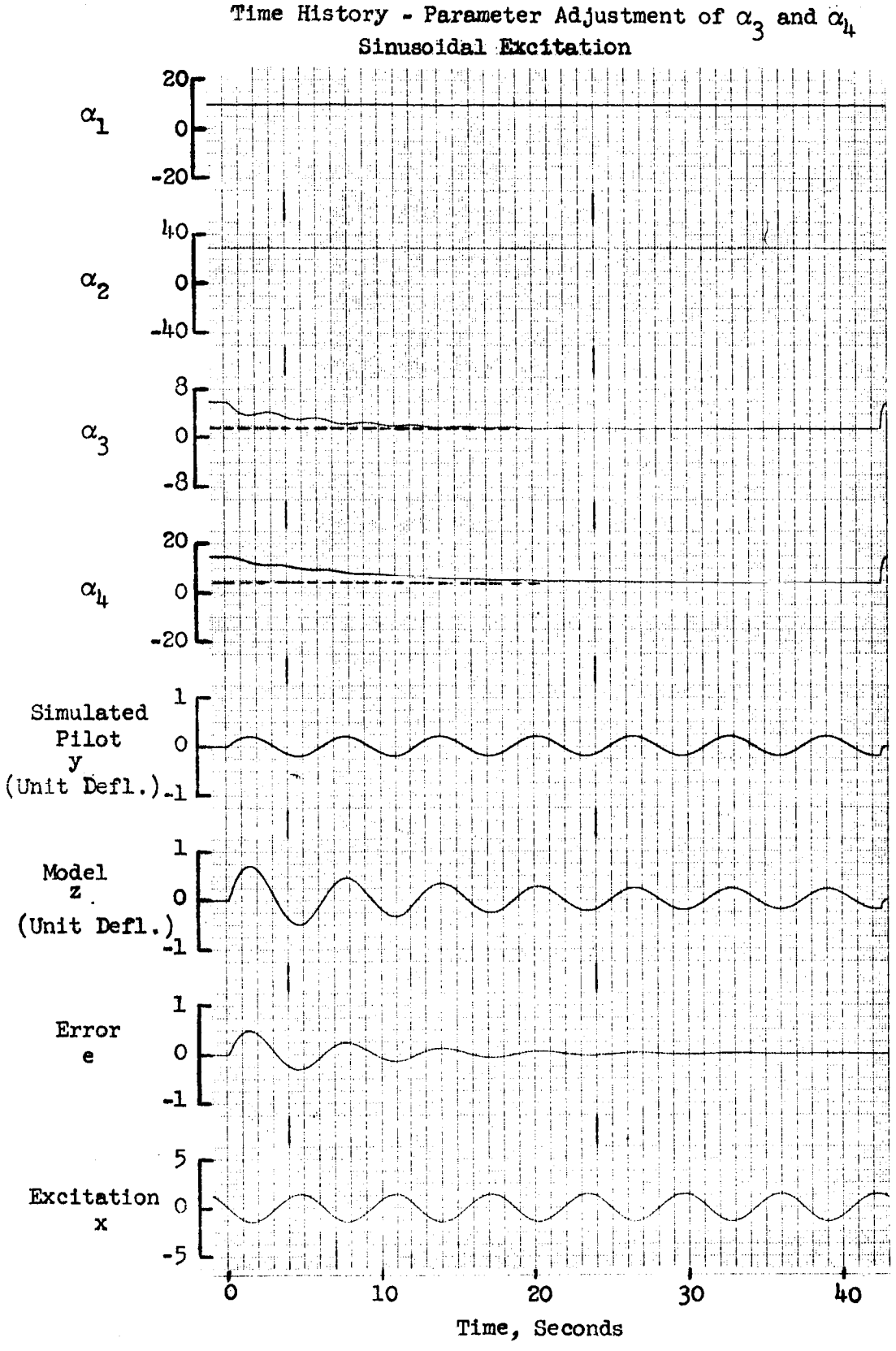
Time History - Parameter Adjustment of α_3 and α_4
Sinusoidal Excitation
α_1
20
0
-20
α_2
40
0
-40
α_3
8
0
-8
α_4
20
0
-20
Simulated Pilot y (Unit Defl.)
1
0
-1
Model z (Unit Defl.)
1
0
-1
Error e
1
0
-1
Excitation x
5
0
-5
0
10
20
30
40
Time, Seconds

Figure A-2

Time History - Parameter Adjustment of α_3 and α_4
Random Excitation

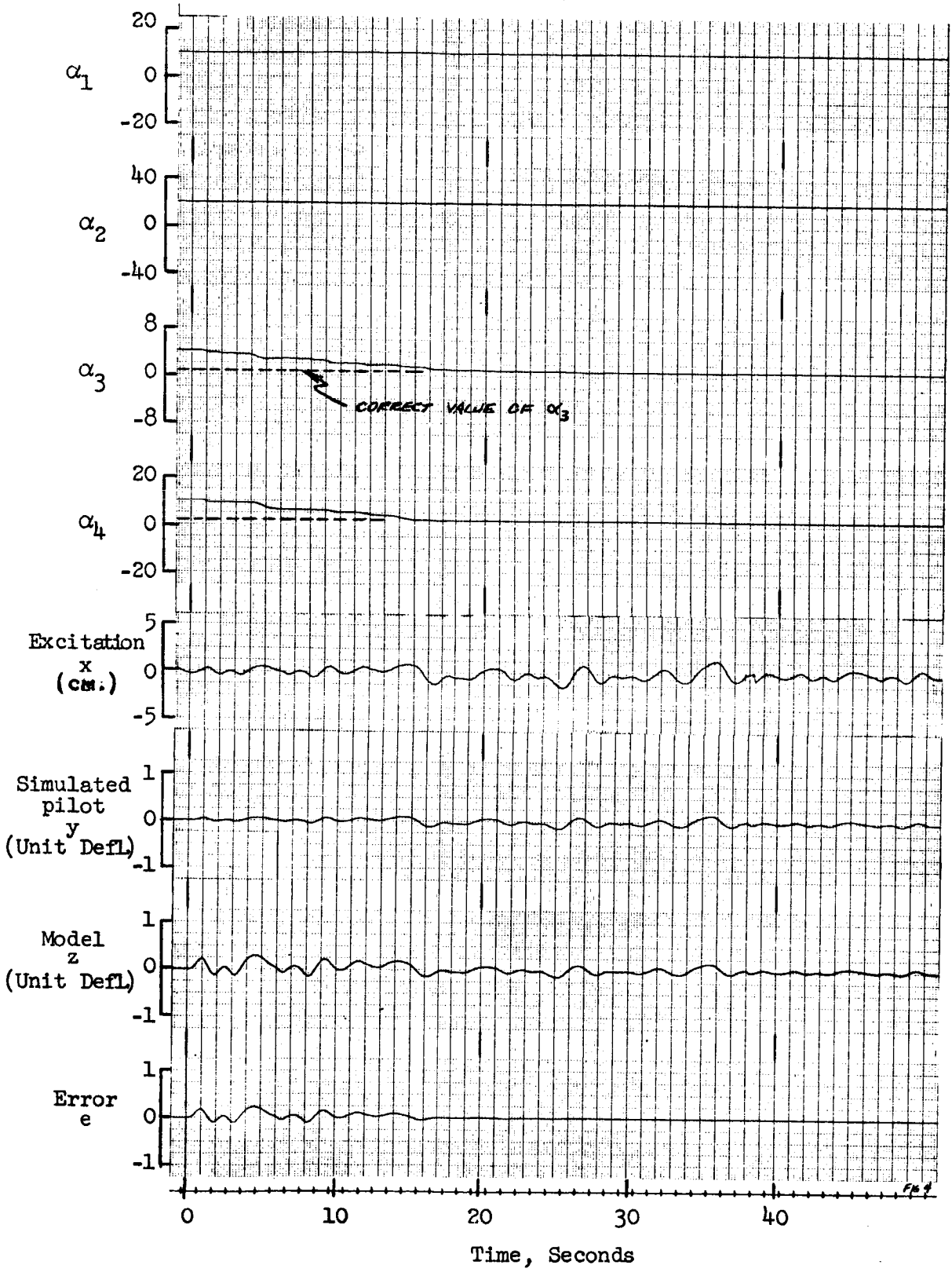

Figure A-3

Effect of Error Criterion on the Time History of
Parameter Adjustment - Sinusoidal Excitation
K = 8 q = 0

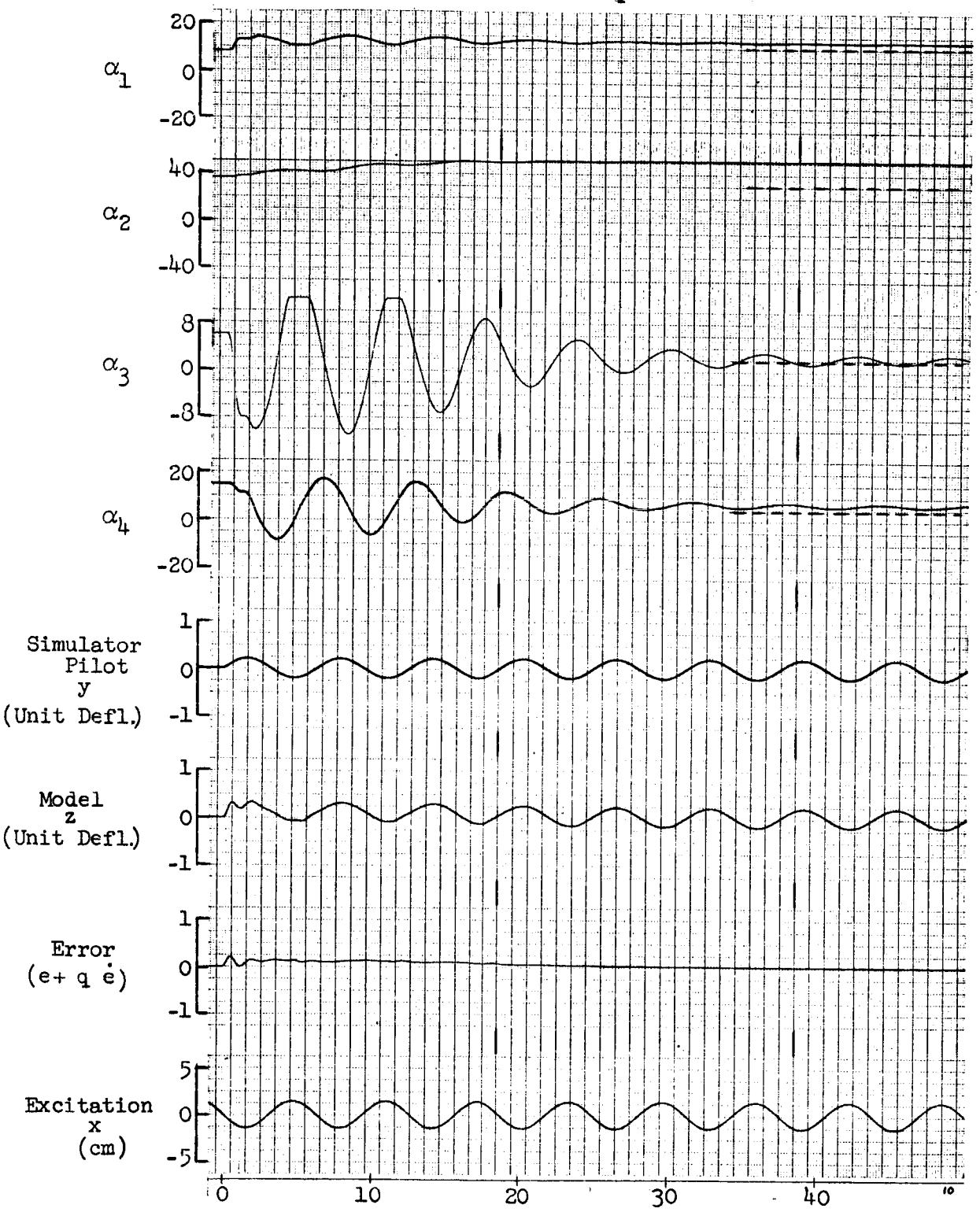

Figure A-4

Effect of Error Criterion on the Time History of Parameter Adjustment - Sinusoidal Excitation
K = 8 $\mathbf{q}$ = .5

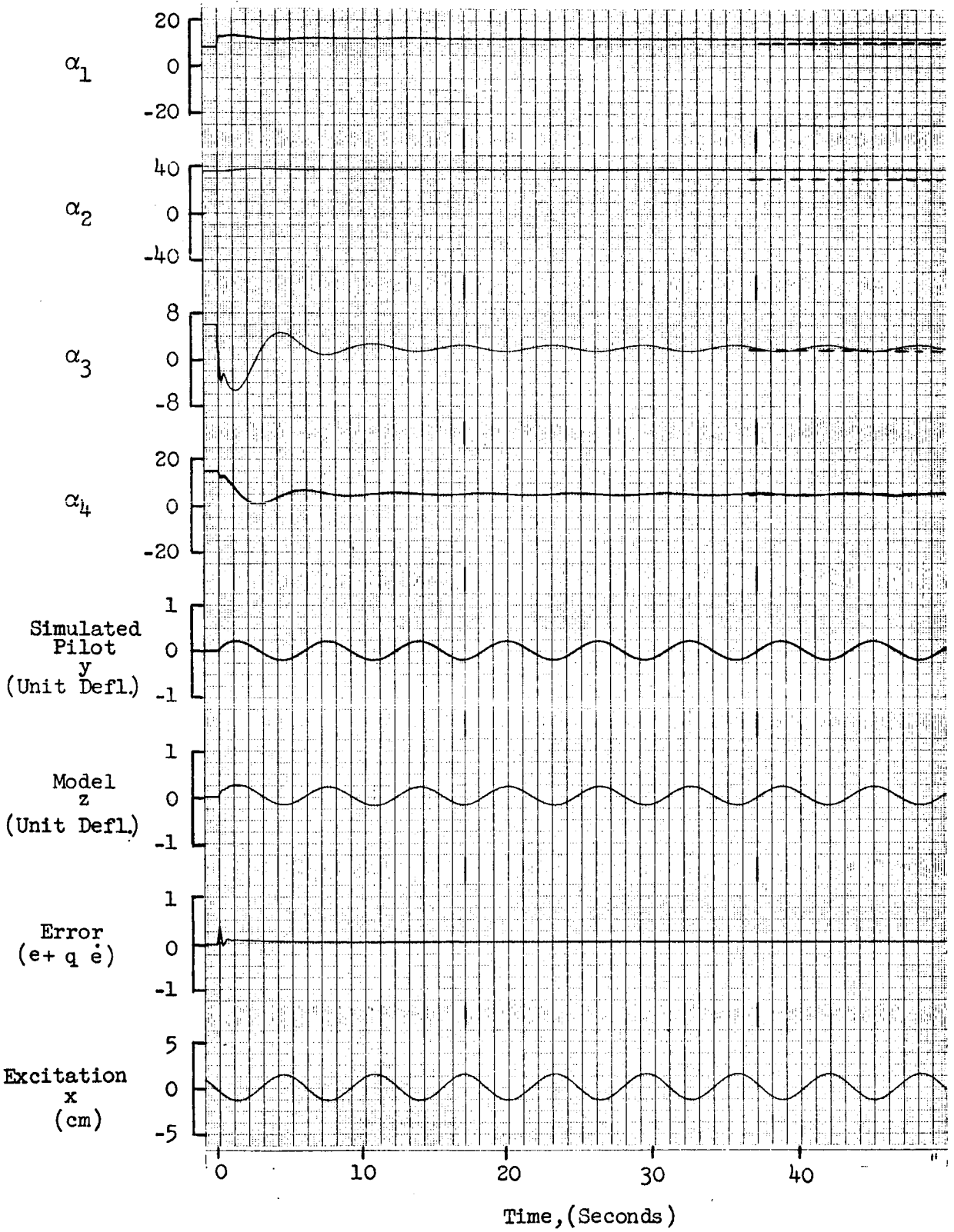

Figure A-5

Effect of Error Criterion on the Time History of
Parameter Adjustment - Sinusoidal Excitation
K = 8 q = 1.0

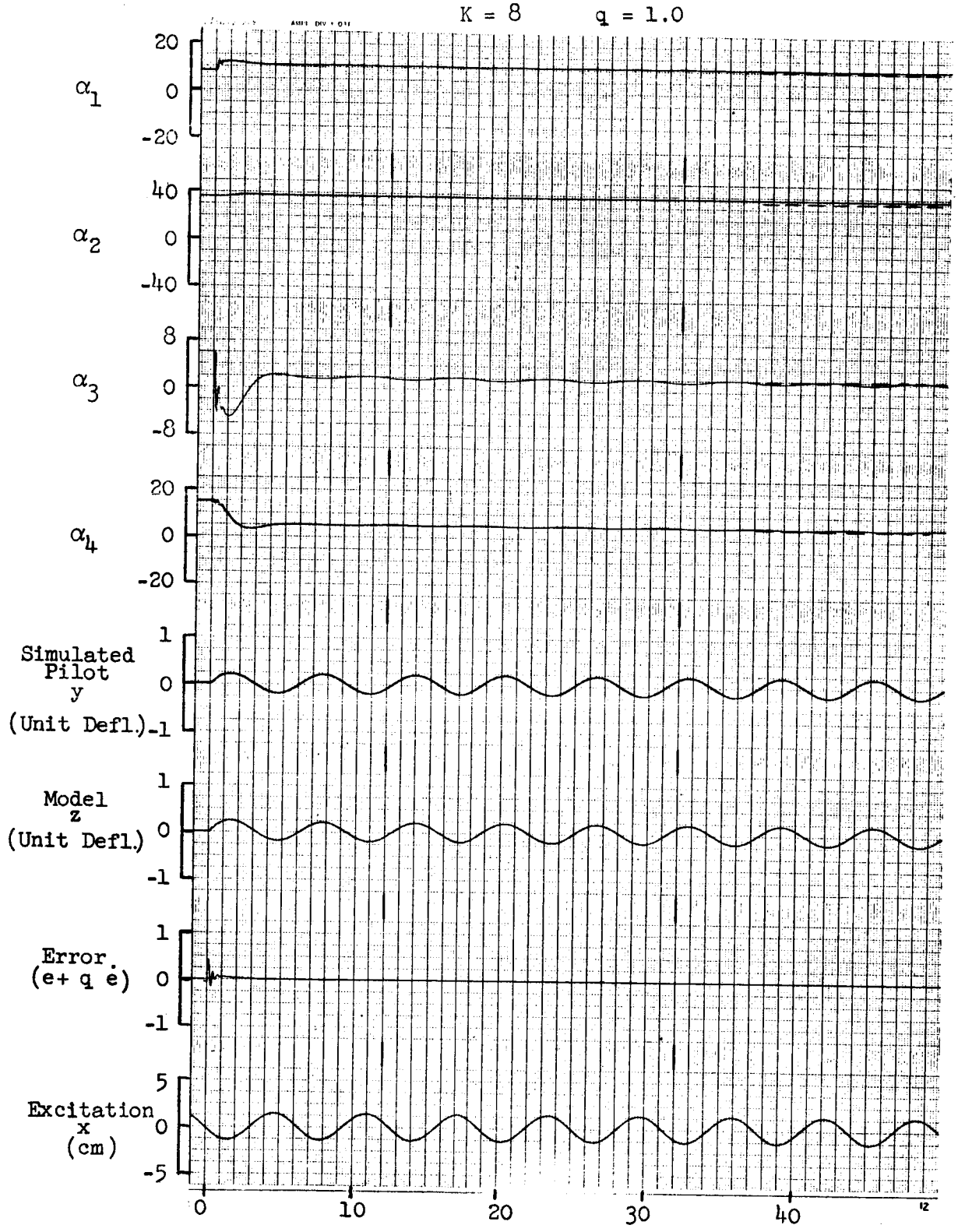

Time, (Seconds)

Figure A-6

Effect of Error Criterion on the Time History of Parameter Adjustment - Random Excitation

K = 16 q = 0

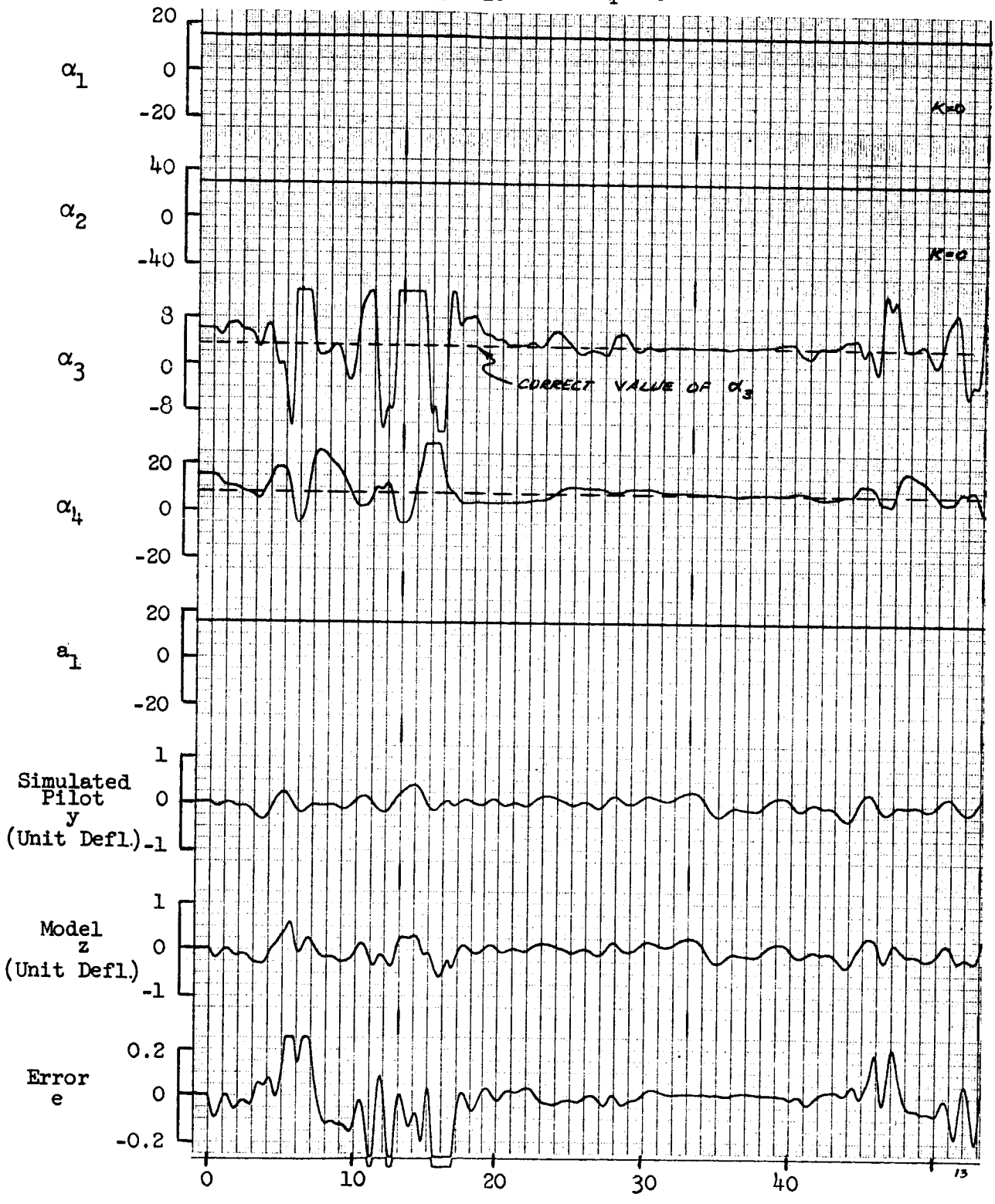

Figure A-7

Effect of Error Criterion on the Time History of Parameter Adjustment - Random Excitation

K = 16 q = .5

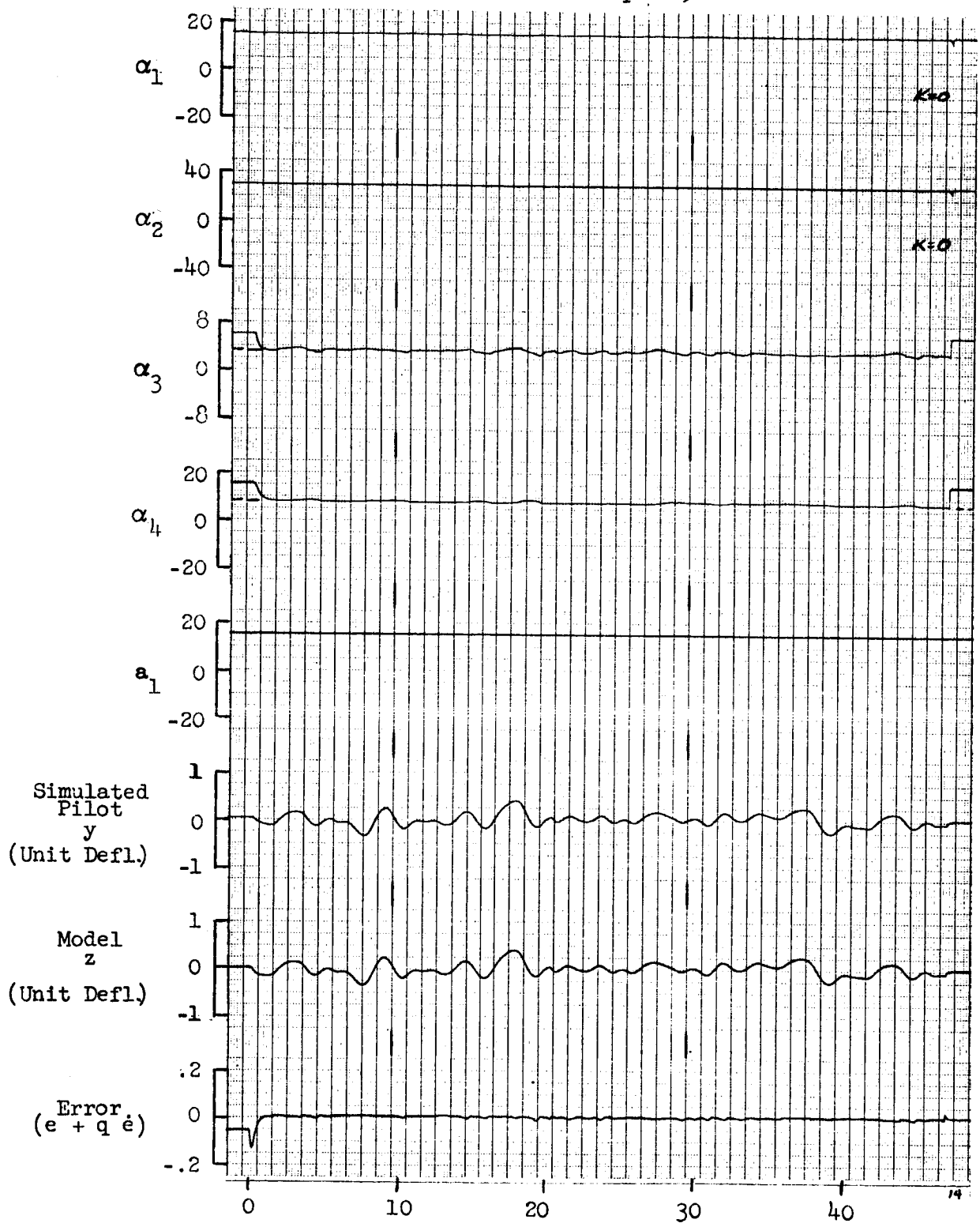

Figure A-8

Time History of Model Adaptation to a Simulated Pilot's Sinusoidal Parameter, a_1

$K_1 = 20 \quad q = 0$

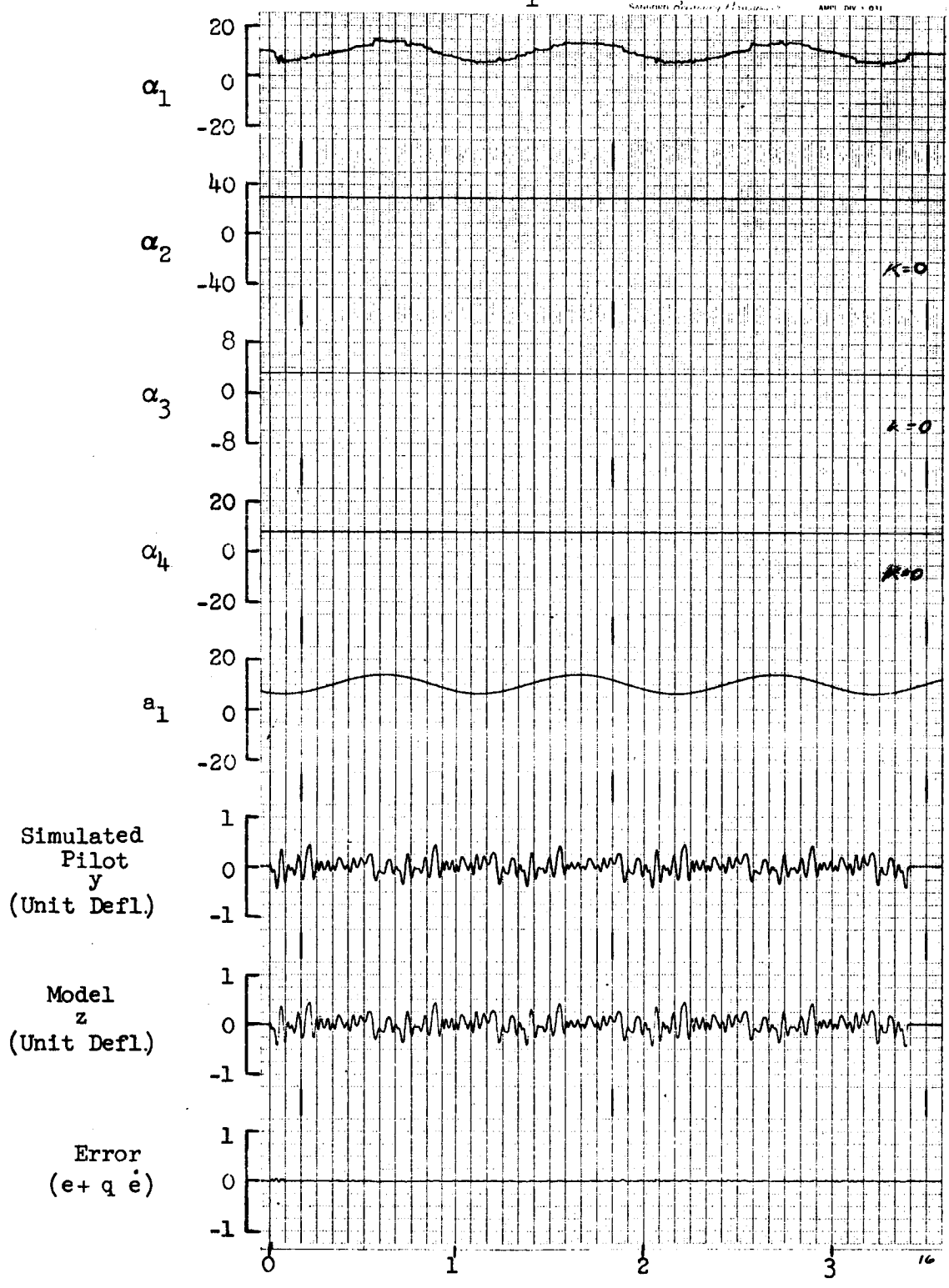

Figure A-9

Time History of Model Adaptation to a Simulated Pilot's Sinusoidal Parameter, a_1
K = 20 q = 0

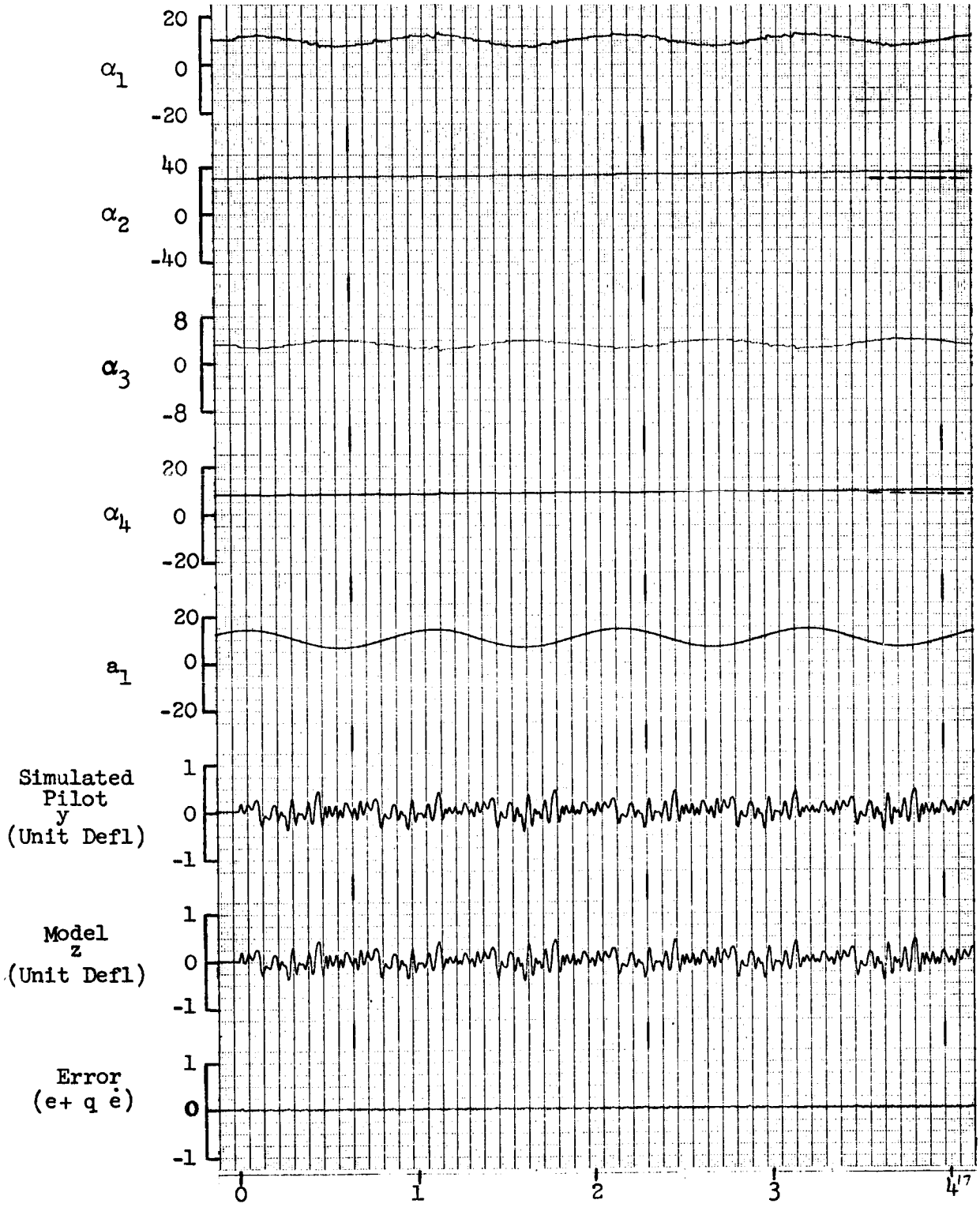

Time (Minutes)

Figure A-10

Time History of Model Adaptation to a Simulated Pilot's Sinusoidal Parameter, a_3
q = 0

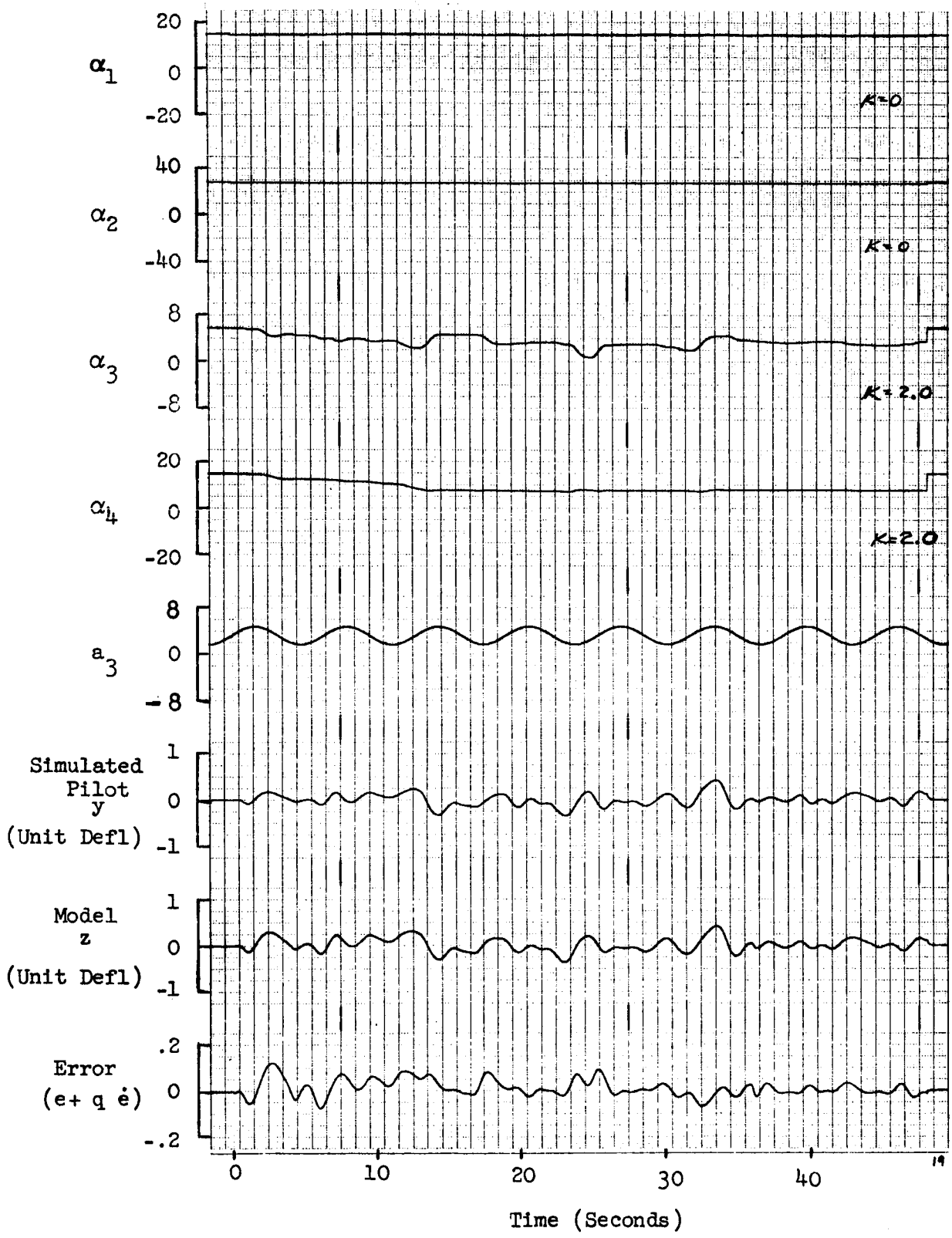

Figure A-11

Time History of Model Adaptation to a Simulated Pilot's Sinusoidal Parameter, a_3
$q = 0$

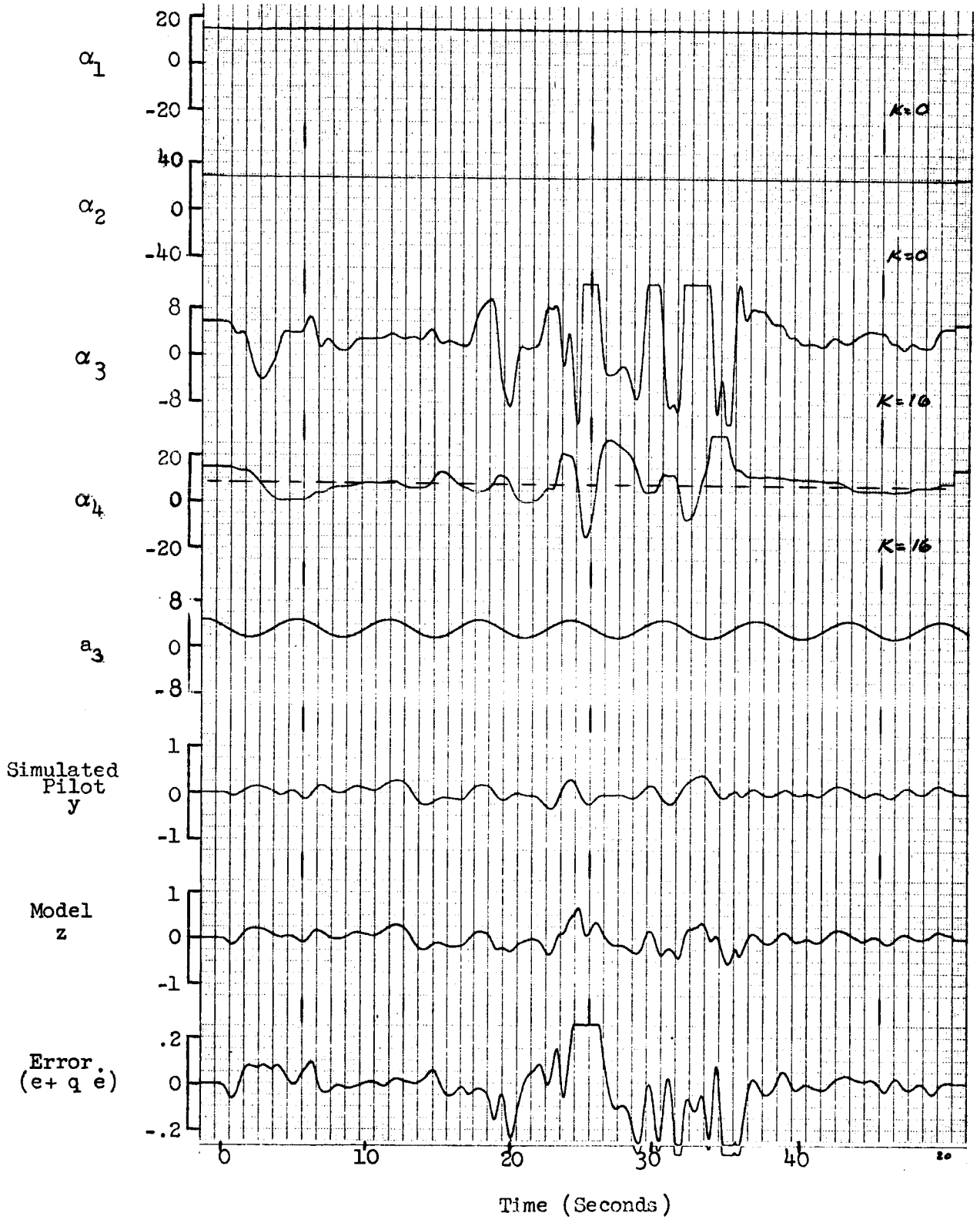

Figure A-12

Time-History of Model Adaptation to a Simulated Pilot's Sinusoidal Parameter, a_3.

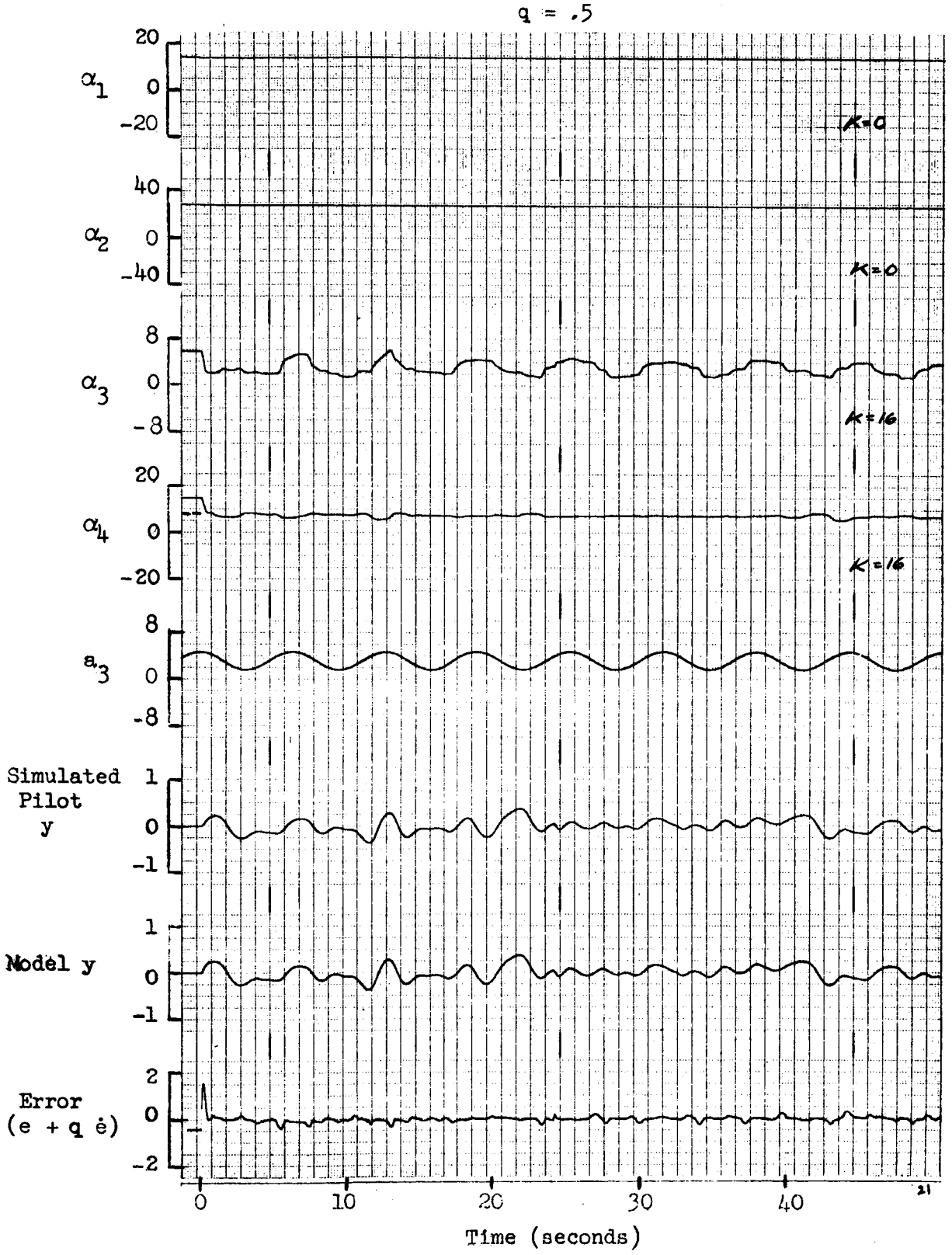

Figure A-13

Time-History of Model Adaptation to a Simulated Pilot s Stepped Parameter, a_3.

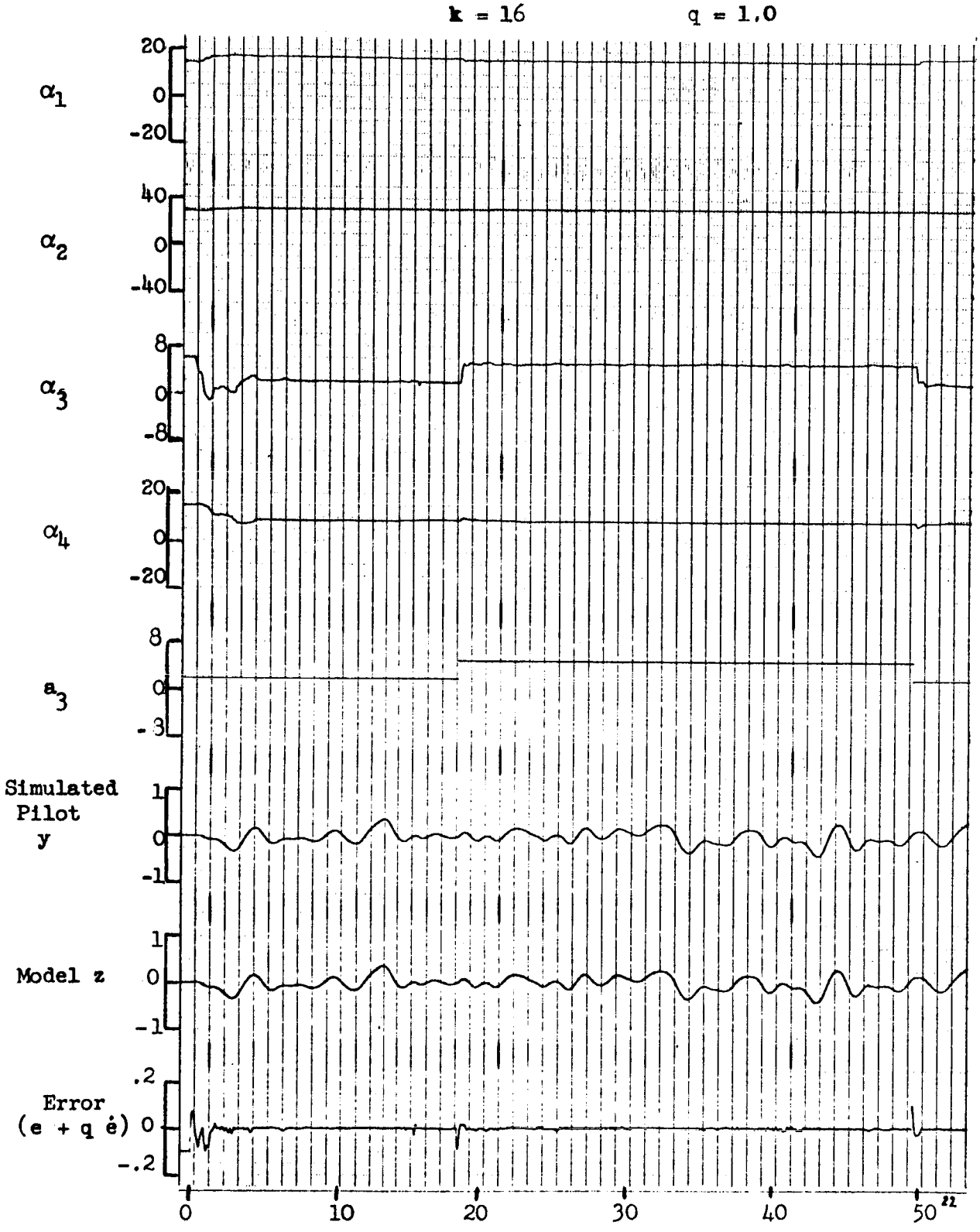

Figure A-14

Time-History of Model Adaptation to a Simulated Pilot's Stepped Parameter, a_3.

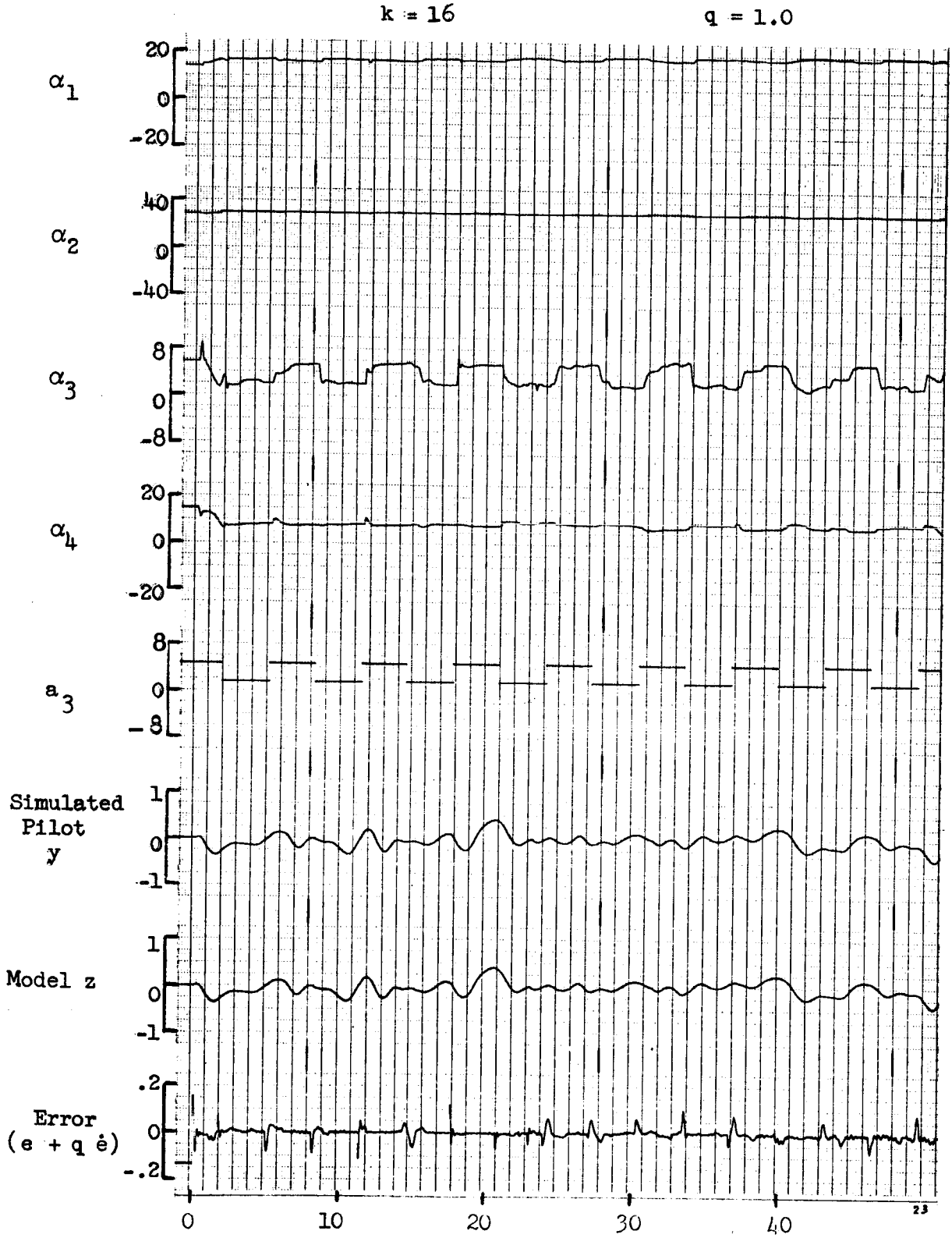

Figure A-15

Time History - Adjustment of Parameter α_5

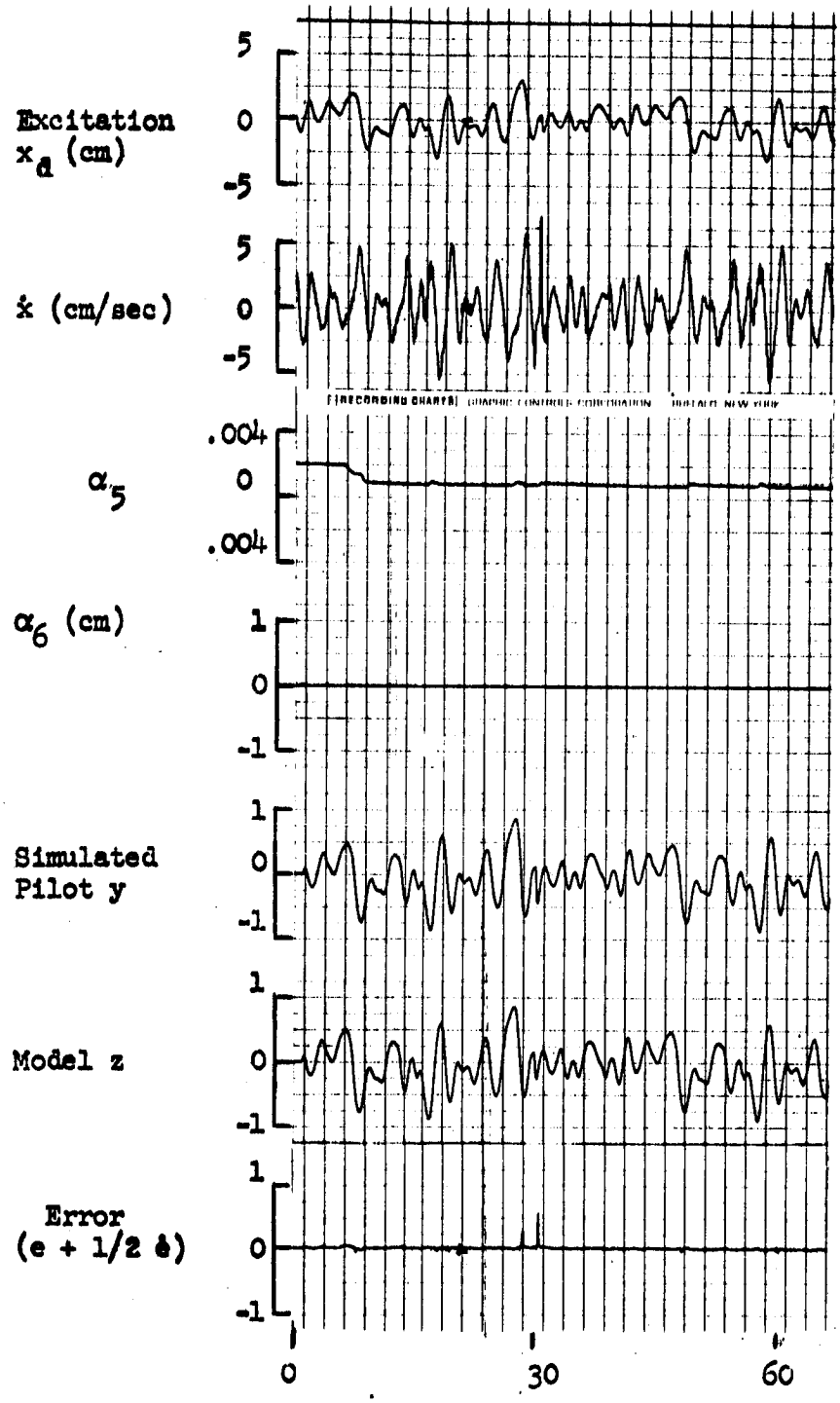

Figure A-16

Time History - Adjustment of Parameter α_6

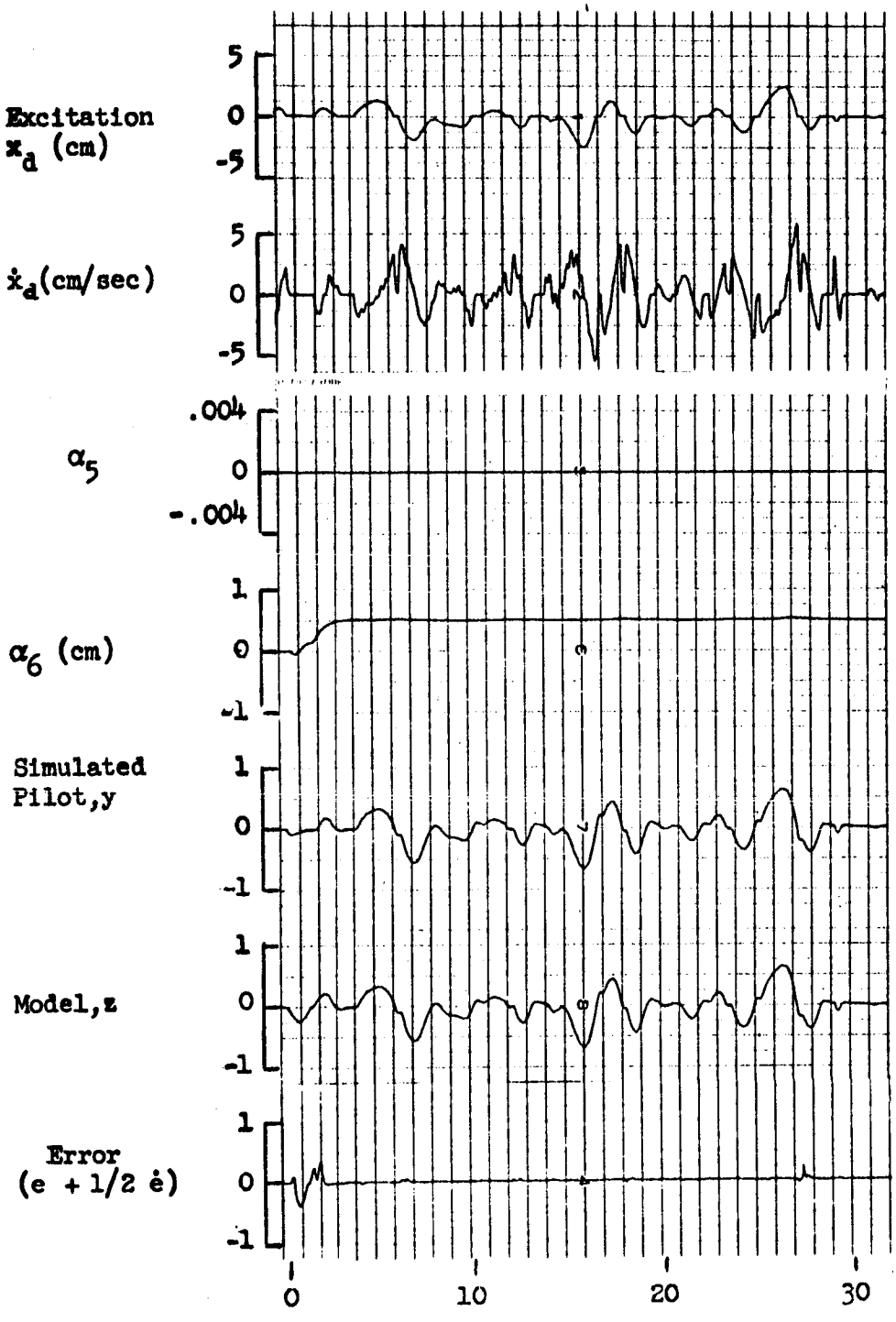

Figure A-17

Time History - Adjustment of Parameter α_7

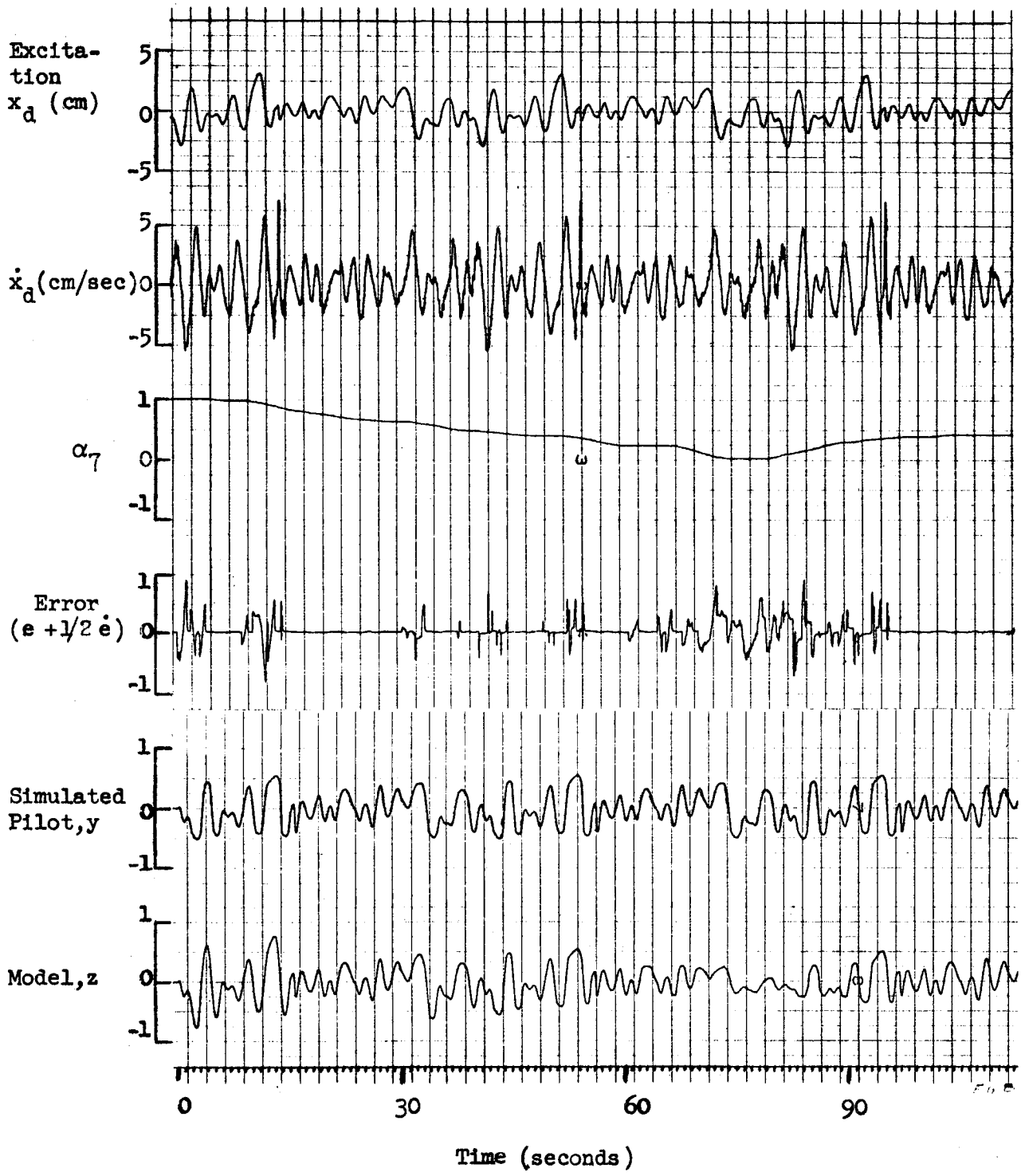

Figure A-18

Time History - Simultaneous Adjustment
of Parameters α_5 and α_6

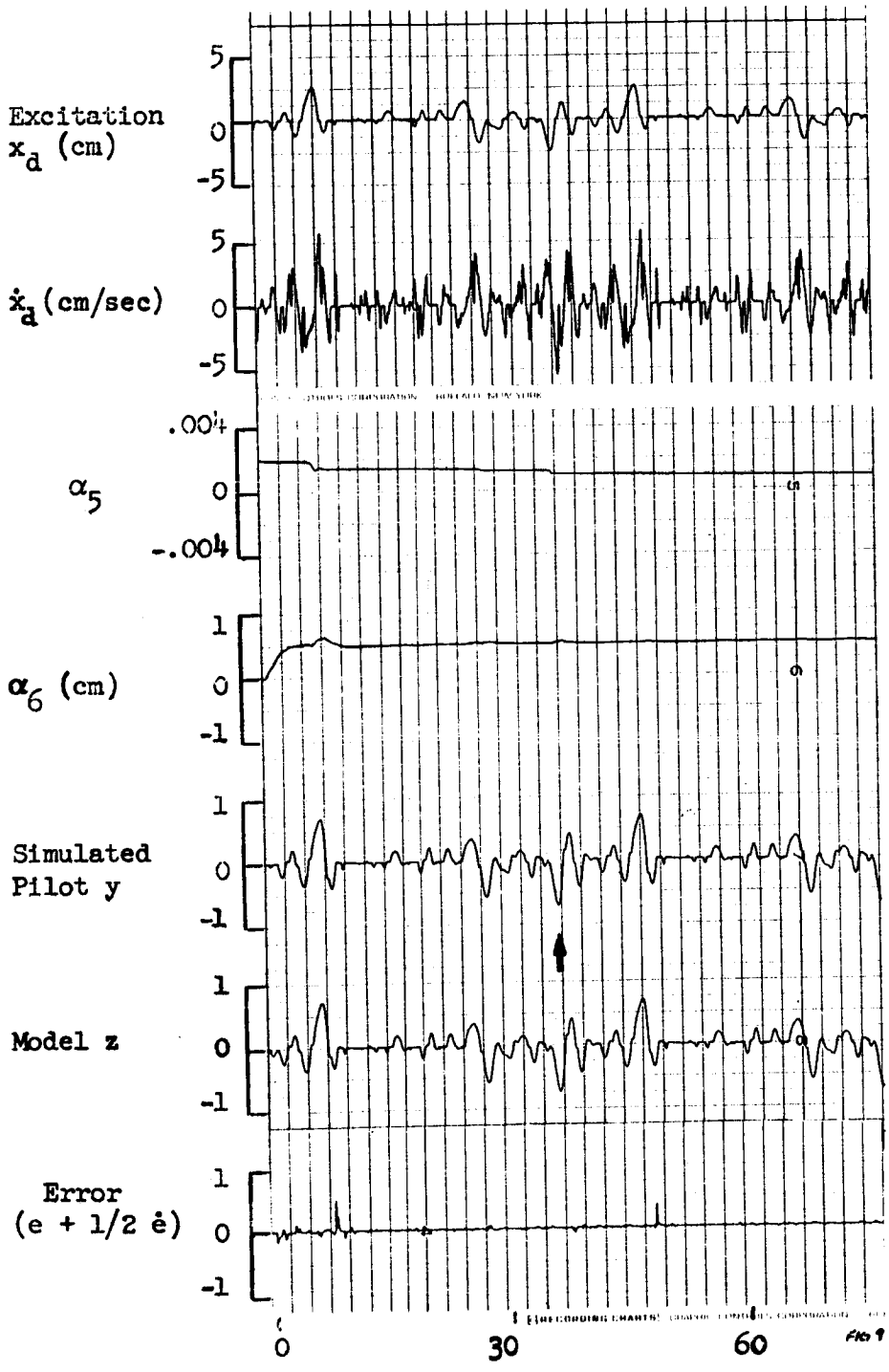

Time (seconds)

Figure A-19

Time History - Adjustment of Two Parameters with Noise Added to Simulated Pilot, c = 0

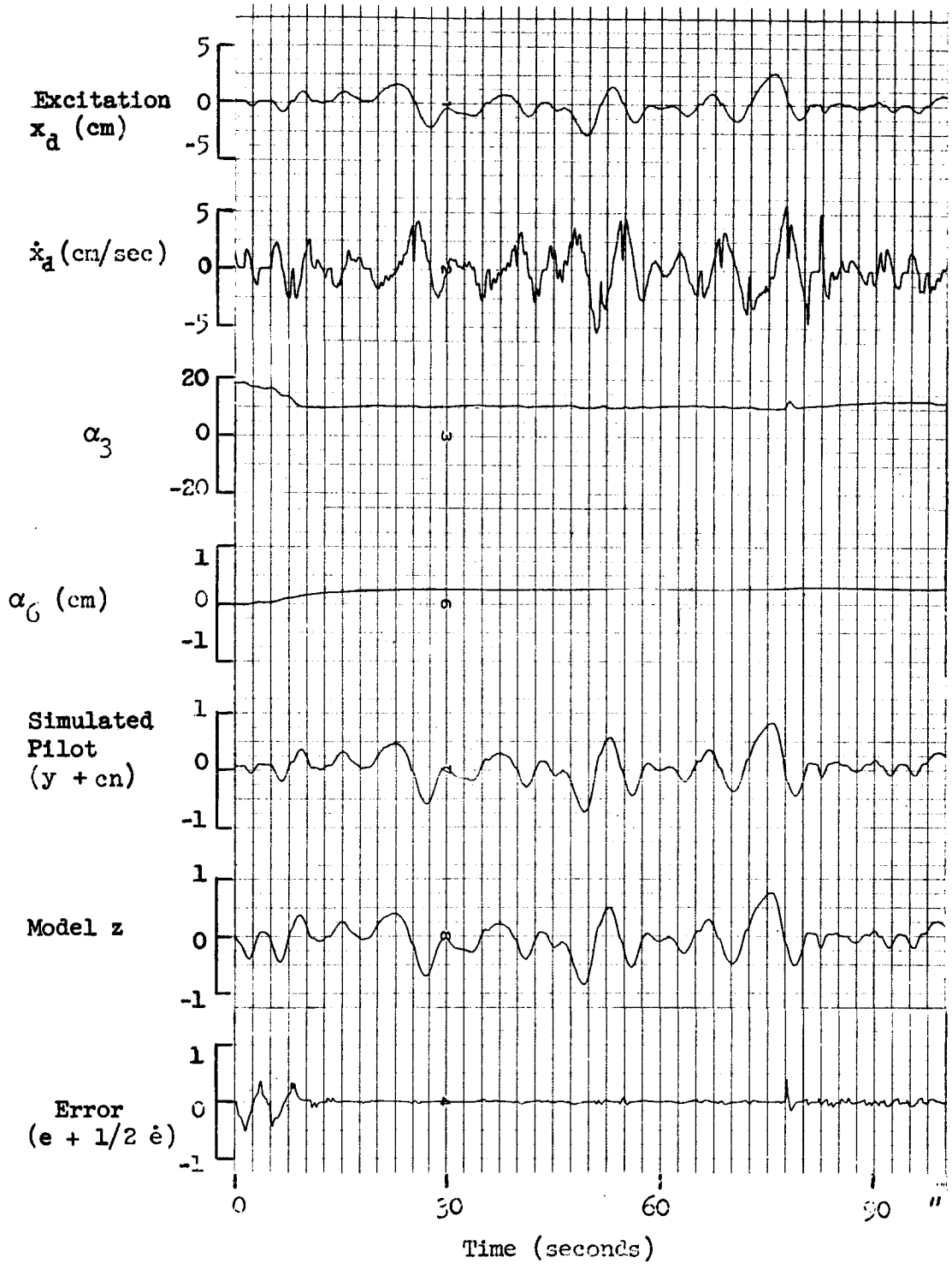

Figure A-20

Time-History - Adjustment of Two Parameters With Filtered Noise Added to Simulated Pilot, c = 8.0

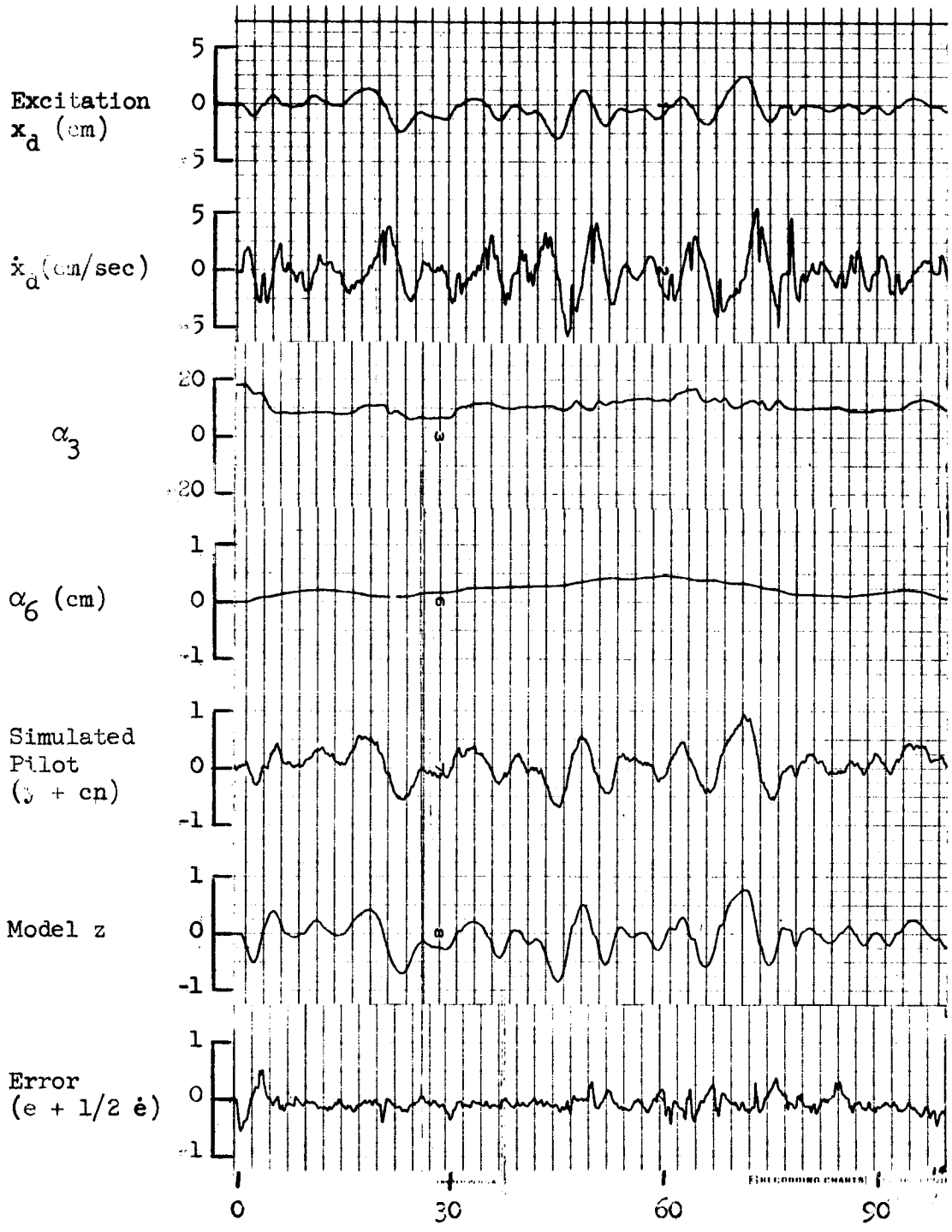

Figure A-21

Time History - Adjustment of Two Parameters with Noise Added to Simulated Pilot, c = 1.0

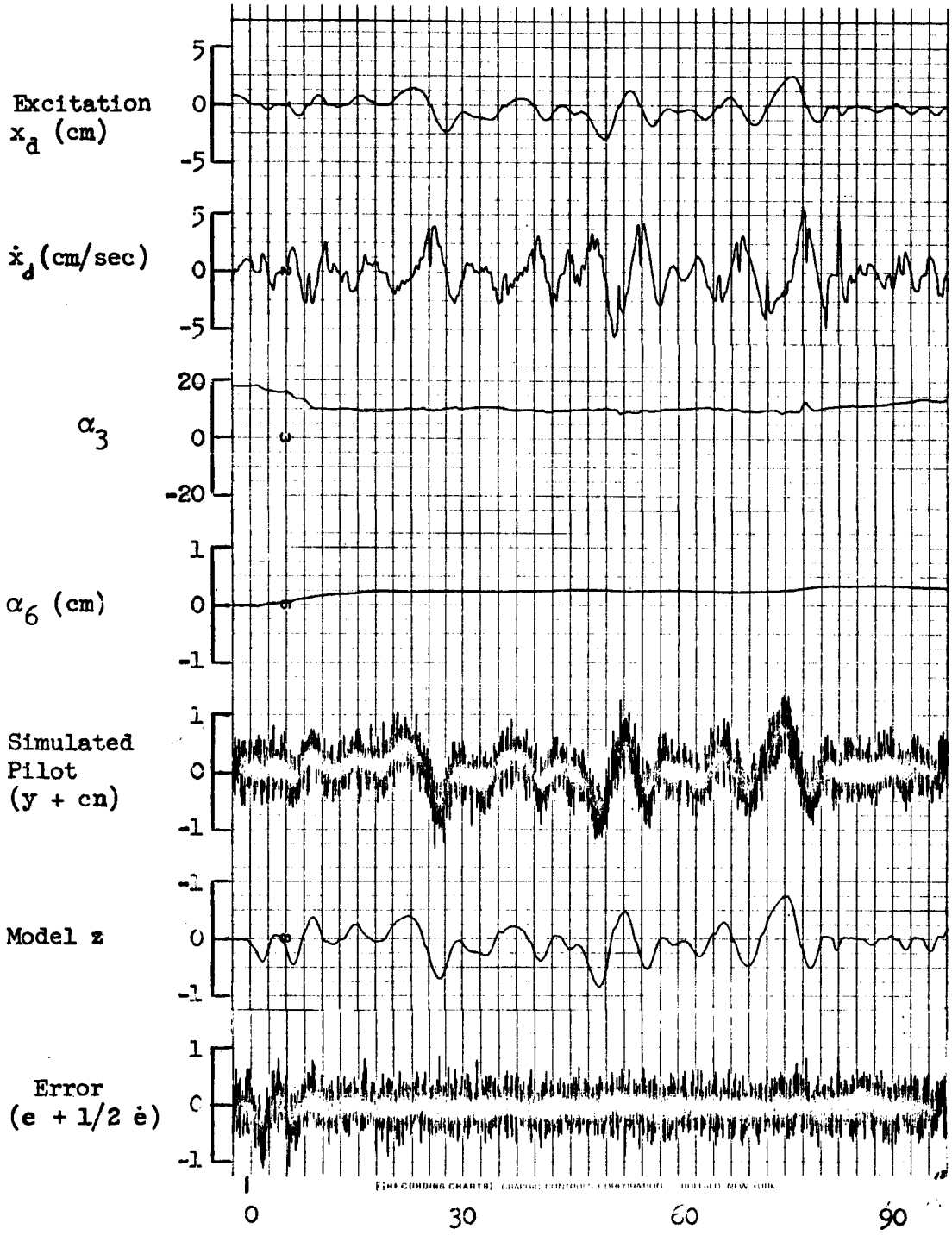

Figure A-22

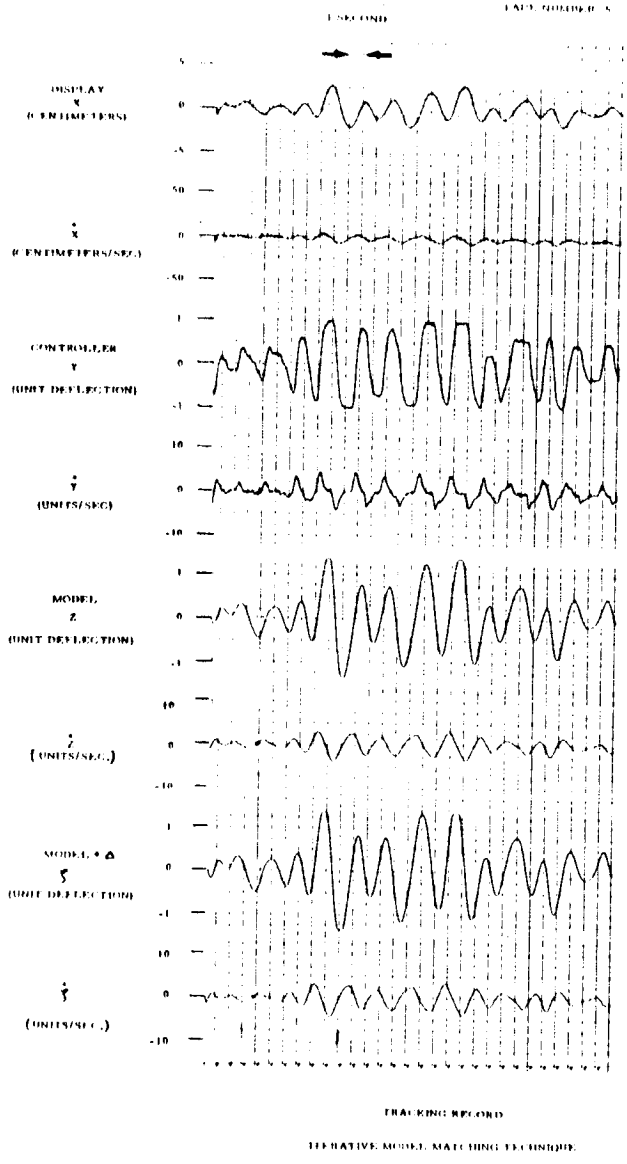
1 SECOND
DISPLAY
X
(CENTIMETERS)
$\dot{X}$
(CENTIMETERS/SEC.)
CONTROLLER
Y
(UNIT DEFLECTION)
$\dot{Y}$
(UNITS/SEC)
MODEL
Z
(UNIT DEFLECTION)
$\dot{Z}$
(UNITS/SEC.)
MODEL + Δ
ζ
(UNIT DEFLECTION)
$\dot{\zeta}$
(UNITS/SEC.)
TRACKING RECORD
ITERATIVE MODEL MATCHING TECHNIQUE

Figure A-23a

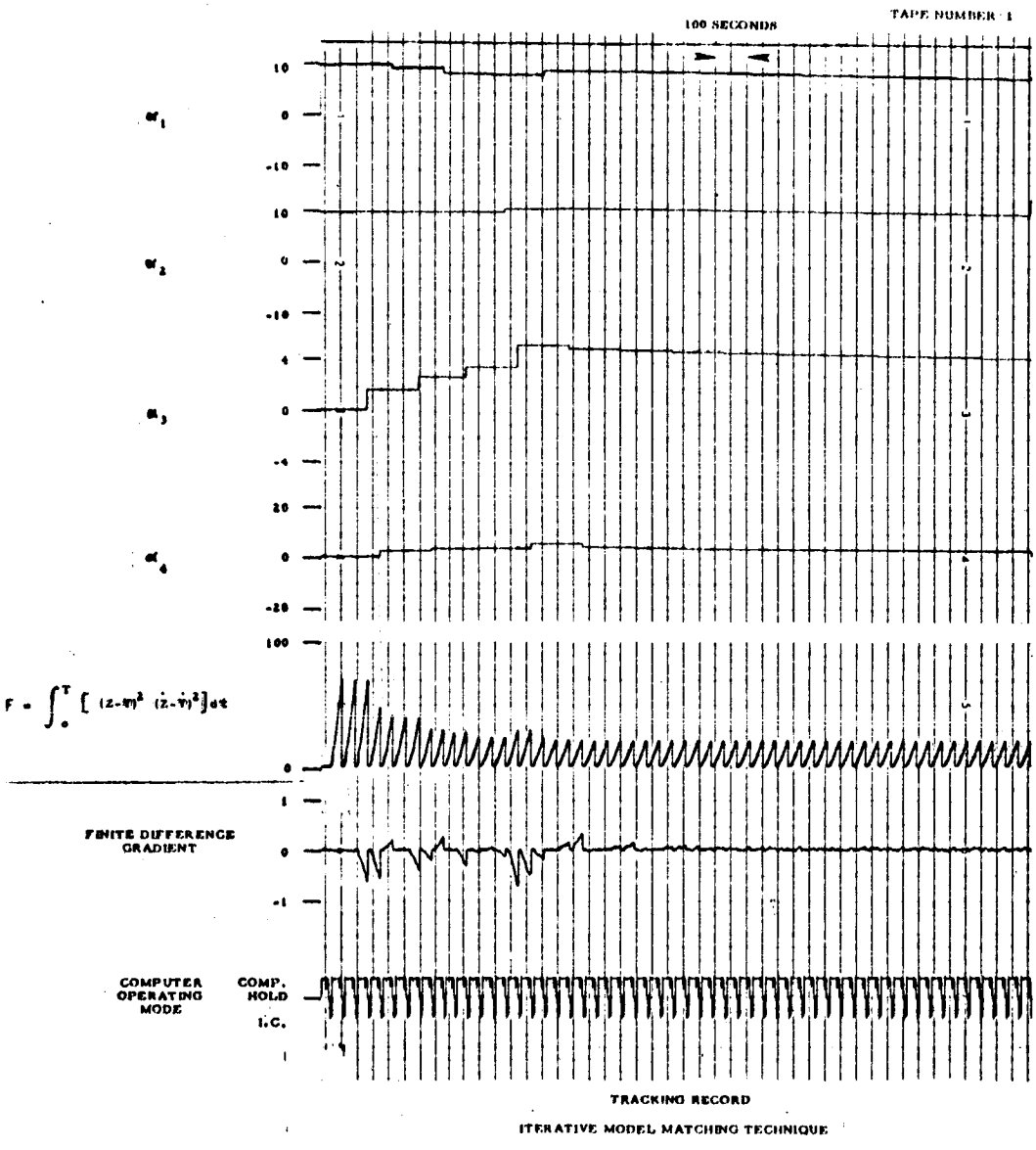
100 SECONDS
TAPE NUMBER 1
α_1
α_2
α_3
α_4
$F = \int_0^T [(z-\hat{z})^2 (\dot{z}-\dot{\hat{z}})^2] dt$
FINITE DIFFERENCE GRADIENT
COMPUTER OPERATING MODE
COMP. HOLD
I.C.
TRACKING RECORD
ITERATIVE MODEL MATCHING TECHNIQUE

Figure A-23b

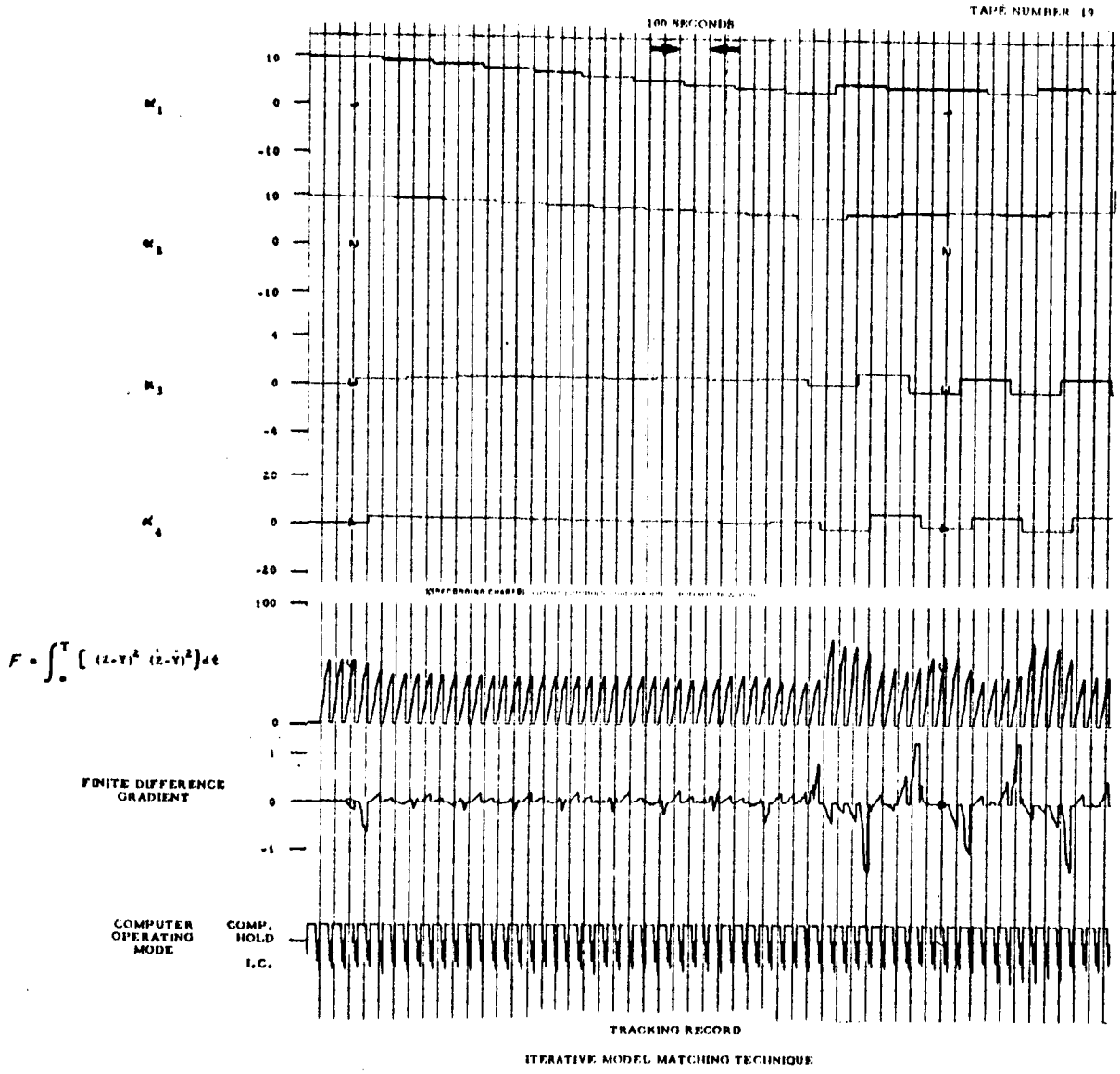

ITERATIVE MODEL MATCHING TECHNIQUE

Figure A-24

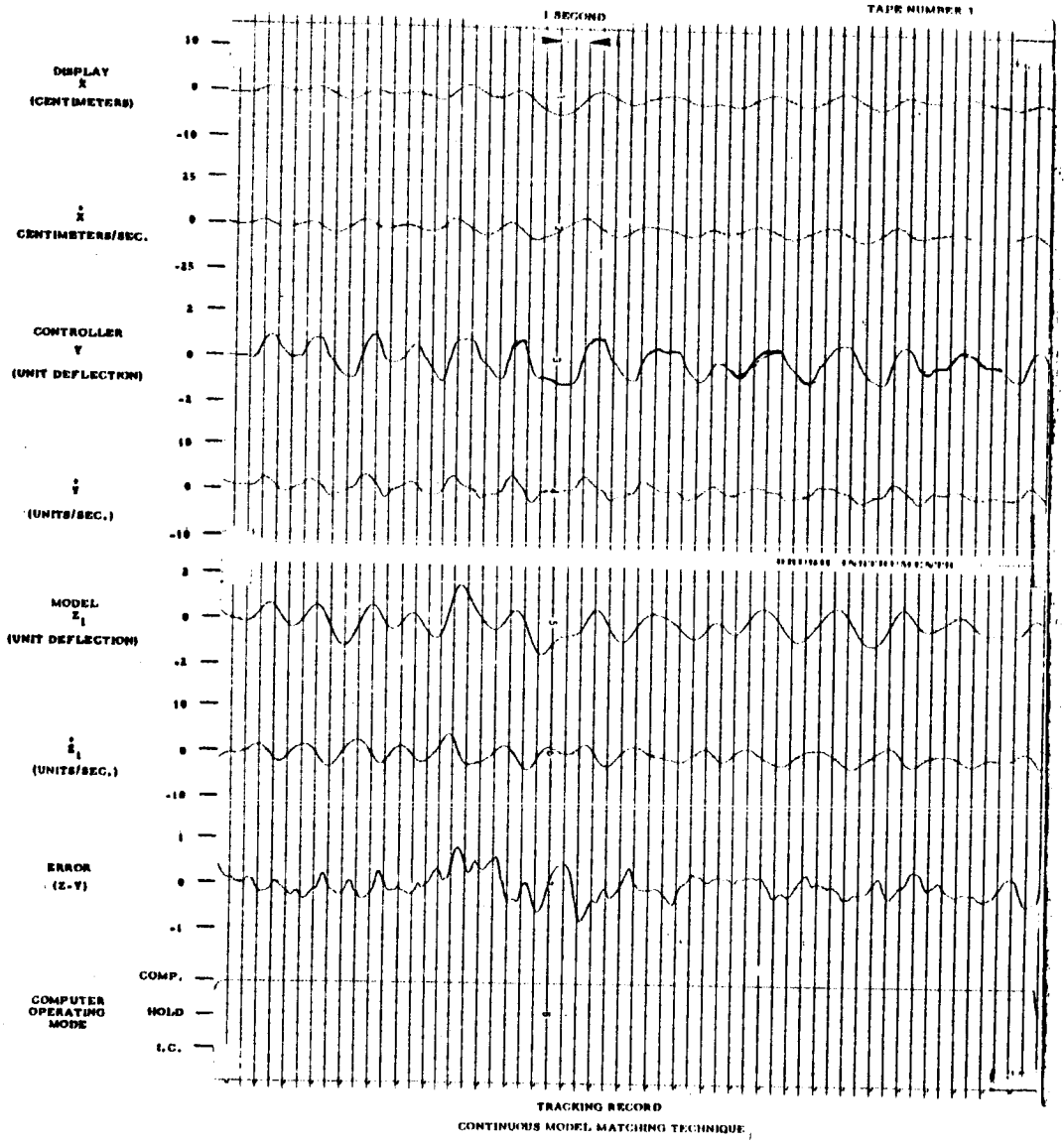
1 SECOND
TAPE NUMBER 1
DISPLAY
$\dot{X}$
(CENTIMETERS/SEC.
CONTROLLER
V
(UNIT DEFLECTION)
$\dot{V}$
(UNITS/SEC.)
MODEL
Z_1
(UNIT DEFLECTION)
$\dot{Z}_1$
(UNITS/SEC.)
ERROR
(Z-V)
COMPUTER
OPERATING
MODE
COMP.
HOLD
I.C.
TRACKING RECORD
CONTINUOUS MODEL MATCHING TECHNIQUE

Figure A-25

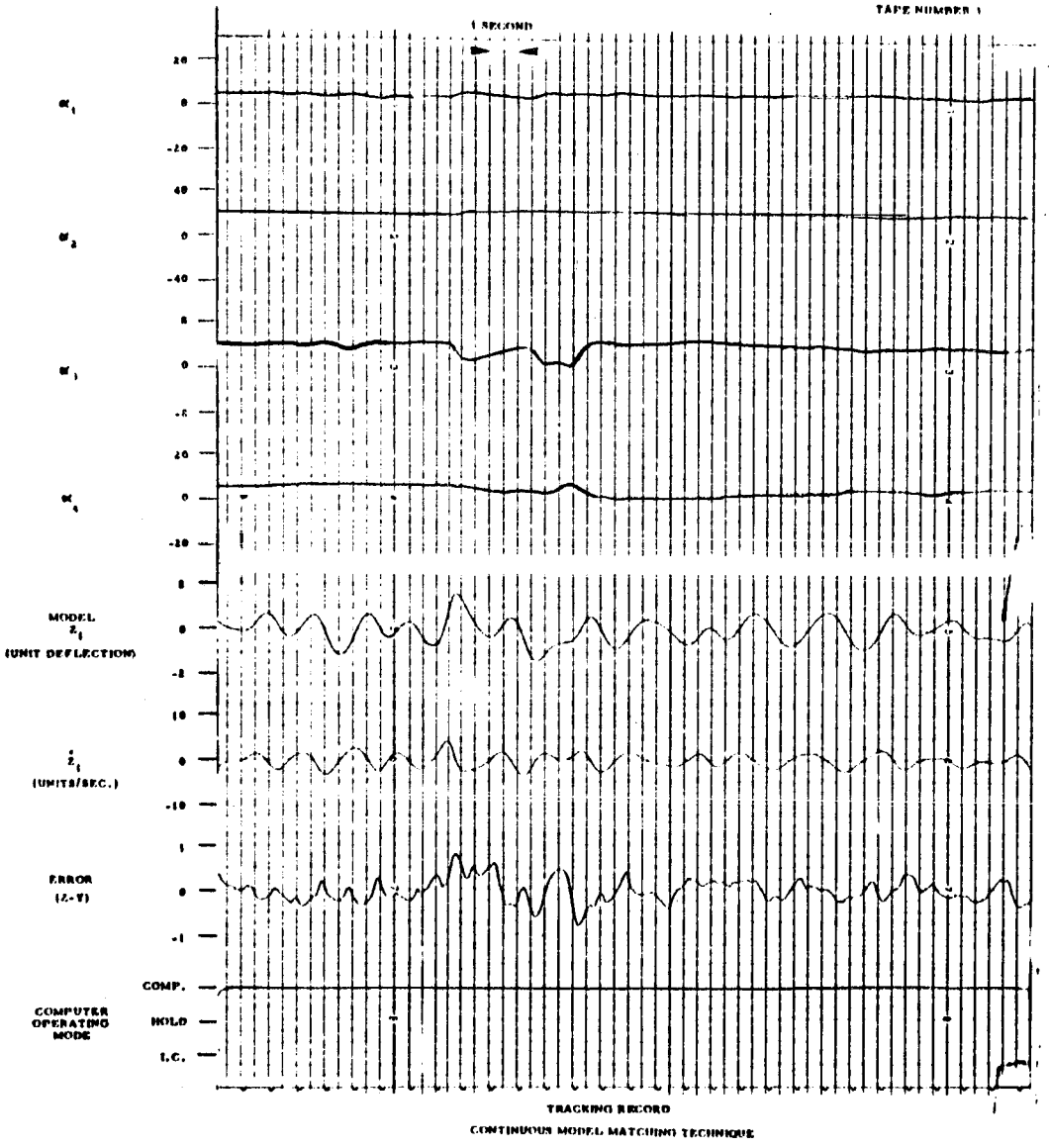
1 SECOND
TAPE NUMBER 1
MODEL
(UNIT DEFLECTION)
(UNITS/SEC.)
ERROR
(Z-Y)
COMP.
HOLD
I.C.
COMPUTER OPERATING MODE
TRACKING RECORD
CONTINUOUS MODEL MATCHING TECHNIQUE

Figure A-26

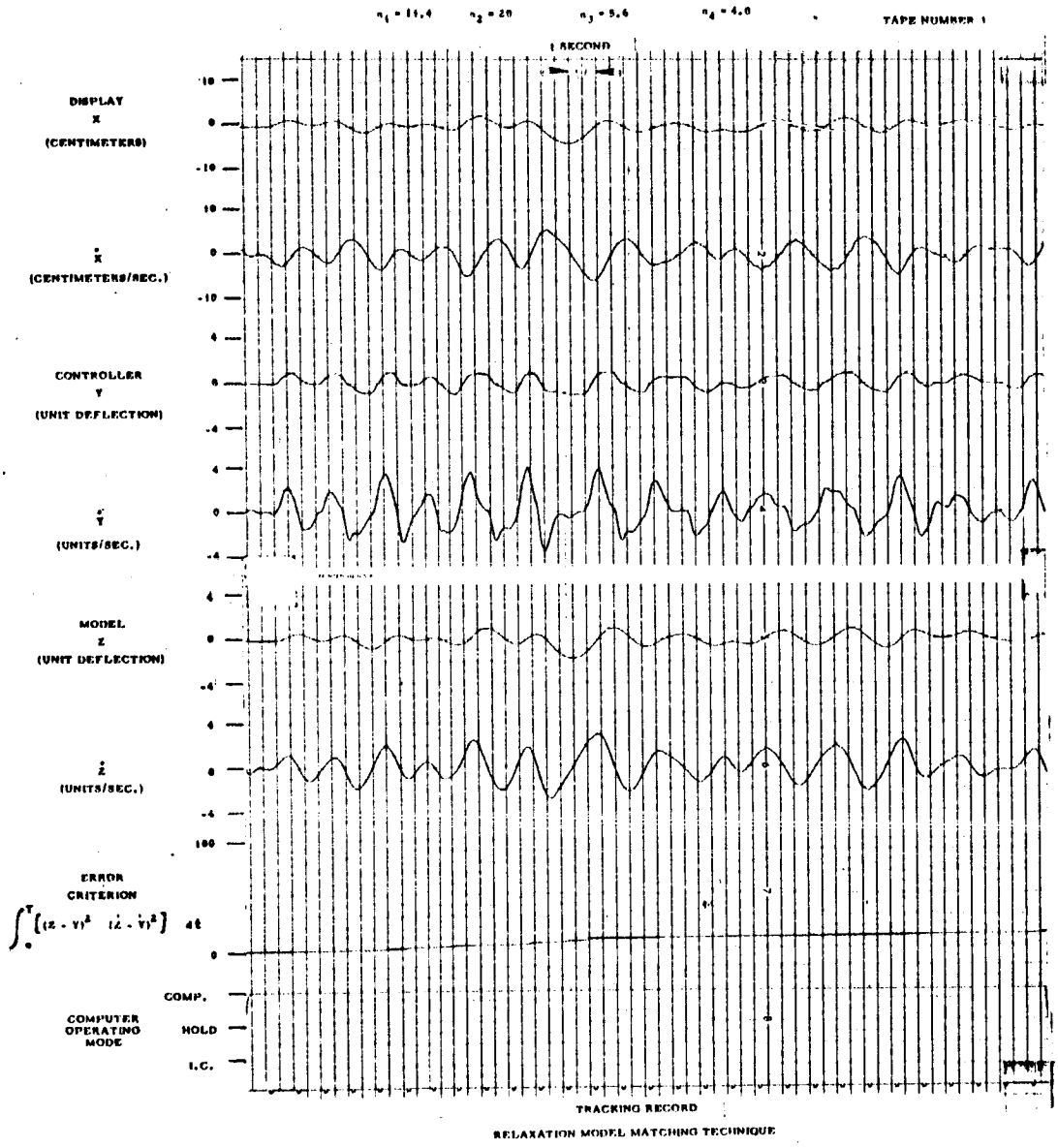
$n_1 = 11.4$
$n_2 = 20$
$n_3 = 5.6$
$n_4 = 4.0$
TAPE NUMBER 1
1 SECOND
DISPLAY
x
(CENTIMETERS)
$\dot{x}$
(CENTIMETERS/SEC.)
CONTROLLER
y
(UNIT DEFLECTION)
$\dot{y}$
(UNITS/SEC.)
MODEL
z
(UNIT DEFLECTION)
$\dot{z}$
(UNITS/SEC.)
ERROR
CRITERION
$\int_0^T [(z-y)^2 \quad (\dot{z}-\dot{y})^2]\, dt$
COMPUTER
OPERATING
MODE
COMP.
HOLD
I.C.
TRACKING RECORD
RELAXATION MODEL MATCHING TECHNIQUE

Figure A-27

Time-History of Human Pilot Compensatory Tracking
in a Time Varying Task
Pilot "R"

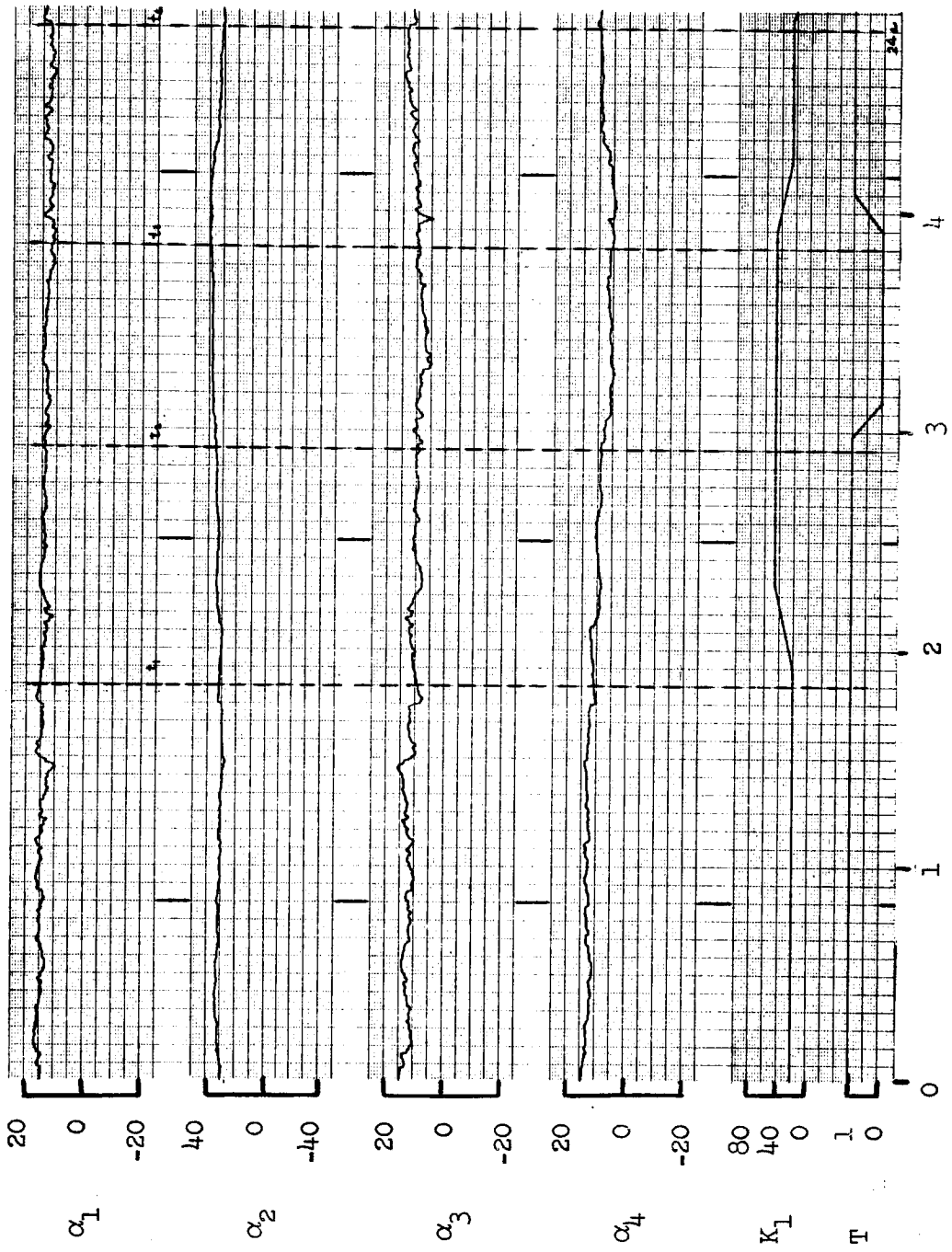

Figure A28a

Time-History of Human Pilot Compensatory Tracking

in a Time Varying Task

Pilot "R"

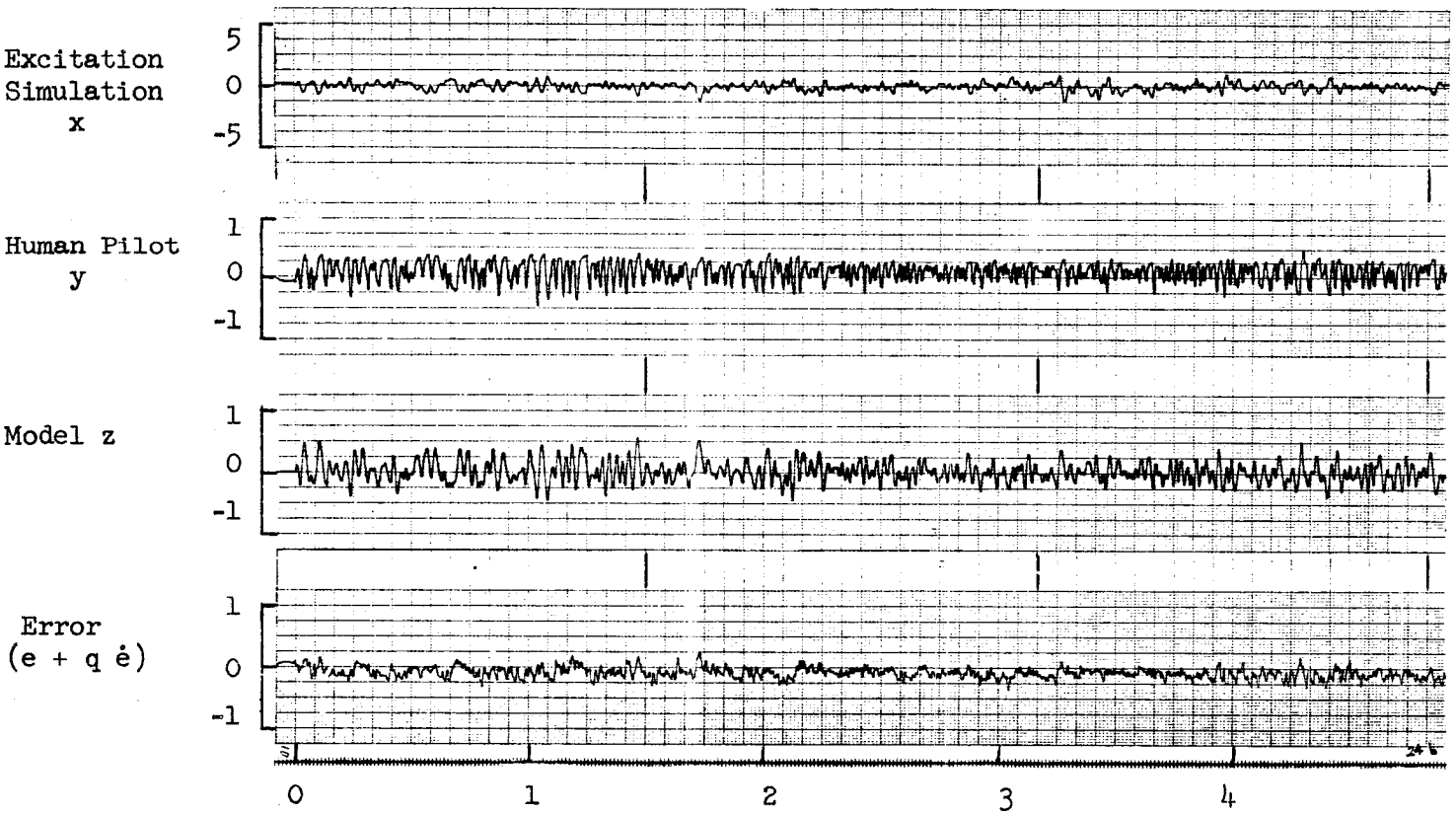

Figure A-28b

Time-History of Human Pilot Compensatory Tracking
in a Time Varying Task

Pilot "B"

Time (Minutes)

Figure A29a

Time History of Human Pilot Compensatory Tracking

in a Time Varying Task

Pilot "B"

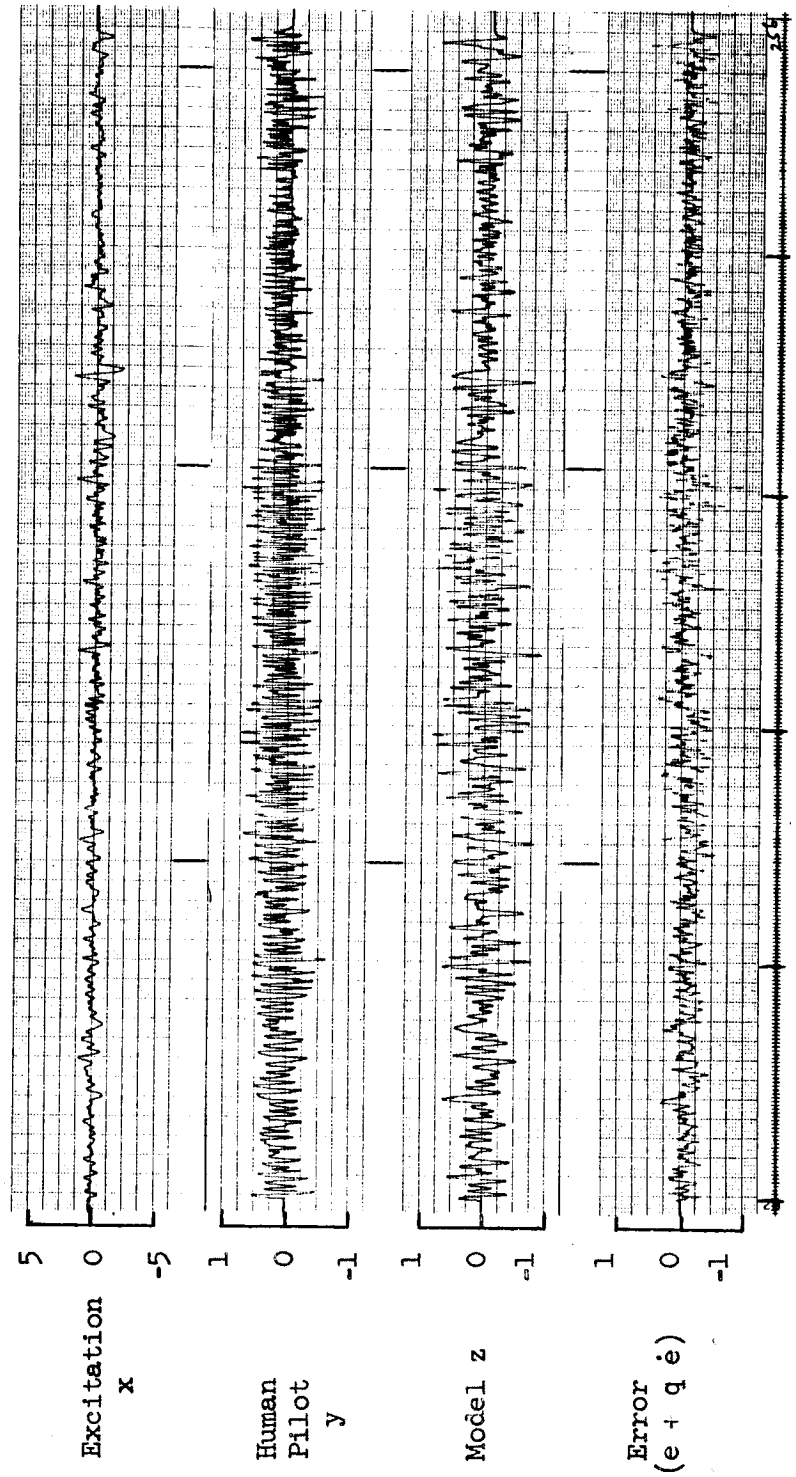

Figure A29b

Time History of Parameter Adjustment - Human Pilot R

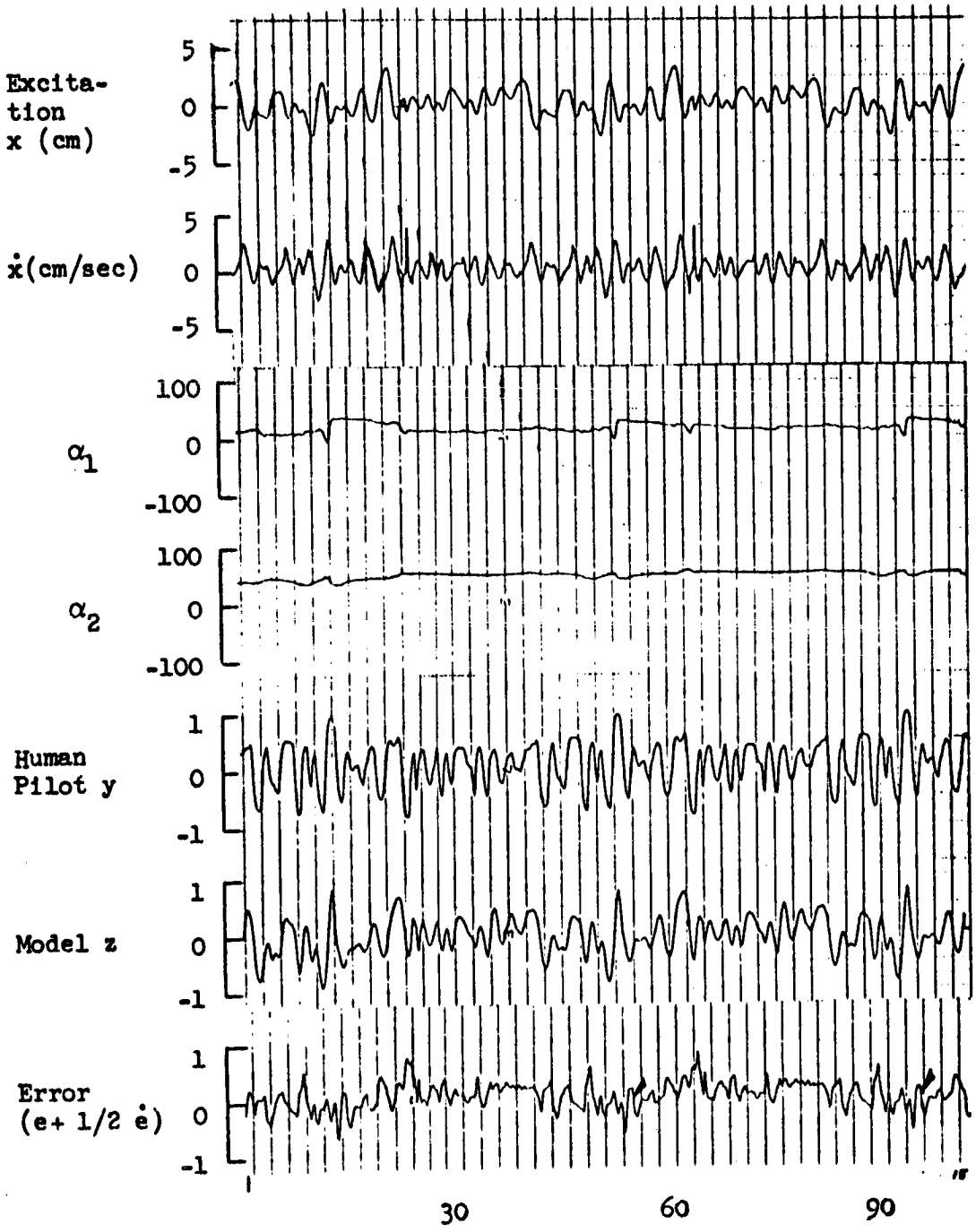

Time (seconds)

Figure A-30

Time History of Parameter Adjustment - Human Pilot R

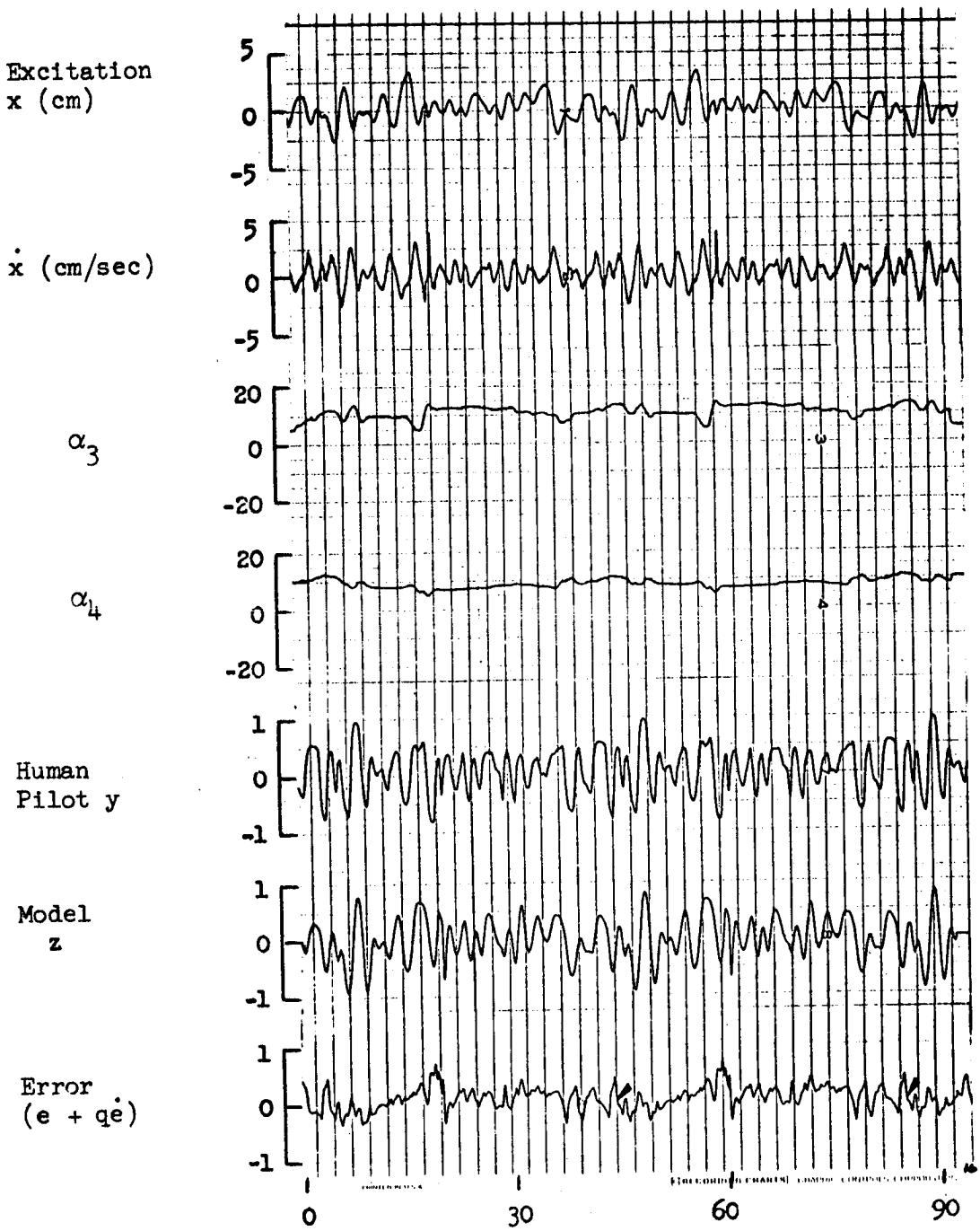

Figure A-31

Time History of Paremeter Adjustment - Human Pilot R

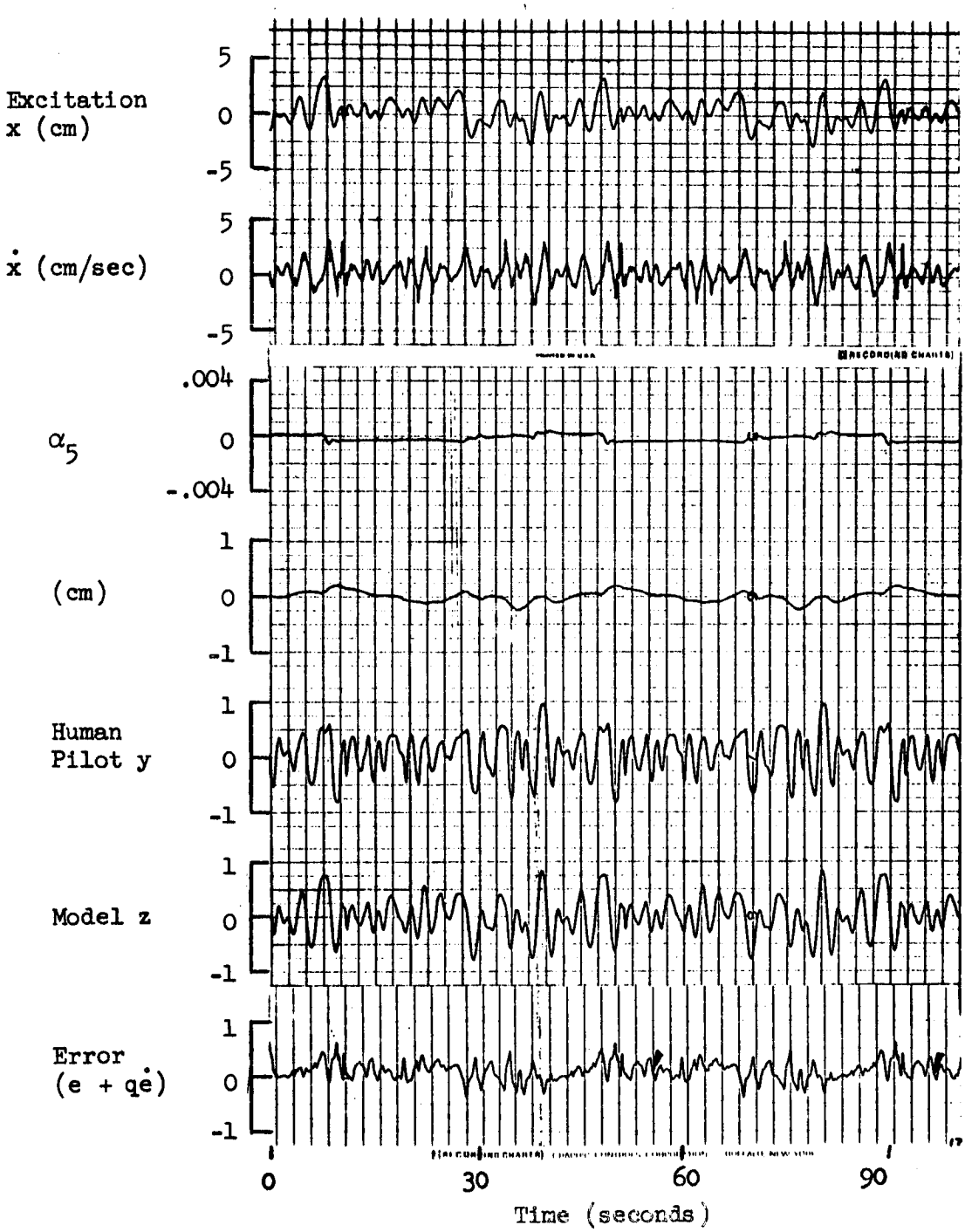

Figure A-32

Time History of Parameter Adjustment
Pilot R, Vertical Axis

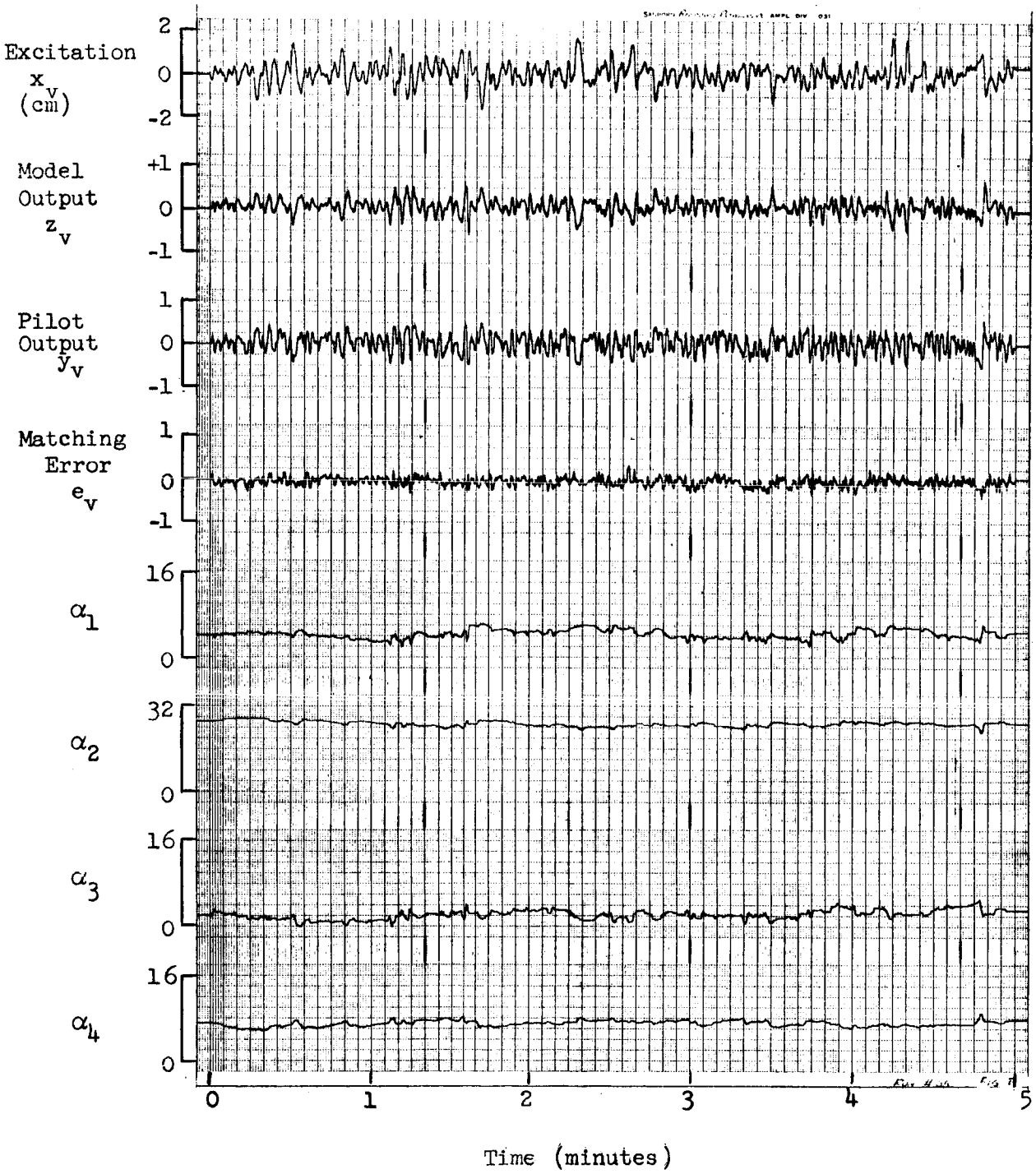

Figure A-33

Time History of Parameter Adjustment

Pilot R, Horizontal Axis

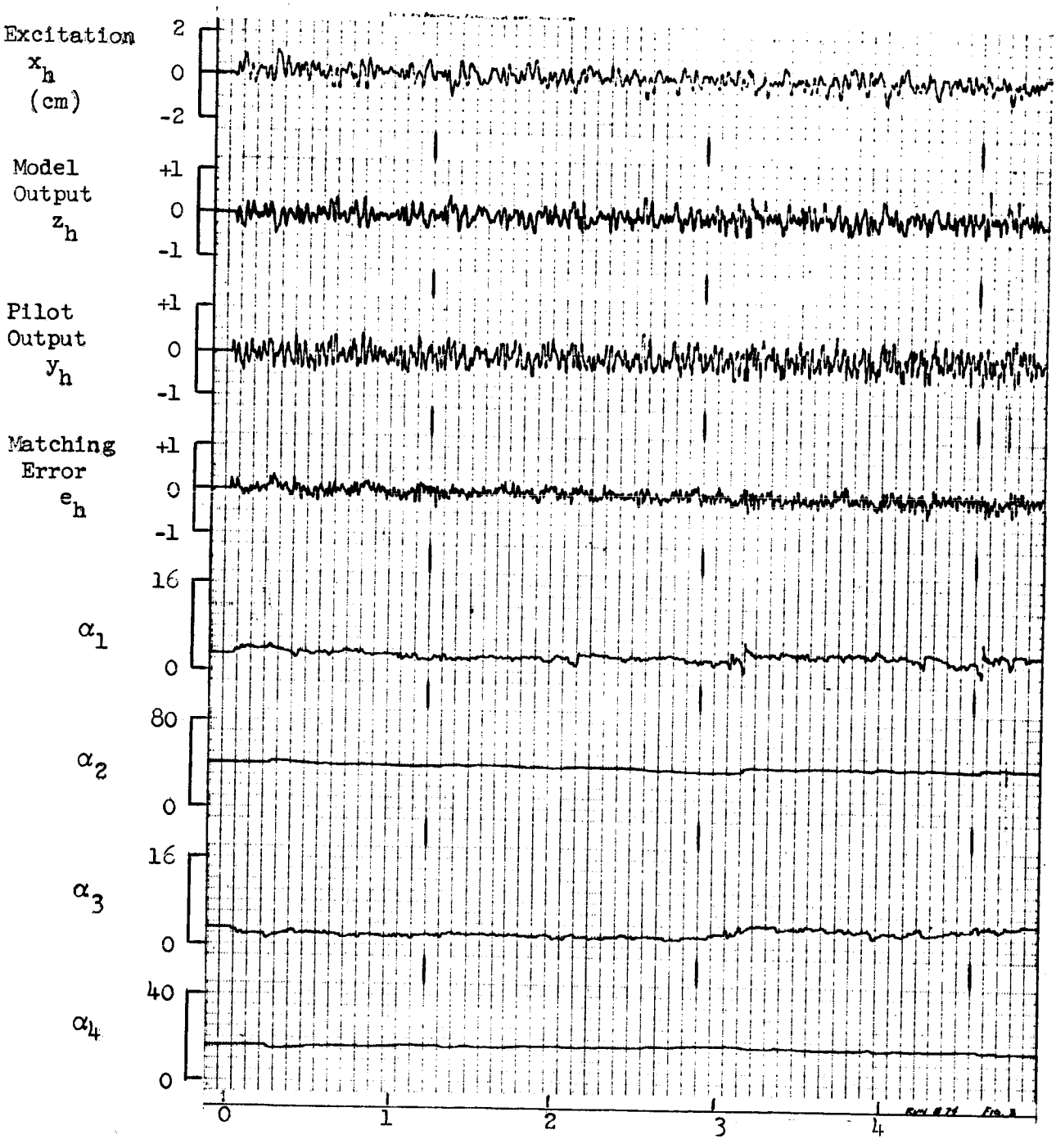

Time (minutes)

Figure A-34

Time History - Adjustment of Parameter β_3
Pilot R

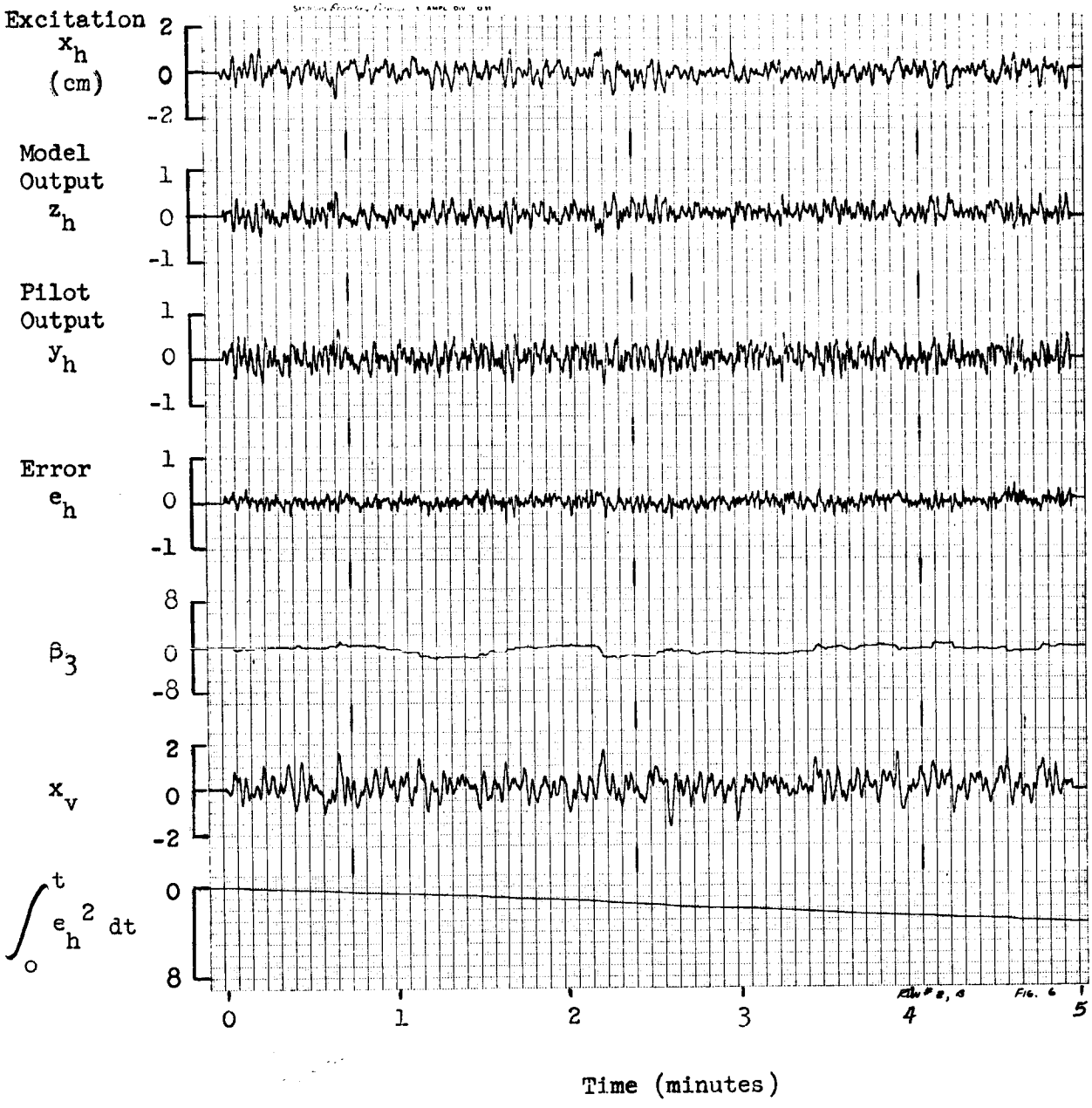

Figure A-35

APPENDIX B

A COMPARISON OF THE NASA AND STL MODEL MATCHING IMPLEMENTATION

The purpose of this section is to compare the analog computer technique used at NASA/Langley Research Center (2), (18) with the method used at STL for the "continuous model matching method" in the present study.

The NASA method is based on the work of Whitaker, Osburn and Kezer on adaptive control (1), while the "output error" method used in the STL study is based on the work of Margolis and Leondes (21). The method will be compared on the basis of a) error criterion, b) determination of sensitivity coefficients, c) inherent errors and limitations.

B1. Error Criterion

Both the NASA work and the STL work are based on minimization of a quadratic function of the matching error. Specifically, Whitaker's work is based on the criterion

$$F_w = \tfrac{1}{2}\int_{t_o}^{t_o = T} e^2\, dt \tag{B.1}$$

which represents the integral squared matching error. In practice, however, when continuous parameter adjustment is desired, the work is based on a new criterion

$$f_w = \frac{df_w}{dt} = \tfrac{1}{2}e^2 = \tfrac{1}{2}(z - y)^2 \tag{B.2}$$

where z is the model output and y is the output of the system being modeled.*

The STL work uses a somewhat more general criterion given by

$$f_m = \tfrac{1}{2}(e + q\dot{e})^2 \tag{B.3}$$

*In Whitaker's work the words "model" and "system" must be interchanged to be applicable for model matching work, since the model-referenced adaptive control theory uses a fixed model and an adjustable system.

where the term $q\dot{e}$ is introduced for improved convergence. It is clear that the two criteria are equivalent for $q = 0$.

B2. Determination of Sensitivity Coefficients u_i

The coefficients u_i can be evaluated in several ways. First, we note that

$$u_i = \frac{\partial e}{\partial p_i} = \frac{\partial (z - y)}{\partial p_i} = \frac{\partial z}{\partial p_i} \tag{B.4}$$

since the system output y is independent of the model parameter p_i. The method used by Whitaker is based on block diagram manipulation. Sensitivity coefficients are obtained by mechanizing a filter whose output is the desired coefficient u_i, and whose inputs are one or more model signals. For example, consider the model defined by

$$\dot{z} + p_1 z = p_2 x \tag{B.5}$$

In transfer function form

$$Z(s) = \frac{p_2 X(s)}{(s + p_1)} \tag{B.6}$$

Formal differentiation can be used to obtain

$$\frac{\partial Z}{\partial p_2} = \frac{X(s)}{(s + p_1)} \tag{B.7}$$

which is interpreted to mean that the coefficient $u_2 = \frac{\partial z}{\partial p_2}$ can be obtained from a filter with an input x(t), as shown below:

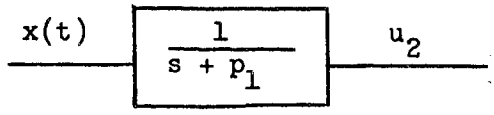

Figure B-1

Similarly

$$\frac{\partial Z}{\partial p_1} = - \frac{p_2 \; X \; (s)}{(s + p_1)^2} = - \frac{Z(s)}{s + p_1} \tag{B.8}$$

and the filter configuration is given below:

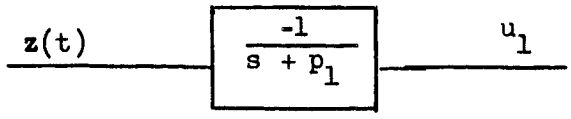

Figure B-2

It should be noted that (as Whitaker points out) the partial derivatives employed above are only used formally, and are strictly valid only when the parameters are constant.

Now, the parameter adjustment is based on the relationship

$$\dot{p}_i = - K \frac{\partial \mathfrak{F}}{\partial p_i} = - K \, e \, u_i \tag{B.9}$$

Consequently, the filters of Figure B-1 and B-2, followed by multipliers and integrators, are used to provide the variable parameters in the model.

The method used at STL is based on explicit computation of the influence coefficient by differentiation of the model differential equation with respect to the parameter. Thus, for equation (B.5), the sensitivity equations obtained are

$$\begin{aligned} \dot{u}_1 + p_1 u_1 &= -z \\ \dot{u}_2 + p_1 u_2 &= x \end{aligned} \tag{B.10}$$

which can be solved for the u_i. Clearly, the filters of Figures B-1 and B-2 are identical with the equations (B.10).

The use of model signals in the implementation of the influence coefficients can be further illustrated by the following example:

$$\ddot{z} + \alpha_1 \dot{z} + \alpha_2 z = \alpha_3 \dot{x} + \alpha_4 x$$

which corresponds to the model used in this study. Consider the influence coefficients u_3 and u_4. These can be obtained from the equations

$$\ddot{u}_3 + \alpha_1 \dot{u}_3 + \alpha_2 u_3 = \dot{x} \qquad \text{(B.11)}$$

$$\ddot{u}_4 + \alpha_1 \dot{u}_4 + \alpha_2 u_4 = x \qquad \text{(B.12)}$$

If we set up a model to solve (B.12) it can be drawn in the "filter" notation as:

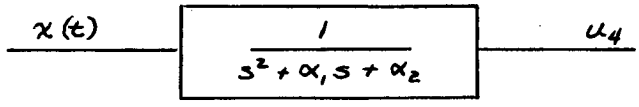

Figure B-3

But from (B.11) it can be seen that

$$\dot{u}_4 = u_3$$

and consequently u_4 is also available from the same filter output.

It should be noted that finite differences can also be used to determine influence coefficients, so that

$$\frac{y(p_1 + \Delta p_1) - y(p_1, t)}{\Delta p_1} \cong \frac{\partial y}{\partial p_1} \qquad \text{(B.13)}$$

B.3 Inherent Errors, Differences and Limitations

It follows from the preceding discussion that the "filter" method and the influence coefficient programming method (14) are essentially identical when the parameters are constant. If the parameters are being adjusted, then in the STL method the parameters are adjusted both in the model and in the sensitivity equation. In the NASA approach, the filter parameters remain invariant. The latter approach is clearly valid when the parameters are close to their true values, but may suffer from poorer convergence when the parameters are far from their correct values. When the parameters p_i are close to their "true" values a_i, it is even possible to use system influence coefficients as approximate equivalents to the model sensitivities, i.e. let

$$\frac{\partial y}{\partial a_i} \cong \frac{\partial z}{\partial p_i}$$

This approach is mentioned by Whitaker and was used extensively by Donalson (20). When the values of p_i and a_i are far apart, however, or when the a_i are completely unknown, the choice of the fixed parameters in the filter becomes another degree of freedom in the problem and a particular choice may have to be justified analytically or experimentally. An extension of Whitaker's method using variable filters was studied extensively at STL by W.J. Klenk and termed "dynamic model reference adaptive control" (17).

Neither method yields the actual sensitivities when the parameters are varying, since then the u_i are not defined.

The explicit parameter influence method is directly applicable to nonlinear system. Since transfer function manipulation is not possible in the nonlinear case, the time domain or differential equation approach is indicated.

Finally, the explicit parameter influence coefficient method makes it possible to generalize the criterion function by addition of rate terms, absolute value terms, etc.

Summary

The signal filtering method of Whitaker and the influence coefficient method employed by Margolis are equivalent for linear time-invariant systems. They differ only in whether the parameters in the sensitivity equations (or filters) remain constant or are adjusted. The influence coefficient method is readily extended to more general criterion functions and to nonlinear systems where transfer functions are not applicable.

REFERENCES

1. Osburn, P. V., Whitaker, H. P., and Kezer, A., "New Developments in the Design of Model Reference Adaptive Control Systems," IAS Paper No. 61-39, January 1961.

2. Adams, James J., "A Simplified Method for Measuring Human Transfer Functions," NASA Technical Report TN D-1782, April 1963.

3. McRuer, D. T., and Krendel, E., "Dynamic Response of Human Operators," WADC Technical Report TR 56-524, October 1957.

4. Goodyear Aircraft Corporation, "Final Report: Human Dynamics Study," GAC Report GER-4750, April 1952.

5. Ornstein, G. N., "Applications of a Technique for the Automatic Determination of Human Response Equation Parameters," Ph.D. Dissertation, Ohio State University, 1961.

6. Graupe, K. K., "The Analog Solution of Some Functional Analysis Problems," Transactions of the American Institute of Electrical Engineers (Communications and Electronics), January 1961.

7. Wertz, H. J., "Adaptive Control of Systems Containing the Human Operator," Ph.D. Dissertation, University of Wisconsin, 1962.

8. Margolis, M., "On the Theory of Process Adaptive Control Systems, the Learning Model Approach," Ph.D. Dissertation, University of California at Los Angeles, June 1960, and Report AFOSR TN 60-618, May 1960.

9. Humphrey, R. E., "Determination of the Values of Parameters in Mathematical Models of Physical Systems," STL Internal Memorandum No. 9352.1-258, September 1963.

10. Humphrey, R. E., and Bekey, G. A., "A Technique for Determining the Parameters in a Nonlinear Model of a Human Operator," STL Report No. 9865-6003-MU000, March 1963.

11. Elkind, Jerome I, and Green, David M., "Measurement of Time-varying and Nonlinear Dynamic Characteristics of Human Pilots," ASD Technical Report 61-225, December 1961.

12. Tompkins, C. B., "Methods of Steep Descent," in Modern Mathematics for the Engineer, ed. by E. F. Beckenback, (pp. 448-479), McGraw-Hill Book Co., 1956.

13. McGhee, R. B., "Identification of Nonlinear Dynamic Systems by Regression Analysis Methods, Ph.D. Dissertation, University of Southern California, June 1963.

14. Meissinger, H. F., "The Use of Parameter Influence Coefficients in Computer Analysis of Dynamic Systems," Proc. Western Joint Computer Conference, pp. 181-92, May 1960.

15. Humphrey, R. E., "Results of Preliminary Experiments on the Characteristics of a Human Operator in a Two-axis Manual Control Task," Unpublished STL Memorandum No. 9352.8-126, 24 October, 1962.

16. Potts, T. F., Ornstein, G. N., and Clymer, A. B., "The Automatic Determination of Human and Other System Parameters," Proc. Western Joint Computer Conference, Los Angeles, May 1961.

17. Klenk, W. J., "Preliminary Investigation of a Model Adaptive Control System," STL Document No. 0000-0001-MU000, 19 July 1961.

18. Adams, James J., and Bergeron, H. P., "Measured Variation in the Transfer Function of a Human Pilot in a Single Axis Task," NASA Technical Note TN D-1952, October 1963.

19. Adams, James J., and Bergeron, Hugh P., "Measured Transfer Functions of Pilots During 2-axis Tasks with Motion," NASA Technical Note D-2177, March 1964.

20. Donalson, D. D., "A Model Referenced Parameter Tracking Technique for Adaptive Control Systems," Ph.D. Dissertation, University of California at Los Angeles, 1961.

21. Margolis, M., and Leondes, C. T., "A Parameter Tracking Servo for Adaptive Control Systems," IRE Wescon Conv. Record, p. 104, August 1959.

GLOSSARY

a - Parameter in the system to be identified.

α - Parameter in the model of the human operator.

β - Cross-coupling parameter in the model of the human operator.

γ - Nonlinear cross-coupling parameter in the model of the human operator.

c - Initial condition model parameter.

e - Output error ($e = z-y$).

F - Time-integrated error criterion.

f - Instantaneous error criterion.

h - Subscript refers to the horizontal axis in a two-axis tracking task.

K - Gain.

(k) - Iterative notation - refers to the kth iteration.

n - Random noise - zero frequency spectral density = 2.41 $\frac{\text{volts}^2}{\text{cps}}$.

q - A constant introducing error rate compensation.

$Q(t)$ - Finite difference approximation of the gradient.

$r(t)$ - Input disturbance function.

s - Laplace operator.

t - Time.

u_i - Influence coefficient, $\partial z/\partial \alpha_i$.

v - Subscript refers to vertical axis of a two-axis task.

x - Oscilloscope display displacement, centimeters.

y - Output of the human operator, $\pm$ 1 unit full stick deflection of $\pm$ 30 degrees.

z - Output of the model of the human operator.

ζ - Output of a second model of the human operator with the ith parameter increased by $\Delta\alpha_i$.